Universidad de Concepción

Dirección de Postgrado

Facultad de Ciencias Químicas

Programa Doctorado en Ciencias Geológicas

Modelo de fuente de sismicidad volcánica y su relación con deformación cortical de gran escala en un sistema riolítico: Complejo Volcánico Laguna del Maule.

Tesis para optar al grado de Doctor en Ciencias Geológicas

CARLOS EDUARDO CARDONA IDARRAGA

Concepción - Chile

2018

Profesor Guía: Andrés Tassara Oddó

Dpto. de Ciencias de la Tierra, Facultad de Ciencias Químicas

Universidad de Concepción

Co-guía: Luis Lara Pulgar

Servicio Nacional de Geología y Minería

Sernageomin

Dedicatoria

En el año 1985 una tragedia ocurrió en mi país de origen, la erupción del volcán Nevado del Ruiz cobró la vida de más de 23000 personas, mi padre tenía unas tierras cerca de una localidad altamente impactada por dicha erupción, al día siguiente de la erupción fuimos con él a la zona y no puedo recordar panorama más lúgubre que el observado. Desde ese entonces me inquietaron los volcanes, quería saber por qué razón un sistema natural tan majestuoso, puede llegar a ser tan destructivo, tengo el convencimiento que ésta fue una de las principales razones para escoger la geología como mi carrera profesional y dedicar toda mi experiencia profesional en trabajar en observatorios volcanológicos. Por este motivo, agradezco todo el apoyo de mi familia, especialmente a mi Madre por su tozudez y soporte, sin el cual probablemente no hubiese sido posible terminar mi carrera profesional, Madre te debo todo lo que soy y te dedico este nuevo logro.

La vida me ha regalado la oportunidad de conocer personas maravillosas, en especial me siento inmensamente afortunado de poder compartir mi proyecto de vida con una mujer invaluable, Jimena gracias por

tu apoyo incondicional, por siempre darme fuerzas, por construir una familia juntos, por regalarme la dicha de ser padre de mis dos invaluables tesoros Valentina e Isabella, quiero agradecer a las tres por estar siempre a mi lado, por aceptar todas mis horas de ausencia, les dedico con mucho orgullo este logro, sin ustedes en mi vida no hubiese sido posible conseguir lo que hasta ahora hemos logrado.

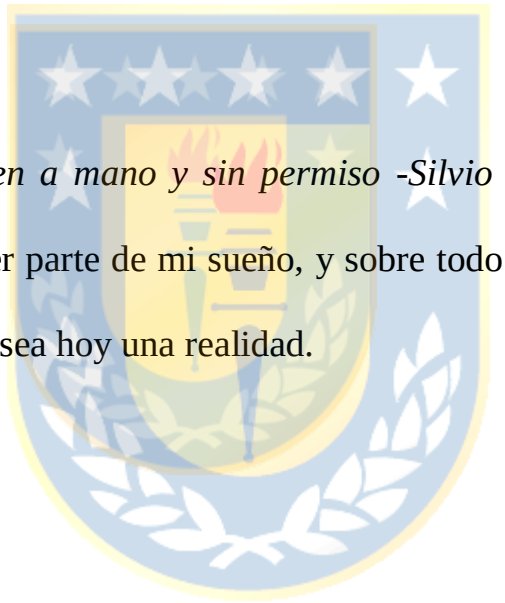

"*Los sueños se hacen a mano y sin permiso -Silvio Rodríguez-*", gracias mis mujeres por hacer parte de mi sueño, y sobre todo por ayudar a que mi sueño de doctorarme sea hoy una realidad.

AGRADECIMIENTOS

Esta tesis doctoral no hubiese sido posible sin el apoyo de muchas personas, que contribuyeron de una u otra manera a su consecución final, y de los cuales nombraré solamente algunas a continuación:

El autor agradece considerablemente al Servicio Nacional de Geología y Minería por el apoyo institucional recibido para realizar esta investigación, a través del proyecto 'Red Nacional de Vigilancia Volcánica'. Especialmente agradezco al Dr. Luis Lara Pulgar y al Sr. Fernando Gil Cruz por impulsar la inclusión de esta investigación dentro del plan regular de trabajo del Observatorio Volcanológico de los Andes del Sur. El apoyo presupuestario y logístico recibido fueron esenciales para el desarrollo de esta investigación.

Agradezco a mi esposa Jimena, ella fue la que impulso a tomar la decisión de empezar mi estudio doctoral, y ante dificultades siempre me ha dado una voz de aliento, me ha hecho sentir importante y capaz de lograrlo, gracias por ser un cimiento en momentos difíciles, gracias por llevar nuestra familia en mis horas de ausencia.

Quiero agradecer a mi madre, por inculcar todos los valores que me han formado, por alentarme a seguir estudiando, todo lo que he conseguido ha sido gracias a tu esfuerzo y dedicación, madre te debo todo lo que soy.

Agradezco a mi profesor guía Dr. Andrés Tassara Oddó, quien me acompañó a lo largo del trabajo de investigación dándome consejos acertados, realizando un criticismo constructivo e impulsando de manera desinteresada a finalizar la investigación. Estoy seguro que la vida pone las personas adecuadas en el momento oportuno. Andrés, estoy eternamente agradecido por tu apoyo.

Dos personas fueron fundamentales en todo el proceso del doctorado, mis compañeros de estudio Luis Franco (mi eterno amigo) y Daniel Basualto, con ellos compartí varias noches en la cabina de doctorantes. Además de considerarlos mis amigos, les agradezco enormemente sus buenos consejos y ayuda en el procesamiento. Debo decir que sin ustedes, todo hubiese sido más difícil.

Debo agradecer enormemente a mi amigo y colega de OVDAS, el ingeniero electrónico Christian Delgado, quien ayudó en el despliegue y mantenimiento de las estaciones de la red Laguna del Maule. Sin su

esfuerzo y profesionalismo hubiese sido imposible obtener los datos para realizar este trabajo de investigación.

Hace 20 años tuve la fortuna de conocer al señor Fernando Gil-Cruz, quien fue mi primer maestro de sismología volcánica y asesor de mi tesis de pregrado. Fernando, gracias por enseñarme todo tu conocimiento, por mostrarme el maravilloso mundo de la vigilancia volcánica.

De igual forma, agradezco a todos los compañeros del Observatorio Volcanológico de los Andes del Sur -OVDAS-, por ayudar en el procesamiento primario de los datos. En especial a Sergio Morales que colaboró en el procesamiento de datos y realización de figuras, muchas gracias por su colaboración. De igual forma, quiero agradecer a Loreto Córdova por el procesamiento de los datos GPS.

Finalmente, quiero agradecer al Dr. Bradley Singer y al Dr. Clifford Thurber por su invitación a hacer parte del grupo de investigación del Proyecto National Science Foundation del Complejo Volcánico Laguna del Maule, gracias por el apoyo económico, por gestionar y facilitar mi pasantía en la Universidad de Wisconsin, y por recibir entrenamiento en técnicas de procesamiento de datos sísmicos.

Resumen

El Complejo Volcánico Trasarco Laguna del Maule (LMVC, 33°S – 46°S) es considerado como uno de los más peligrosos sistemas volcánicos de los Andes, lo cual es sugerido por una combinación de un impresionante vulcanismo riolítico holocénico y un proceso actual de alzamiento superficial de alta tasa, detectado por medidas geodésicas. La actividad holocénica comprende aproximadamente 40 km^3 de lavas riolíticas y riodacíticas que han sido eruptadas desde 24 centros de emisión separados, que circundan el lago. Recientes estudios multiparamétricos que involucran datos InSAR, GPS, magnetotelúrica, microgravimetría, sísmica y petrocronología, sugieren la actividad de un cuerpo de magma riolítico superficial, localizado a 5 km de profundidad, el cual está produciendo grandes levantamientos corticales a tasas (> 25 cm/y) consideradas como las más grandes medidas en un sistema volcánico que no presente un ciclo eruptivo en curso. El modelo sugerido de ésta deformación ha sido asociado a un sill inclinado inflándose, de aproximadamente 9 km de largo y 5 km de ancho, con valores de apertura anual promedio de 1 m. Con estas evidencias de actividad, el Observatorio Volcanológico de los Andes del Sur (OVDAS) dependiente del Sernageomin desplegó una red de vigilancia en

abril de 2011, compuesta por sismómetros y estaciones GPS, lo cual confirmó las grandes tasas de alzamiento y evidenció actividad sísmica superficial alrededor de la zona de inflación. Esta investigación presenta la primera caracterización sistemática de la actividad sísmica registrada en el CVLM, entre los años 2011 y 2016, mostrando su evolución espacial y temporal, identificando familias sísmicas y resolviendo la fuente que produce la sismicidad volcánica. Un aspecto destacable es el reconocimiento de enjambres sísmicos repetitivos (21 en total) ocurriendo en el vértice SW del sill propuesto como fuente del alzamiento superficial. Después de resolver la fuente sísmica de los enjambres como una falla strike-slip, nosotros integramos estos resultados con aquellos derivados de un mapeo estructural del área del CVLM. Nuestro principal hallazgo es descubrir dos principales estructuras que producen la sismicidad, La Falla Troncoso cuyos mecanismos focales y evidencia de campo sugieren un fallamiento strike-slip, y la segunda estructura un lineamiento WNW-ESE con evidencias de campo de un fallamiento normal. Adicionalmente, se construyeron las series diarias de tiempo para la sismicidad volcánica y los datos de GPS, con el propósito de evaluar el nivel de acoplamiento entre ambos procesos. Parece existir una conexión temporal, ya que cuando un

alto/bajo número de enjambres sísmicos fueron registrados correlaciona con incrementos/decrementos de las tasas de alzamiento. Para soportar lo anterior, se realizó un cálculo de esfuerzos tipo Coulomb, asumiendo como fuente de esfuerzos el sill inflándose y como estructuras receptoras fallas strike-slip de componente dextral, los resultados sugieren que el proceso causante del impresionante alzamiento vertical podría afectar el campo de esfuerzos local del área, promoviendo el deslizamiento en fallas vecinas.

Abstract

The rear arc Laguna del Maule Volcanic Complex (LMVC, 33°S – 46°S) is considered as one of the most hazardous volcanic system on Andean Volcanic Zone, as suggested by the combination of an impressively Holocene volcanism and large rates of current surface uplift detected by geodetic measurements. The Holocene activity comprises approximately 40 km^3 of rhyolites and rhyodacites lavas that have erupted from 24 separated vents surrounding the lake. Recent multiparametric studies involving InSAR, GPS, magnetotelluric, and microgravimetry, seismic and petrochronology data, have suggested the activity of a shallow rhyolitic magma body located 5 km depth, which is producing a large crustal uplifting with rates (> 25 cm/y) considered as the highest ever recorded at a volcano system that is not actively erupting (Singer y otros 2014). The source of this deformation has been suggested as an inflating and dipping sill, approximately 9 km length and 5 km width, with a media value of opening rate of 1 m by year. Given this evidences of unrest, the Observatorio Volcanologico de los Andes del Sur (OVDAS; the Chilean Volcano Observatory depending on the Geological Survey SERNAGEOMIN) deployed a survey network in April 2011, composed by

seismometers and GPS station, confirming the extreme uplift rates and showing clear evidence of shallow seismic activity surrounding the inflating zone. This investigation presents the first systematic characterization of the seismic activity recorded at LMVC between 2011 and 2016, showing the temporal and spatial evolution of the seismicity, identifying seismic families and resolving the sources that produce the volcano seismicity. A noteworthy aspect was recognizing the repetitive seismic swarms (21 in total) occurring on the SW corner of the sill proposed as source of the surface uplift. After resolved the source of seismic swarms as a strike slip fault, we integrated these results with those derived from a structural mapping of the LMVC. Our main finding is to discover two main active structures producing seismicity, the Troncoso fault with focal mechanism and clear field evidences of a strike-slip fault, and one WNW-ESE lineament with field evidences of normal faulting. Additionally, we constructed time series for daily volcano seismicity and GPS data, in order to evaluate the level of coupling between both phenomena. There seems to be a temporal connection, since periods with a greater/smaller number of seismic swarms were recorded could correlate with periods with increasing/decreasing of the uplifting rates. To support this assumption, we

did a Coulomb stress calculation, assuming as source of stresses a sill inflating and as receiver structures strike-slip faults. Our results suggest that the inflation process causing the astonishing surface uplift could affect the local stress field of the area, promoting the failure on neighbor faults.

Tabla de contenidos

Índice de Figuras

Índice de Tablas

CAPITULO 1: INTRODUCCIÓN GENERAL

1.1Introducción

El Complejo Volcánico Laguna del Maule (CVLM), se ubica en el límite entre Chile y Argentina, en la región del Maule (36.1° S, 76.5° W), es un campo volcánico de trasarco, localizado a ~330 km al E de la trinchera, ~200 km de la costa y entre ~130-150 km por encima de la zona de Benioff (Fig. 1.1). Alberga numerosos centros volcánicos en su interior, con actividad Holocena reconocida, y magmas composicionalmente diversos que incluyen desde basaltos hasta riolítas (Hildreth y otros, 2010). Aunque el CVLM no tiene registros de erupciones históricas, durante los últimos años, el CVLM ha llamado la atención de la comunidad científica debido a la observación de síntomas inequívocos de actividad endógena acompañada de una deformación cortical catalogada como una de las mayores a nivel mundial (Fournier y otros 2010, Feigl y otros, 2014, Le Mével y otros 2015, 2016), en un volcán activo que no presente un proceso eruptivo en curso. Un interferograma de imágenes satelitales entre 2003 y 2004 analizado por Fournier y otros (2010) no mostró ningún tipo de deformación cortical

detectable, pero imágenes satelitales para en un periodo comprendido entre enero de 2007 y enero de 2008, revelaron una zona de deformación inflacionaria a una tasa cercana a los 18.5 cm/año. Los autores modelaron la fuente causante de la deformación como un 'sill' rectangular, localizado en el centro del complejo a 5 km de profundidad, con tasas de apertura cercanas a los 60 cm/año. Posteriormente, interferogramas analizados por Feigl (2014), entre enero de 2007 y febrero de 2010, sugieren que la deformación del complejo continuaba activa, e inclusive con una clara tendencia al ascenso, calculando tasas máximas de alzamiento vertical de ~25 cm/año, y confirmando como fuente de deformación un sill rectangular ubicado a 5 km de profundidad. Estudios posteriores realizados por Le Mével y otros (2015), combinando datos InSar y estaciones GPS locales, muestran que la tasa de deformación debió comenzar en el año 2007, alcanzado su tasa de alzamiento máximo antes de la ocurrencia del gran sismo de subducción del Maule, Mw=8.8 de febrero de 2010, con tasas cercanas a los 25 cm/año, y nuevamente decreció en enero de 2013, para estabilizarse alrededor de 20 cm/año. Le Mével y otros (2016) desarrollaron modelos numéricos de inyección de magma para analizar la evolución temporal de la fuente de deformación, y sugiere que entre el 2007 y el

2009, la presión de inyección aumentó a un máximo de 11.5 MPa, con una tasa de flujo de volumen de 1.3 m^3/s, la que decreció a 0.7 m^3/s en 2014, y se mantuvo con una tasa decreciente hasta el año 2016.

Por otro lado, mediciones gravimétricas realizadas por Miller y otros (2016) reportan un notable cambio de masa al interior del CVLM, entre los años 2013 y 2014, calculando cambios residuales de gravedad de 124 ± 12 microgales. Finalmente, nuevos indicios de actividad endógena fueron reportados por Cordell y otros (2018) los cuales usando medidas magneto telúricas desarrollaron un modelo tridimensional de resistividad eléctrica para el CVLM, donde se destacan dos zonas anómalas, la primera de carácter superficial localizada al oeste del complejo a 4 km de profundidad y otra más profunda en la porción norte del complejo a 10 km de profundidad.

Debido a las evidencias de actividad interna observadas, en el año 2011, el Observatorio Volcanológico de los Andés del Sur (OVDAS) perteneciente al proyecto "Red Nacional del Vigilancia Volcánica" del Servicio Nacional de Geología y Minería (Sernageomin), decidió instalar

estaciones sísmicas de banda ancha y GPS alrededor del campo volcánico. La red de vigilancia instalada registró actividad sísmica asociada con el complejo, con registro de al menos 21 enjambres sísmicos próximos al área de deformación, entre los años 2011 y 2017, localizados a niveles superficiales < 5 km. Asimismo, las medidas de GPS realizadas desde febrero de 2012, reafirmaron que la deformación continuaba activa, con tasas verticales calculadas de aproximadamente 25 cm/año. De acuerdo con los estudios geológicos previos y los datos obtenidos sobre su actividad reciente principalmente datos sísmicos y geodésicos, indican que el CVLM es un sistema con síntomas inequívocos de reactivación y con potencial de evolucionar hacia ciclos eruptivos de alta explosividad con la evacuación de magma riolítico. De esta manera, el estudio de las condiciones actuales constituye una oportunidad invaluable para comprender la dinámica de este tipo de sistemas y las características que se presentan en fases pre-eruptivas.

El objetivo de este proyecto consistió en la implementación de una red de monitoreo multidisciplinaria en el CVLM, basada especialmente en estaciones sísmicas de banda ancha y GPS, con el objetivo primordial de entender su dinámica actual y modelar la configuración en profundidad de

la fuente generadora de la actividad sísmica observada, permitiendo a su vez la comprensión de los procesos corticales internos que pudiesen conducir eventualmente hacia un nuevo ciclo eruptivo.

1.2 Marco tectónico y geológico regional.

La parte central de Chile (33°S – 46°S) está enmarcada por una convergencia oblicua entre las placas Nazca y Suramericana, con tasas de convergencia promedio de 6.6 cm/año (Cembrano y Lara 2009; Lavenue y Cembrano 1999; Bonali y otros, 2013). El límite de placas a estas latitudes posee una particularidad especial de particionamiento de la deformación cortical, generando grandes sismos de subducción y un complejo sistemas de fallas intraarco de componente transpresional-dextral, como el conocido sistema de fallas 'Liquine-Ofqui' (LOFZ) en su porción sur y la falla el Melado en la región central. Estos sistemas de fallas intraarco han sido reconocidos como zonas de fragilidad cortical y de circulación por donde magmas han alimentado el volcanismo Andino durante el Holoceno. El LOFZ ha sido sugerido como la principal estructura cortical con una marcada influencia para la localización en el segmento central de Chile del arco volcánico activo moderno. El CVLM se localiza al norte de la zona

volcánica sur de los Andes (Stern, 2004), y específicamente en la subzona volcánica denominada Transicional de dicho segmento (TSVZ). Algunos autores sugieren que el límite sur de dicha subzona, y donde se ubican algunos centros volcánicos activos como el Longaví (Rodríguez, 2007), Complejo volcánico San Pedro de Tátara- Pellado (Feeley y otros, 1998) y el CVLM (Frey y otros 1984), podrían coincidir espacialmente con la extensión continental de la zona de fractura La Mocha. Así mismo, el CVLM se ubica a ~330 km al E de la trinchera, ~200 km de la costa, entre ~130-150 km por encima de la zona de Benioff, y a 20 km al E del complejo volcánico San Pedro Tatará – Pellado (Hildreth y otros, 2010) el cual se sitúa sobre el eje del arco volcánico cuaternario, por lo que el CVLM es considerado como un campo volcánico tras-arco. Los depósitos asociados con su historia eruptiva cubren secuencias de rocas volcánicas del Mioceno y Plioceno depositadas sobre basamento del Oligoceno (Stern, 2004).

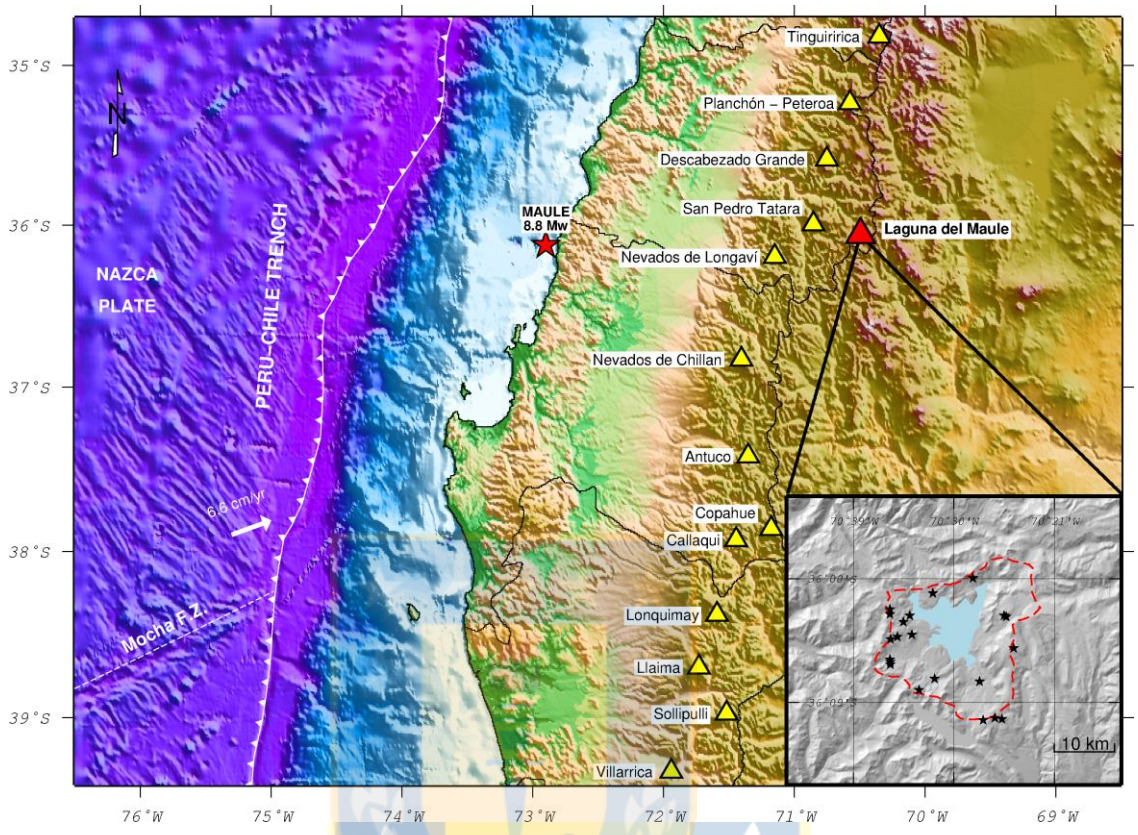

Figura 1.1 Mapa de localización y marco tectónico regional del Complejo Volcánico Laguna del Maule (triangulo rojo), los volcanes actualmente vigilados por el Observatorio Volcanólogico de los Andes del Sur (OVDAS) son señalados por los triángulos amarillos. La estrella roja muestra la localización del terremoto Mw=8.8. Fuente: Elaboración propia.

Aunque diversos estudios regionales han considerado que los centros volcánicos pertenecientes al TSVZ han sido relacionados con procesos que involucran la mezcla de magmas basálticos con magmas evolucionados, y contribución de rocas corticales al magmatismo (Hildreth y Moorbath,

1988; Stern, 2004), parece ser que dicho factor no tuviese un rol preponderante en el magmatismo generador de las rocas eruptadas por el CVLM; levantamientos geológicos y estudios isotópicos de sus rocas volcánicas (Hildreth y otros, 2010; Frey y otros, 1984; Singer y otros, 2014; Andersen y otros, 2017), sugieren procesos complejos para la generación de dichos magmas, donde un modelo relacionado con cristalización fraccionada (>80%) desde un magma basáltico, podría ser un factor fundamental que explicaría la similitud isotópica encontrada entre los basaltos y las riolítas asociadas con el CVLM (Hildreth y otros, 2010).

1.3 Geología Local.

Con relación a la geología local del CVLM, los primeros levantamientos cartográficos realizados corresponden a los estudios de González y Vergara (1962) y Drake (1976), incluyendo el área del CVLM en estudios a nivel de escala regional. Posteriormente, Munizaga (1978) y Frey y otros (1984), realizaron levantamientos cartográficos específicos del CVLM, los estudios realizados enfatizan en el amplio abanico composicional encontrado en las rocas pertenecientes al CVLM, y la progresión lineal desde basaltos como

rocas más antiguas hasta riolitas como las rocas más recientemente eruptadas, desde varios centros de emisión ubicados alrededor del lago. El objetivo principal del estudio de Frey y otros (1984), era determinar si las rocas pertenecientes al CVLM tenían una correlación entre sus características isotópicas y la localización de los diversos centros volcánicos, sugiriendo que dicha información era relevante para evaluar el efecto de la contaminación cortical y en determinar variaciones en la composición de la fuente; sin embargo, la principal conclusión a que llegó el estudio fue que las riolítas que rodean la laguna, están genéticamente relacionadas con cristalización fraccional y/o fusión parcial de rocas basálticas antiguas, las cuales presentan una composición isotópica similar, sugiriendo que dichos magmas básicos evolucionaron sin una significativa contaminación de la corteza superior. Posteriormente, Hildreth y otros (2010), realizaron un levantamiento muy detallado de las unidades antiguas del Pleistoceno y las rocas riolíticas post-glaciales de la laguna (Fig. 1.2), identificando 36 ‘coulees’ y domos riolíticos y riodacíticos, que hicieron erupción desde 24 centros de emisión separados y que cubren un área de ~100 km^2, sugiriendo una prolongada historia de erupciones explosivas recientes, desde centros de emisión dispersos a lo largo del lago, con un

abanico composicional continuo desde 49% a 77,6% de SiO_2. Este estudio concluye que ninguno de los basaltos es primitivo y que todos los productos presentan una fuerte marca geoquímica tipo arco. Finalmente, aunque sus productos van desde basaltos hasta riolítas, el área del CVLM puede ser considerado como un coherente campo volcánico, tomando en cuenta: 1- La alta densidad espacial de sus centros de emisión cuaternarios distribuidos, 2- La dispersión de numerosos sitios eruptivos a lo largo del campo persistentemente durante los últimos 1.5 Ma, 3- La ininterrumpida continuidad (desde 49% a 77% de SiO2) de su estrecho arreglo composicional para sus múltiples productos en los diversos centros de emisión, y 4- Recurrentes erupciones rioliticas, restringidas regionalmente a unos pocos centros volcánicos, pero extendidos a lo largo del CVLM.

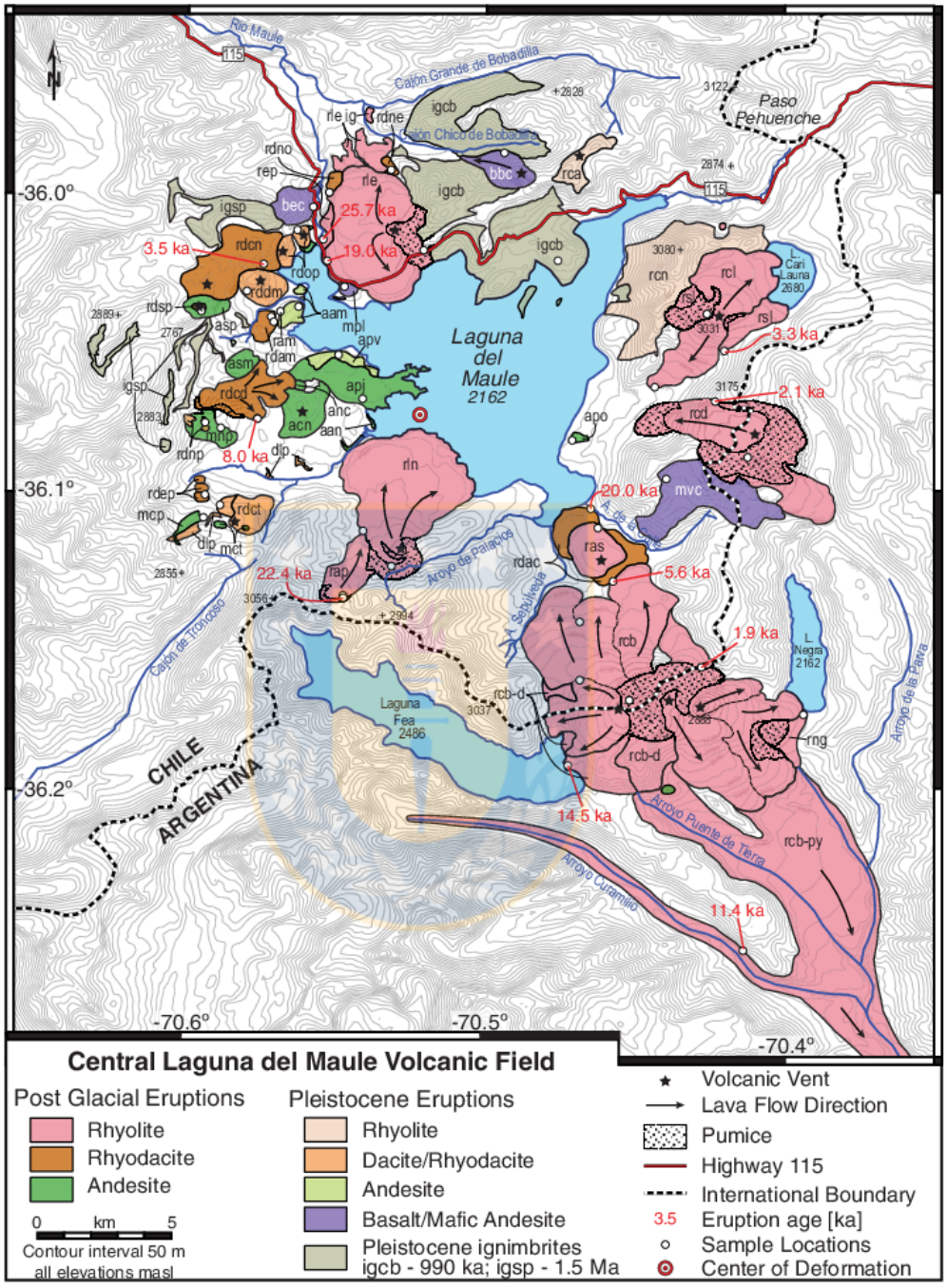

Figura 1.2. Mapa geológico simplificado del CVLM y su periferia, las estrellas marcan la ubicación de los centros de emisión y los cráteres son mostrados como depresiones achuradas. Fuente: Andersen y otros 2018, modificado de Hildreth y otros, 2010.

1.4 Actividad y estudios recientes

1.4.1 Estudios de deformación

Los primeros síntomas de actividad en el CVLM fueron observados usando imágenes InSAR. Fournier y otros (2010) estudiaron interferogramas para un periodo de tiempo entre enero del 2007 y enero de 2008, reportando una zona inflacionaria asociada al CVLM, la fuente productora de dicha deformación fue modelada como un 'sill' inclinado dispuesto en dirección SW-NE, ubicado en el centro de laguna a 5 km de profundidad y con una tasa de deformación anual de 18.5 cm/a (Fig. 1.3).

Los niveles de deformación reportados por el estudio de Fournier y otros (2010) se categorizaron como una de las deformaciones volcánicas activas más grandes a nivel mundial (Fig. 1.4), y tomando en cuenta su historia geológica asociada con grandes erupciones de tipo riolítico, llamó la atención de la comunidad científica internacional.

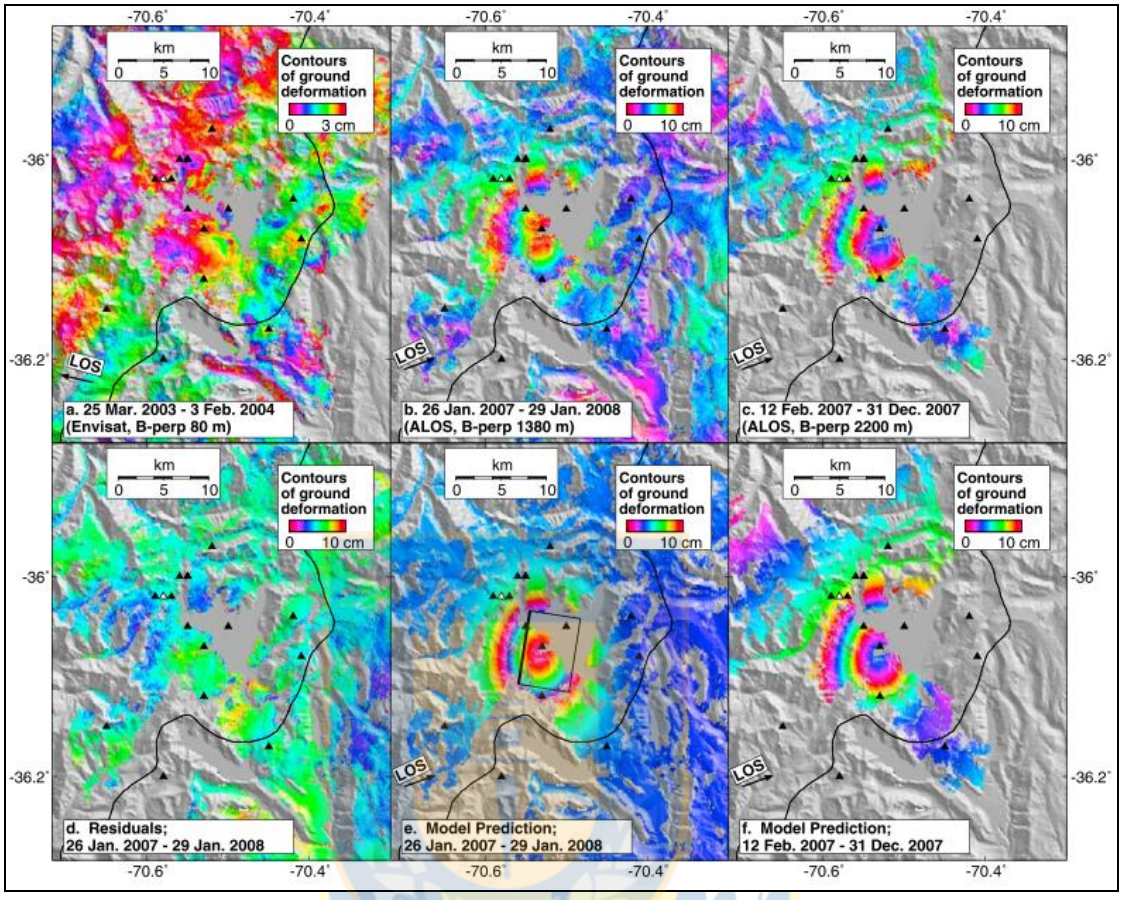

Figura 1.3 Interferogramas obtenidos en el estudio realizado por Fournier y otros (2010), nótese que para el periodo comprendido entre marzo de 2003 y febrero de 2004, el área no presentaba deformación asociada, y para el periodo enero de 2007 y enero de 2008, fue observado un centro de deformación que fue modelado con un 'sill' inflándose localizado en el centro del CVLM. Fuente: Fournier y otros (2010).

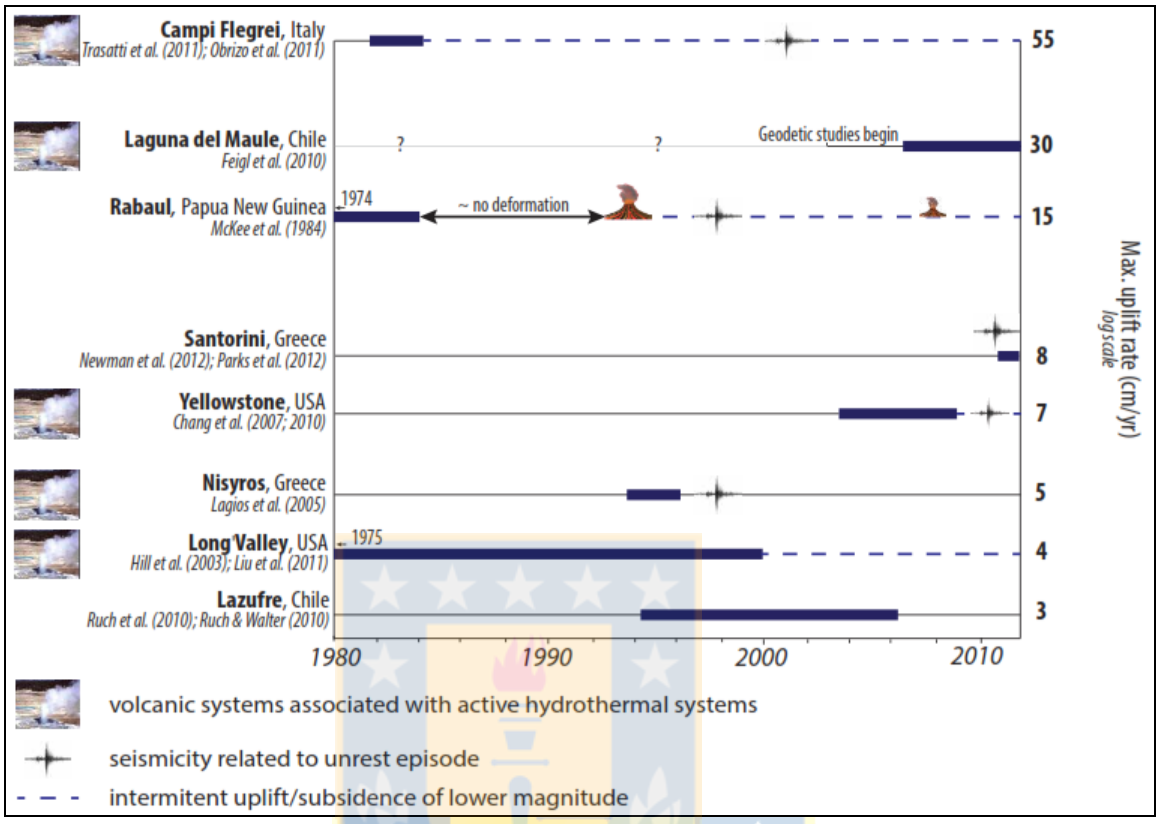

Figura 1.4 Comparación de grandes tasas de deformación volcánica observadas en periodos recientes. Fuente: Le Mével y otros 2012.

Posteriormente, Feigl y otros (2014) realizaron nuevos estudios InSAR con imágenes adquiridas entre los años 2007-2012, confirmando que la fuente de deformación permanecía activa y con una tendencia al incremento, calculando tasas máximas de ~28 cm/a, con un alzamiento acumulado hasta el 2012 de cerca de 150 cm en 5 años (Fig. 1.5a). El modelamiento de los datos InSAR, asumiendo una dislocación rectangular con propiedades elásticas uniformes, sugieren un cuerpo cuya geometría

representa un ‘sill’ localizado a 5.2 ± 0.3 km de profundidad, con 9.0 ± 0.3 km de largo, 5.3 ± 0.4 km de ancho, una inclinación de 20° ± 3° hacia el E y un rumbo de 14° ± 5° (Fig. 1.5b). Los autores calculan una tasa de apertura de 1.1 m/año, con tasas de incremento de volumen en el sill modelado de 51 ± 5 millones de m^3/año, dando un incremento total de volumen de 0.15 km^3 entre los años 2004 y 2012. La geometría sugerida es muy similar a los resultados encontrados previamente por el trabajo de Fournier y otros (2010).

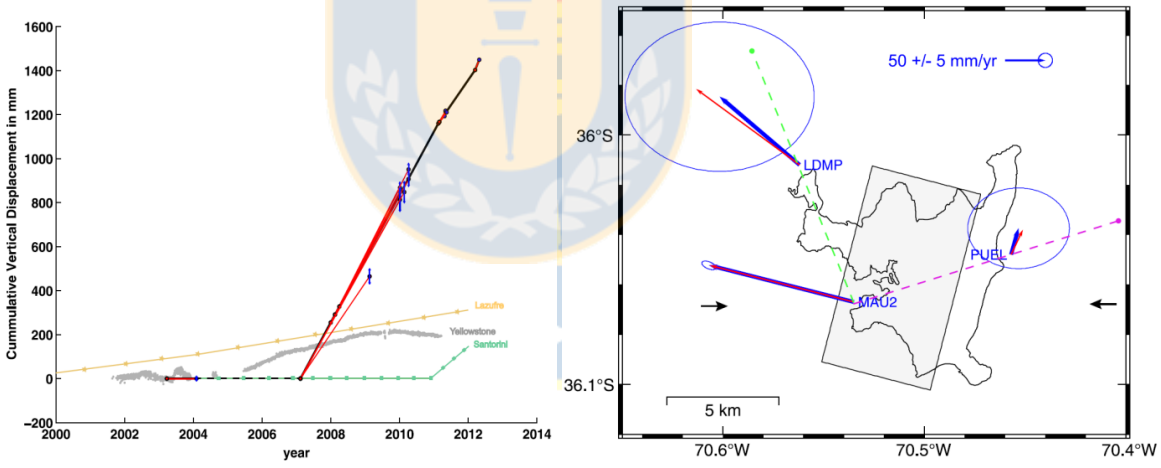

(a) (b)

Figura 1.5 Resultados del trabajo de Feigl y otros (2014). **(a)** Series de tiempo de desplazamiento vertical calculado sobre la zona de máximo alzamiento del CVLM, entre los años 2004 y 2012, con un total acumulado de cerca de 1,5m, y su comparación con otras áreas volcánicas riolíticas alrededor del mundo. **(b)** Mapa del campo de velocidades horizontales de las estaciones GPS del CVLM para el año 2012 (líneas azules) y el ajuste de

las velocidades modeladas (líneas rojas) asumiendo una fuente rectangular ('Sill') ubicada a 5.2 Km de profundidad. Fuente: Feigl y otros (2014).

Le Mével y otros (2015), analizaron nuevos datos de GPS e imágenes InSAR entre el 2003 y 2014, donde sugieren que el proceso de alzamiento comenzó en algún periodo del año 2007, mostrando un comportamiento incremental hasta el año 2010, donde se alcanza los máximos alzamientos históricos de 25cm/a, posteriormente el proceso sufre una desaceleración llegando a tasas anuales de 22 cm/a. Algunos autores sugieren que la desaceleración coincide con cambios en el stress regional observado posterior a la ocurrencia del terremoto Mw=8.8 del Maule (Pritchard y otros 2013). En enero de 2013 las tasas de alzamiento nuevamente sufren un proceso de desaceleración llegando a tasas anuales de 19 cm/a (Fig. 1.6a), este cambio coincide temporalmente con la ocurrencia del enjambre sísmico más energético que se haya registrado en el CVLM. El total de desplazamiento vertical acumulado entre los años 2007 y 2014 fue de ~1850 mm (Fig. 1.6b). Continuando con su trabajo, Le Mével y otros (2016) realizaron modelamientos numéricos de la deformación por medio de soluciones analíticas, asumiendo un esferoide localizado a 4.5 Km de profundidad, llegando a la conclusión que en los dos primeros años de

inicio del proceso de alzamiento el proceso presentó una aceleración con tasas de flujo de magma de 1.2 m^3/s, para mediados de 2009 la tasa de flujo de volumen decrece a 0.7 m^3/s, y en 7.3 años (entre 2007 y 2014) al menos un volumen de magma de 0.19 km^3 fue inyectado.

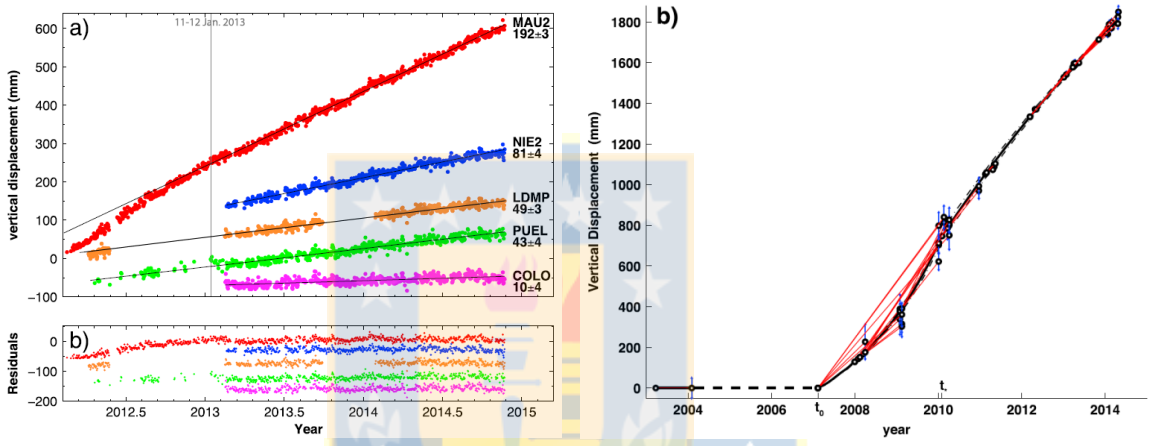

(a) (b)

Figura 1.6 Resultados del trabajo de LeMével y otros (2015). **(a)** Series de tiempo de desplazamiento vertical para las cinco estaciones GPS del OVDAS, entre los años 2012 y 2014, nótese que en enero de 2013 la pendiente cambia debido a la desaceleración del proceso de alzamiento, lo cual coincide temporalmente con la ocurrencia del enjambre sísmico más energético registrado en la zona del CVLM. **(b)** Desplazamiento vertical acumulado observado en la zona de máxima deformación, para un intervalo de tiempo entre los años 2007-2014, se presentó un levantamiento total de 1850 mm. Fuente: LeMével y otros (2015).

1.4.2 Mediciones gravimétricas

Entre los años 2014-2016, Miller y otros (2016) realizaron mediciones de microgravedad en 239 puntos alrededor del CVLM, con el fin de realizar la inversión de un modelo 3D de gravedad para el sistema volcánico, encontrando una zona de baja densidad de 30 Km^3, localizado a 2 Km de profundidad, la cual fue interpretada como un reservorio de magma rico en volátiles, conteniendo al menos 85% de fundido, alojado dentro de un mush de 115 Km^3 total o parcialmente cristalizado (>70% cristales). El reservorio es adyacente a la falla Troncoso y se ubica sobre el sill sugerido por los estudios InSAR. Dicho reservorio está cercano a uno de los centros eruptivos holocénicos (Nieblas) que eruptó 2 Km^3 hace 2-3 ka, correspondiente al 7% del reservorio de magma indicado (Fig. 1.7).

Por otro lado, Miller y otros (2017) realizando un estudio de cambios temporales de las mediciones de microgravedad sugieren que durante el año 2013 ocurrió una inyección de masa de $1.5x10^{11}$ Kg, localizada a lo largo de la falla Troncoso y estructuras paralelas ubicadas bajo la laguna a 1.5-2 km de profundidad, siendo sugerido como mecanismo responsable de estos

cambios temporales de densidad la movilización de fluidos hidrotermales dentro de fisuras existentes o nuevas fisuras creadas por el proceso de alzamiento.

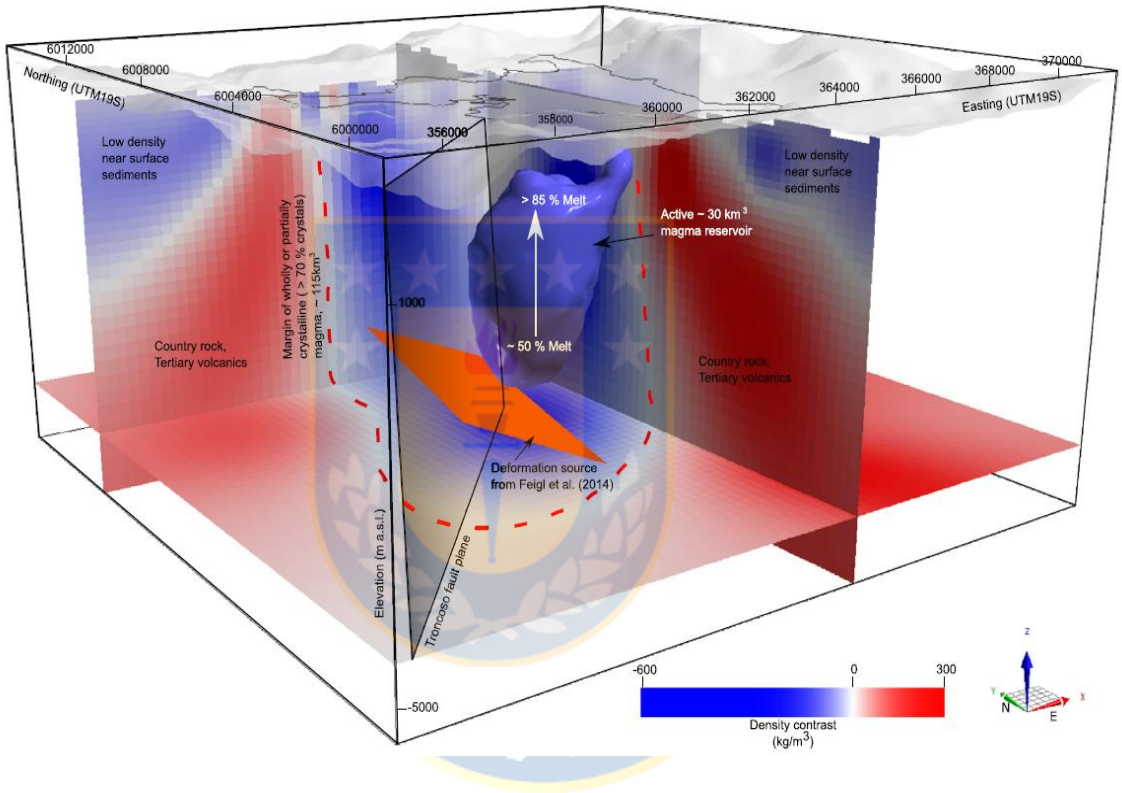

Figura 1.7 Modelo de contraste de densidad del CVLM. En púrpura se muestra la zona de baja densidad 30 Km^3 localizada sobre el 'sill' modelado por los estudios INSAR, el cual se encuentra rodeado por una zona de 115 Km^3 (línea roja discontinua) interpretada como un mush total o parcialmente cristalizado (>70% cristales). Fuente: Miller y otros (2016)

1.4.3 Mediciones Magnetotelúricas

Cordell y otros (2018), crearon un modelo 3D de resistividad eléctrica para el CVLM y áreas circundantes, identificando cuatro anomalías de conductividad. La primera de ellas (C1) ubicada 100 m bajo el lago, la cual es interpretada como el reservorio hidrotermal superficial. La segunda (C2) a 1 km de profundidad, que coincide espacialmente con el área de máxima inflación, sin embargo, los autores remarcan que esta anomalía esta en el límite de detección del método, por lo tanto su constricción es baja, y podría corresponder a un artefacto. En el modelo se resaltan dos anomalías importantes altamente conductivas, identificadas como C3 y C4. La más profunda de ellas (C4) está localizada al norte del CVLM a más de > 8 km de profundidad, la cual es interpretada como un reservorio magmático profundo riolítico a andesítico de larga vida. Este reservorio profundo aporta fundido y fluidos hidrotermales a un reservorio más superficial (C3) localizado al NW del CVLM a 4 Km de profundidad, que coincide espacialmente en superficie con algunos centros de emisión holocénicos y fuentes termales (Fig. 1.8).

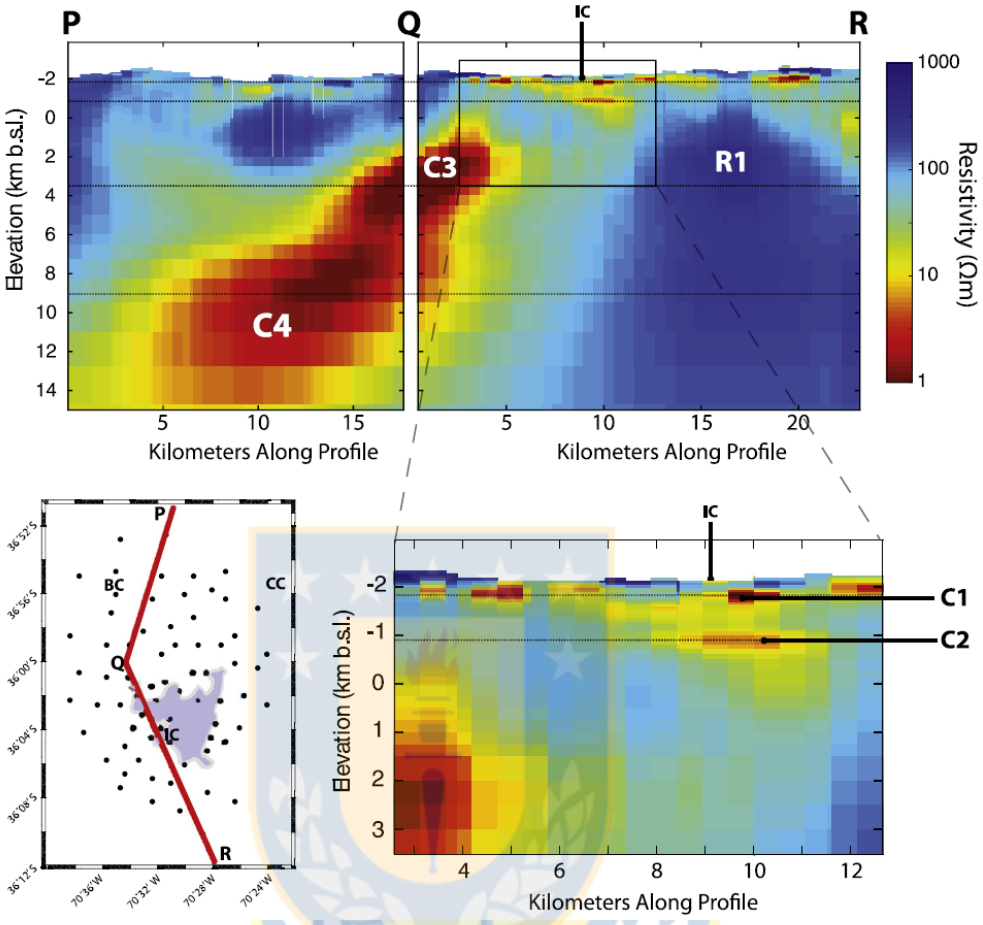

Figura 1.8 Modelo de resistividad eléctrica para el CVLM. Cortes transversales PQ y QR donde se muestra las cuatro zonas conductivas. Fuente: Cordell y otros (2018).

1.4.4 Estudios Petrológicos

Andersen y otros (2017, 2018) realizaron estudios petrocronológicos e isotópicos de las erupciones ocurridas durante el Holoceno, encontrando

que durante este periodo aproximadamente 40 km^3 de riolítas fueron eruptadas efusiva y explosivamente de al menos 24 centros de emisión, ocurriendo al menos 50 erupciones durante los últimos 26 Ka (Fig. 1.9). Las razones $^{238}U/^{230}Th$ de las lavas del CVLM están desacopladas de las características de fluidos provenientes del slab, el magma silícico es generado por hibridización y cristalización en la corteza superior. Los datos petrocronológicos muestran que las riolítas más nuevas, eruptadas durante los últimos 3200 años, residen en la corteza superior por únicamente décadas, seguidas por extracción desde un reservorio superficial. Ellos proponen como la acumulación de fluidos derivados de la desgasificación de un fundido máfico profundo es capaz de presurizar cuerpos de magma riolítico de baja densidad. Además, sugieren que la notoria ausencia de desgasificación superficial acompañando los síntomas recientes de actividad podría sugerir que los fluidos son atrapados en capas impermeables, lo cual podría catalizar una futura erupción explosiva.

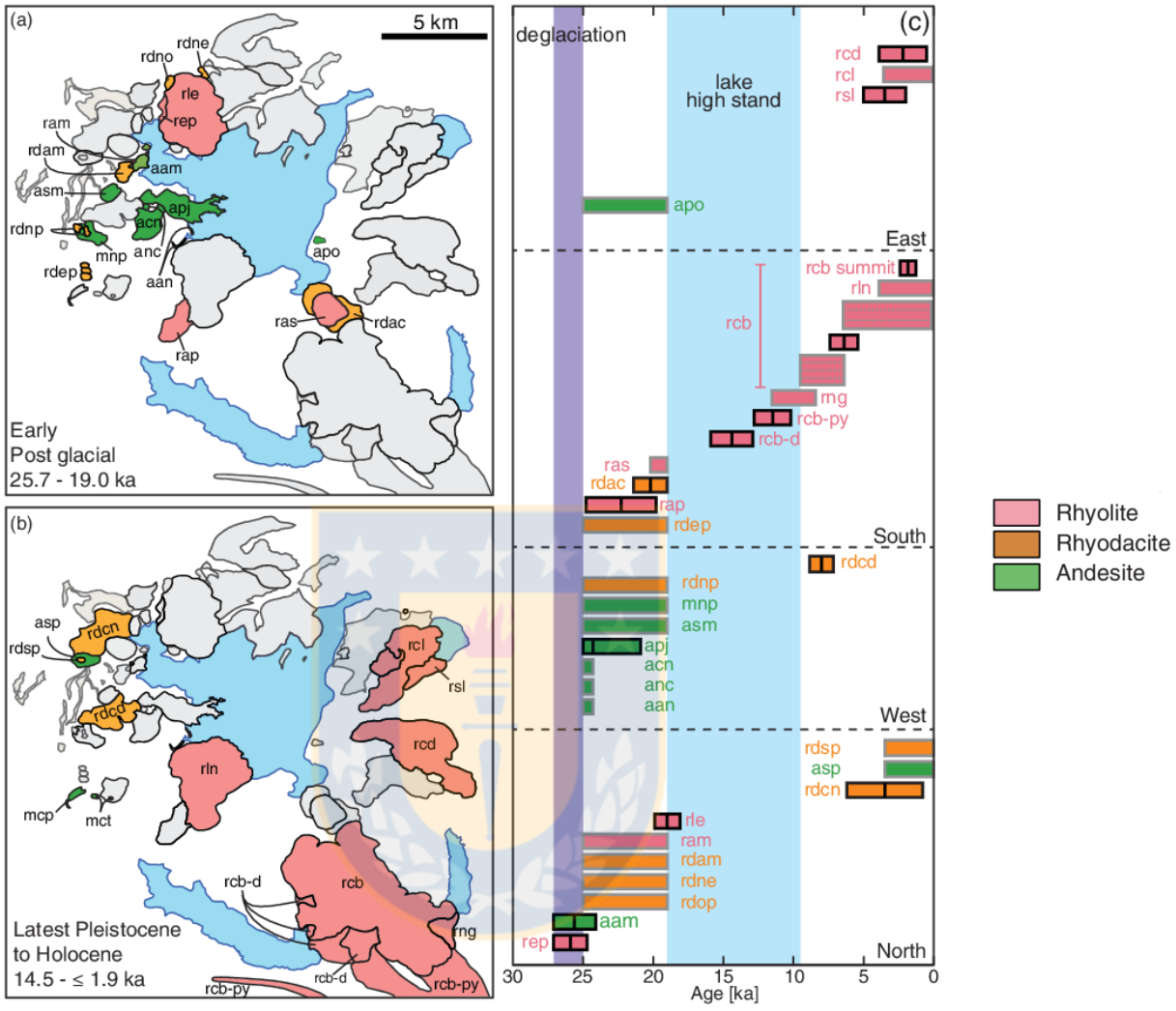

Figura 1.9 Secuencia eruptiva post glacial de las lavas de la cuenca central del CVLM. Las composiciones de las diferentes unidades son identificadas de acuerdo a colores: riolítas con color rosado, riodacítas con color anaranjado y andesitas con color verde. El gráfico (a) muestra las unidades del periodo Post-glacial tempano, el gráfico (b) las unidades del Pleistoceno tardío a Holoceno, y en el gráfico (c) se observa la evolución temporal de cada una de las unidades. Fuente: Andersen y otros (2017)

1.5 Planteamiento del trabajo de investigación e hipótesis

De acuerdo con los antecedentes geológicos previos, los resultados de estudios anteriores, los datos sísmicos y el campo de velocidad de deformación cortical registrados, se platean los siguientes interrogantes sobre la sismicidad y el estado actual del sistema del complejo volcánico Laguna del Maule:

- ¿Por qué en grandes procesos de deformación cortical volcánica como el caso del CVLM, se presentan enjambres sísmicos de baja magnitud?
- ¿Es posible determinar el nivel de acoplamiento de las fuentes de los diferentes fenómenos observados bajo la corteza del CVLM, existe alguna conexión entre las fuentes de deformación y los enjambres sísmicos?
- ¿Es posible determinar relaciones espaciales y temporales entre la sismicidad, el marco estructural donde está emplazado el sistema volcánico, la ubicación de los centros volcánicos Holocenos identificados y la fuente de alzamiento?

Con base en lo anterior, se plantea como hipótesis: **"La deformación activa del Complejo Volcánico Laguna del Maule transfiere esfuerzos a estructuras activas cercanas, incrementado la actividad sísmica de origen tectónico y volcánico de la región".** La resolución del interrogante proporcionará nuevos elementos sobre el comportamiento de complejos volcánicos riolíticos distribuidos durante fases pre-eruptivas y con potencialidad de acuerdo a los síntomas observados de evolucionar hacia crisis volcánicas.

1.6 Objetivos

1.6.1 Objetivo general:

- Obtener un modelo tridimensional del sistema magmático del CVLM y su relación con el contexto sismotectónico y geodinámico local y regional.

1.6.2 Objetivos específicos:

- Caracterizar las fuentes sísmicas del CVLM, determinando los fallamientos y centros volcánicos activos, y su conexión con el contexto sismotectónico y geodinámico local y regional.
- Definir la relación espacial y temporal entre: Fallamientos activos – Deformación cortical – Sismicidad – Sistemas volcánicos.
- Determinar un modelo conceptual del sistema volcánico del CVLM, basado en el modelamiento de datos sismológicos y su relación con datos provenientes de otras metodologías.

1.7 Datos y metodología

1.7.1 Red de estaciones

En Abril de 2011 el OVDAS desplegó una red sísmica portátil compuesta por cinco (5) estaciones sísmicas de banda ancha, con el propósito de conocer el nivel de actividad interna del CVLM. Posteriormente, en el año 2012 la red fue mejorada instalando la telemetría de las estaciones previamente instaladas, adicionando una (1) nueva estación sísmica e instalando cinco (5) GPS. Durante el año 2014, OVDAS

despliega cinco (5) estaciones sísmicas portátiles adicionales, que operaron en el CVLM entre los años 2014 – 2017. Finalmente, como parte de un proyecto NSF liderado por la universidad de Wisconsin, y en el cual agencias y universidades de USA, Chile, Canadá y Argentina participaron, se desplegaron 38 estaciones sísmicas temporales adicionales, alcanzado un total de 49 estaciones sísmicas y cinco 5 GPS desplegadas alrededor del CVLM, que adquirieron datos entre los años 2011 - 2017 (Fig. 1.10).

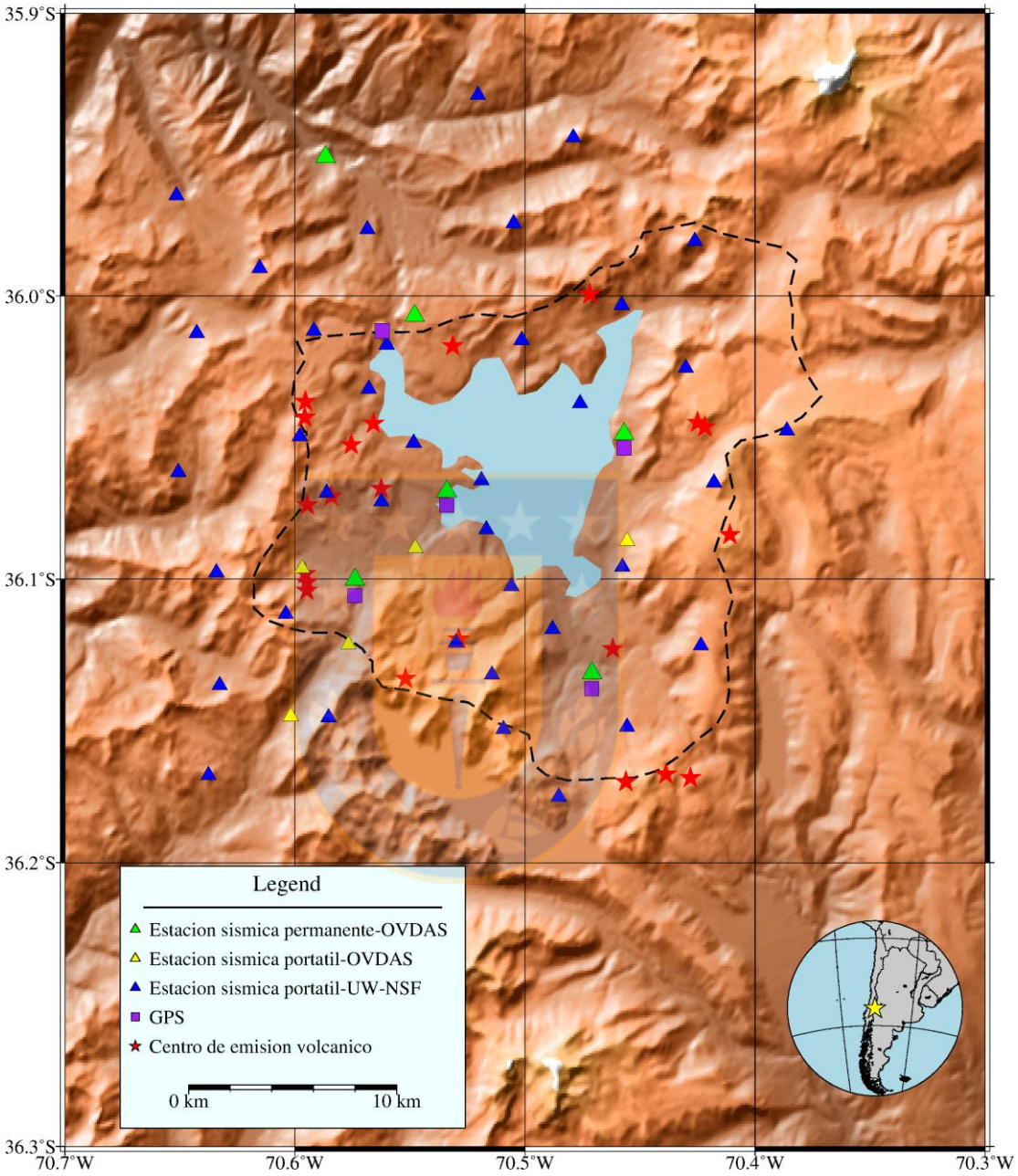

Figura 1.10 Red de estaciones del CVLM, compuesta por 49 estaciones sísmicas (permanentes y portátiles) y 5 estaciones GPS, la línea discontinua negra muestra el borde de la cuenca volcánica. Fuente: Elaboración propia.

1.7.2 Metodología de trabajo

Como se ha descrito anteriormente en la sección de objetivos, el propósito primordial de este trabajo de investigación es contribuir desde el punto de vista sismológico a la obtención de un modelo conceptual 3D del sistema magmático del CVLM y su relación con el marco sismotectónico y geodinámico local y regional, dividiendo el trabajo investigativo en tres objetivos específicos.

El primer objetivo específico tiene relación con la caracterización de la sismicidad volcánica registrada durante los años 2011 – 2016. En el proceso de caracterización fueron examinados manualmente los registros sísmicos de la base datos del OVDAS, clasificando los eventos sísmicos identificados de acuerdo a los criterios propuestos por Lahr y otros (1994) y Chouet (2003), con el fin de construir líneas temporales de ocurrencia diaria de los eventos sísmicos de origen volcánico. Posteriormente, a la base de datos de eventos sísmicos localizados por el OVDAS, se realizó un proceso de relocalización sísmica, debido a que el CVLM no contaba con un modelo local de velocidades, fue necesario obtener un nuevo modelo, utilizando las fases de entrada de las ondas P y S previamente leídas, dicho

proceso fue desarrollado usando el software VELEST (Kissling y otros, 1994) que restituye un modelo de velocidades 1D a partir de la comparación de los tiempos de viaje teóricos y observados. Una vez se obtuvo el modelo de velocidades del CVLM, se realizó un proceso de relocalización sísmica, usando los algoritmos JHD -Join Hypocenter Determination- (Crosson, 1976; Ellsworth, 1977; Thurber,1983) y hypoDD (Waldhauser, 2001), cuyo fin primordial es minimizar los errores en la horizontal y vertical de los epicentros e hipocentros obtenidos, y de este modo construir mapas de distribución espacial de eventos sísmicos, con un mayor nivel de confiabilidad, para que puedan ser confrontados con capas de información provenientes de otras metodologías, con el propósito de encontrar relaciones espaciales con las posibles estructuras productoras de la actividad sísmica observada. Otro aspecto desarrollado en la fase de caracterización de la sismicidad, fue la determinación de familias sísmicas mediante la correlación cruzada de las formas de onda de las señales sísmicas clasificadas, y a su vez la identificación de enjambres sísmicos, con el fin de poder determinar el número de fuentes sísmicas productoras de sismicidad, su ubicación espacial y la determinación de los periodos de tiempo en que dichas fuentes han sido activas. Una vez fueron determinados

el número de fuentes activas durante el periodo evaluado y los enjambres sísmicos fueron identificados, se procedió a realizar el cálculo de la energía sísmica de cada uno de los enjambres identificados, mediante la metodología propuesta por Boatwright(1980), y su vez para los eventos de mayor energía se obtuvo el mecanismo focal mediante la naturaleza del primer arribo de la onda P, usando el software FOCMEC (Snoke y otros, 1984) incluido dentro del programa SEISAN (versión 10.1). A continuación, una vez fueron obtenidas las características de las fuentes productoras de sismicidad, los resultados fueron integrados con un mapeo estructural de la zona de estudio, con el fin de sugerir las estructuras y posibles mecanismos que producen la sismicidad observada.

Para desarrollar el segundo objetivo cuyo propósito es determinar la relación espacial y temporal entre los fallamientos activos, la deformación cortical y la sismicidad observada. En una primera fase, con base en los resultados obtenidos de la caracterización de la fuente productora de los enjambres sísmicos observados, se realizaron series temporales de números de eventos diarios y energía sísmica liberada por cada enjambre sísmico. Además, para el mismo periodo de observación, fueron construidas líneas

temporales de velocidad de las estaciones GPS instaladas alrededor del CVLM, con el fin de separar fases donde fueron observados incrementos temporales de ocurrencia de enjambres y su energía sísmica relacionada, realizando una comparación con lapsos de tiempo donde fueron observados cambios en las tasas de alzamiento cortical, medidos por las estaciones de GPS. Como hipótesis inicial, se sugirió que el proceso de alzamiento podría afectar el campo de esfuerzos local del área, promoviendo la actividad en fallas vecinas. Para validar la hipótesis, un cálculo de esfuerzos tipo coulomb fue desarrollado, empleando el software Coulomb 3.3 (Toda y otros, 2005), el cual se basa en las ecuaciones desarrolladas por Okada (1992). Como estructura productora de esfuerzos fue asumida la geometría de la fuente de alzamiento sugerida por los trabajos de Fournier y otros (2010) y Feigl y otros (2014), y como estructuras receptoras los mecanismos de fuente obtenidos para las fallas donde fueron localizados los enjambres sísmicos identificados. Posteriormente, una vez fueron obtenidos los mapas de distribución de esfuerzos tipo coulomb, se realizó una comparación espacial con los mapas de densidad sísmica, calculados por km^2, para la sismicidad localizada entre los años 2011-2016, con el

propósito de identificar áreas donde confluyen anomalías positivas de cambios de esfuerzos y zonas con una mayor concentración de epicentros.

Finalmente, con el fin de contribuir a la obtención de un modelo conceptual del sistema magmático debajo del CVLM, los resultados obtenidos a través del modelamiento de los datos sismológicos, fueron integrados con los resultados provenientes de otras metodologías, principalmente estudios geodésicos, gravimétricos, magnetotelúricos y petrológicos, con el fin de proponer una configuración del sistema magmático.

La ampliación de los conceptos teóricos de cada una de las metodologías utilizadas puede ser encontrada en el marco metodológico incluido en los capítulos 2, 3 y 4 del presente trabajo de investigación.

1.8 Estructura de la Tesis

En el capítulo 1 de éste trabajo de investigación se describe el contexto tectónico y geológico regional que enmarca el Complejo Volcánico Laguna del Maule, donde destaca su ubicación en el trasarco

volcánico, como diversas calderas riolíticas Chilenas. Posteriormente, se realiza un levantamiento del estado del arte, sintetizando en primer lugar su geología local, que describe un amplio vulcanismo riolítico holocénico, donde se han definido más de 40 erupciones ocurridas en el Holoceno, desde 24 centros de emisión que rodean la laguna, siendo calculado cerca de 40 km^3 de material magmático emitido. Consecutivamente, se abordan los trabajos recientemente realizados sobre la dinámica actual del CVLM, involucrando diversas metodologías (InSAR, deformación, gravimetría, magnetotelúrica, petrocronología y sísmica) que modelan una serie de procesos corticales que han sido gatillados por la intrusión reciente de magma a niveles someros, destacándose un proceso inflacionario de una cámara magmática superficial que ha inducido un proceso de alzamiento superficial, cambios de masa observados por medidas microgravimétricas y sismicidad superficial.

El capítulo 2 incluye el artículo científico denominado "Crustal seismicity associated to rapid surface uplift at Laguna del Maule Volcanic Complex, Southern Volcanic Zone of the Andes", el cual aborda la descripción de la sismicidad cortical asociada con el CVLM, y la

caracterización de las señales sísmicas volcánicas observadas entre los años 2011 y 2014, incluyendo la construcción de las series temporales diarias de las señales sísmicas volcánicas clasificadas, la relocalización de eventos, cálculo de energía sísmica, determinación de un modelo local de velocidades y el cálculo de mecanismos focales. Como aspecto destacable fue la observación de enjambres sísmicos de eventos volcano-tectónicos registrados cíclicamente, lo cual acompaña temporalmente el proceso inflacionario observado. A los episodios de enjambres sísmicos se les realizó un tratamiento especial, detallando su evolución espacio-temporal y agrupándolos en familias sísmicas. Los resultados de la caracterización de la sismicidad observada fueron integrados con las observaciones estructurales levantadas en campo, siendo definidas esencialmente dos estructuras activas ubicadas al SW de la cuenca volcánica como las principales fuentes productoras de la sismicidad. Finalmente, se propone un modelo conceptual 3D para el sistema magmático del CVLM, que reúne los resultados de nuestro trabajo y los artículos científicos recientemente publicados.

En el capítulo 3 se muestra el artículo científico “Repetitive volcano seismic swarms triggered by static stress transfer from sustained volcano deformation: The example of Laguna del Maule Volcanic Complex”, cuyo objetivo primordial es explorar el nivel de acoplamiento existente entre las fuentes productoras de sismicidad y el proceso de levantamiento cortical activo. Para éste propósito se caracterizó la sismicidad volcano-tectónica ocurrida en el CVLM entre los años 2011 y 2016, y se construyeron las series temporales de velocidades de desplazamiento diarias para cinco estaciones GPS instaladas alrededor del complejo para el mismo periodo de tiempo. En primera instancia se realizó una comparación de la evolución temporal de la sismicidad y el proceso inflacionario, destacando fases de incrementos y decrementos de las tasas de alzamiento, que podrían corresponder con periodos cuando un menor/mayor número de enjambres sísmicos fueron registrados. Posteriormente, se realiza un modelamiento de esfuerzos tipo “Coulomb” asumiendo como fuente productora de esfuerzos un sill ubicado a 5 km de profundidad, geometría sugerida por estudios InSAR, y estructuras receptoras fallas strike-slip de componente dextral, fuente sugerida como la principal estructura productora de los enjambres sísmicos. Finalmente, se realiza un mapeo de los valores obtenidos de

cambios de esfuerzos y se comparan con el mapa de densidad sísmica del CVLM, encontrando que zonas de carga de esfuerzos correlacionan espacialmente muy bien con la zona de más alta densidad sísmica del CVLM y donde fueron localizados los enjambres sísmicos registrados.

Finalmente, en el capítulo 4, se detallan las principales conclusiones de este trabajo de investigación, explorando y fundamentando los posibles mecanismos productores de la sismicidad observada y la conexión de nuestros resultados con los hallados por investigaciones recientes realizadas en el CVLM.

CAPITULO 2: Crustal seismicity associated to rapid surface uplift at Laguna del Maule Volcanic Complex, Southern Volcanic Zone of the Andes.

Paper published in Journal of Volcanology and Geothermal research,

https://doi.org/10.1016/j.jvolgeores.2018.01.009

Carlos Cardona[1,3], Andrés Tassara[2,3], Fernando Gil Cruz[1], Luis Lara[1], Sergio Morales[1], Paulina Kohler[2] and Luis Franco[1,3]

1 Observatorio Volcanológico Chileno, Servicio Nacional de Geología y Minería. Rudecindo Ortega 03850, Temuco, Chile.

2 Departamento de Ciencias de la Tierra, Universidad de Concepción, Victor Lamas 1290, Concepción, Chile.

3 Programa de Doctorado en Ciencias Geológicas, Universidad de Concepción, Victor Lamas 1290, Concepción, Chile.

2.1 Resumen

El Complejo Volcánico Laguna del Maule (CVLM, Andes del Sur de Chile) ha experimentado altas tasas (aprox. 30 cm/año) de levantamiento superficial, detectado desde el 2008 a través de medidas geodésicas satelitales. Trabajos anteriores han modelado la fuente de ésta deformación como un sill rectangular subhorizontal inflándose, localizado a 5 km de profundidad, el cual supuestamente está relacionado con un proceso activo de rellenado magmático de un reservorio silícico superficial. Sin embargo, poco es conocido sobre el contexto tectónico en el cual esta actividad está tomando lugar, particularmente en relación con la sismicidad cortical que podría ayudar al entendimiento y monitoreo del actual proceso de deformación. Nosotros presentamos la primera caracterización detallada de la actividad sísmica del CVLM y lo integramos con datos estructurales adquiridos en el campo, con el propósito de dilucidar la posible conexión entre el proceso de alzamiento vertical en progreso y la activación de fallas corticales. Nuestro principal descubrimiento es el reconocimiento de enjambres sísmicos volcano-tectónicos repetitivos (VT) que ocurren periódicamente entre el 2011 y 2017 cerca de la esquina SW del sill modelado por los estudios InSAR. Un análisis de correlación cruzada de

formas de onda para los eventos VT permitió identificar tres diferentes familias sísmicas. Las familias F1 y F3 comparten algunas características comunes de su forma de onda apilada y su localización, lo cual marcadamente difiere de aquellos eventos de la familia F2. Enjambres pertenecientes a esta última familia son más energéticos y su energía fue incrementando desde el año 2011 hasta un pico en el año 2013, el cual coincide con la máxima velocidad vertical de deformación detectada por las estaciones GPS locales. Esto apunta hacia un proceso común relacionando ambos fenómenos. El área donde los enjambres de la familia F2 parecen ocurrir es caracterizada por la intersección de un lineamiento NE-SW con un lineamiento WNW-ESE. El primero es llamado la falla Troncoso y muestra evidencias claras de movimiento strike-slip dextral, que es completamente consistente con uno de los planos nodales de los mecanismos focales determinados para eventos de la familia F2, que fueron finamente localizados. El plano nodal conjugado de estos mecanismos focales podría coincidir con el lineamiento WNW-ESE (paralelo a la laguna la Fea), para el cual nuestro reconocimiento de campo sugiere un movimiento dominantemente normal. Los eventos pertenecientes a las familias F1y F3 están agrupados a lo largo de éste lineamiento, en dirección

W y hasta su intersección con la falla Troncoso, sus mecanismos focales son dominantemente strike–slip pero con alguna mezcla de componentes normales e inversas. Nuestros resultados sugieren una compleja interacción mecánica entre la fuente de inflación y el arreglo de fallas corticales que forman el marco estructural en el cual el sistema magmático del CVLM está emplazado.

2.2 Abstract

Laguna del Maule Volcanic Complex (LMVC, Southern Andes of Chile) has been experiencing large rates (ca. 30 cm/yr) of surface uplift as detected since 2008 by satellite geodetic measurements. Previous works have modeled the source of this deformation as an inflating rectangular sub-horizontal sill underlying LMVC at 5 km depth, which is supposedly related to an active process of magmatic replenishment of a shallow silicic reservoir. However little is known about the tectonic context on which this activity is taken place, particularly its relation with crustal seismicity that could help understanding and monitoring the current deformation process. Here we present the first detailed characterization of the seismic activity taking place at LMVC and integrate it with structural data acquired in the

field in order to illuminate the possible connection between the ongoing process of surface uplift and the activation of crustal faults. Our main finding is the recognition of repetitive volcano-tectonic (VT) seismic swarms that occur periodically between 2011 and 2014 near the SW corner of the sill modeled by InSAR studies. A cross-correlation analysis of the waveforms recorded for these VT events allows identifying three different seismic families. Families F1 and F3 share some common features in the stacked waveform and its locations, which markedly differ from those of family F2. Swarms belonging to this latter family are more energetic and its energy was increasing since 2011 to a pick in January 2013, which coincide with maximum vertical velocities detected by local GPS stations. This point to a common process relating both phenomena. The area where F2 swarms seems to occur is characterized by the intersection of a NE-SW lineament with a WNW-ESE lineament. The former is called Troncoso fault and shows clear field evidences of dextral strike-slip that are fully consistent with one nodal plane of focal mechanism for well-recorded F2 events. The conjugate nodal plane of these focal mechanisms could coincide with the WNW-ESE lineament (parallel to Laguna Fea lake), for which our field reconnaissance suggests a dominant normal motion. Events belonging to

families F1 and F3 are clustered along this latter lineament westward to its intersection with the Troncoso fault and their focal mechanism are also dominantly strike-slip but with some mixture with thrust and normal components. Our results suggest a complex mechanical interaction between the inflating source and the arrangement of crustal faults forming the structural framework on which the magmatic plumbing system of LMVC is emplaced.

Keywords: Rhyolitic volcano system, large-scale deformation, repetitive seismic swarms, cross correlation wave form.

2.3 Introduction

Laguna del Maule Volcanic Complex (LMVC; Fig. 2.1) has a potential to be one of the most hazardous active volcanic systems on Southern Andes volcanic zone (Singer et al., 2014) as suggested by the combination of an impressively large volume of Holocene silicic volcanism (Hildreth et al., 2010; Anderson et al., 2017) and extreme rates of current surface uplift detected by satellite geodetic measurements (Fournier et al., 2010; Feigl et al., 2014; Singer et al., 2014; LeMevel et al., 2015 and 2016).

Preliminary work shown by Singer et al. (2014) indicates that this current deformation is related to active faulting at shallow depth. In this contribution we present the first detailed characterization of the seismic activity taking place at LMVC and integrate it with structural data acquired in the field in order to illuminate the ongoing process of surface uplift.

LMVC comprises 36 rhyolite and rhyodacite coulees and domes that erupted during the Holocene from 24 separated vents surrounding a 9x11 km lake (Fig. 2.1). These silicic products lies on top of more than one hundred pre-Holocene vents from which ca. 350 km3 of intermediate to acidic lavas and pyroclastic rocks were erupted since 1.5 Ma (Hildreth, et. al, 2010; Singer et al., 2014). Part of this activity was related to episodes of caldera-forming eruptions (Hildreth, et. al, 2010), some of them likely occurring during the Holocene (Anderson et al., 2017). Although no historic eruptions are associated to LMVC, the described geological setting implies an important volcanic hazard for this region, which is amplified by the ongoing surface uplift episode that has been recognized using the Interferometric Satellite Aperture Radar (InSAR) method (Fournier et al., 2010; Feigl et al., 2014; Singer et al., 2014; LeMevel et al., 2015 and 2016).

An interferogram between 2003 and 2004 analyzed by Fournier et al. (2010) indicated no detectable deformation, but a clear inflation signal with maximum 18.5 cm/yr line of sight (LOS) deformation centered on the lake basin appears in an InSAR image for 2007-2008. These authors modeled this surface deformation as caused by a shallowly dipping rectangular sill located 5 km below the lake and opening at rates of 60 cm/yr. Interferograms analyzed by Feigl et al. (2014) indicated LOS deformation rates exceeding 28 cm/yr at the surface between 2007 and 2012, and confirmed the inflating sill at 5 km depth as the most likely deformation source. Further studies combining InSAR with local GPS data published by LeMevel et al. (2015) show that the uplift rate achieved its maximum just before the Mw8.8 February 2010 Maule great subduction earthquake and that this rate decreased again in January 2013 to stabilize around 20 cm/yr until at least mid 2014. Le Mevel et al. (2016) using analytical models of magma injection suggest that during the first two years (from 2007 to 2009) the injection pressure rise up to 11. 5 Mpa with a volume flow rate of 1.3 m3/s, decreasing to 0.7 m3/s in 2014 and at least during the last two the years the deformation rates have a tendency to decrease. Magnetotelluric and gravimetric data collected by Miller et al. (2016) detected a mass

change between 2013 and 2014, suggesting a magmatic melt located about 4 to 6 km below surface. This uplift rates are the highest ever recorded at a volcano that is not actively erupting (Singer et al., 2014).

Given the indirect evidences of volcanic unrest available by the end of 2010, the Observatorio Volcanologico de los Andes del Sur (OVDAS; the Chilean Volcano Observatory depending on the Geological Survey SERNAGEOMIN) decided to deploy seismic and continuous GPS instruments to monitor LMVC. This network started recording data in April 2011 confirming the extreme uplift rates and showing clear evidence of shallow seismic activity surrounding the inflating zone.

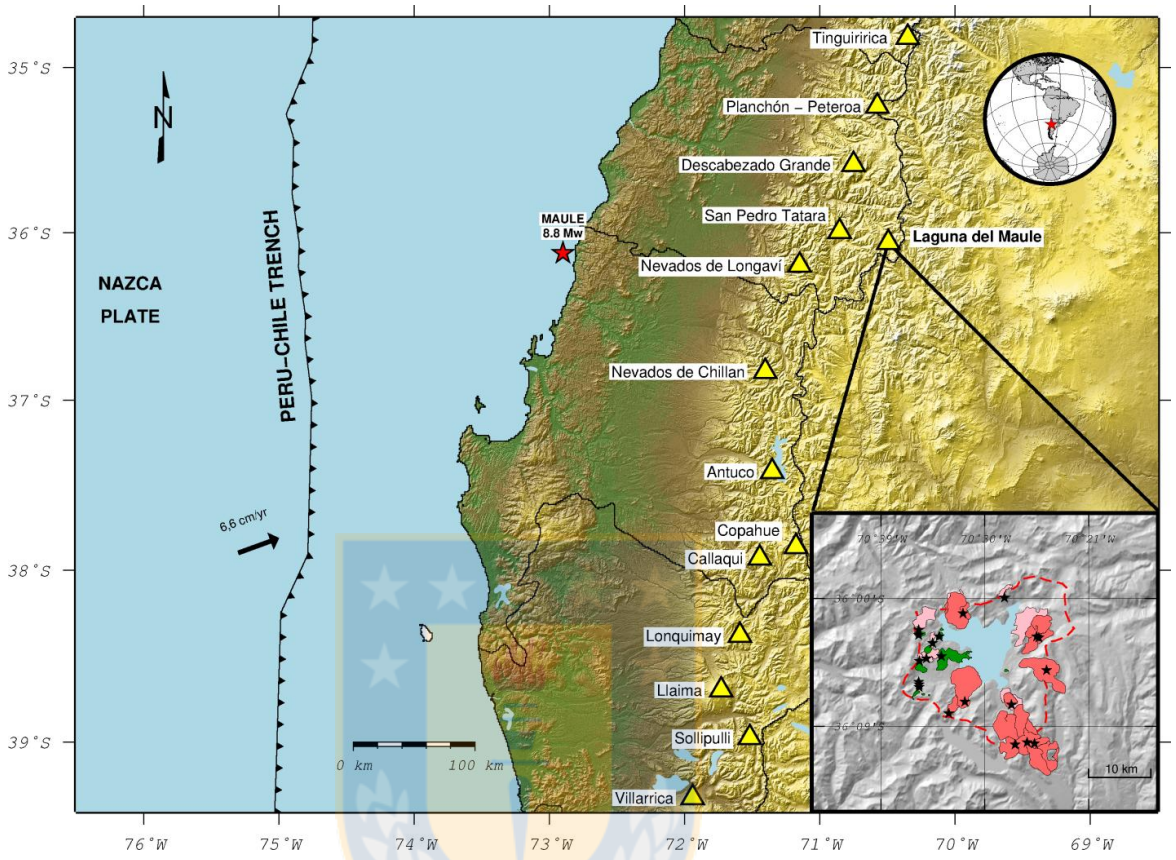

Figure 2.1 Tectonic setting of Laguna del Maule Volcanic Complex (LMVC). Shaded relief topographic image showing the location of the Southern Andes Volcanic zone with yellow triangles being volcanoes under surveillance by OVDAS, the epicenter of the Mw=8.8 27-Feb-2010 Maule earthquake (red star). Inset shows a simplified geological map (adapted from Hildreth et al., 2010) of LMVC, showing the 36 postglacial lava flows and domes (pink=rhyolites; light pink=rhyodacites; green=andesites) that are surrounding the volcanic complex, the black stars are the volcanic vents and the red discontinuous line represents the rim of the basin.

The goal of this contribution is to present the first systematic characterization of the seismic activity recorded by the local OVDAS network at LMVC between 2011 and 2014. After describing the network,

data and methods, we first show the different types of seismic events that can be recognized through a classification scheme. Then we describe the temporal evolution of these events, which allows recognizing the repetitive occurrence of seismic swarms at the SW extreme of the inflating source. We then show the spatial distribution of relocated seismicity along with the 1D seismic velocity model resulting from the relocation process. For seismicity occurring in the region of the swarms we present a cross correlation waveform analysis that allows the identification of different seismic families and the resulting focal mechanisms for a number of these well-located events. Finally we integrate these results with those derived from a structural mapping of the LMVC in order to establish a possible connection of the recorded seismicity with the current surface deformation.

2.4 Seismic Network, Data and Methods

During April 2011 OVDAS deployed a surveillance network composed by 5 portable 30 seconds Guralp broadband (BB) stations, installed around the volcanic complex at distances between 0 and 9 km from the center of the deforming zone. First seismic records showed clear evidence of shallow seismicity and therefore OVDAS installed a telemetric

communication system during austral summer 2012 in order to transmit data in real time to the observatory. During this field campaign 3 dual-frequency continuous GPS stations were also installed close to the deformation zone. A year later (February 2013) the network was improved with the installation of other 2 Guralp 30 seconds BB seismometers and 2 additional GPS stations. Between February and April 2014, a temporary seismic network composed by 5 portable Guralp BB stations was deployed in order to improve the azimuthally coverage and to obtain accurate seismic locations. The network is complemented with 10 additional 30 seconds and 120 seconds BB seismometers, installed previously on neighboring volcanoes. In summary (Fig. 2.2), between April 2011 and October 2014 a monitoring network composed by 21 BB stations and 5 dual-frequency continuous GPS stations was consolidated.

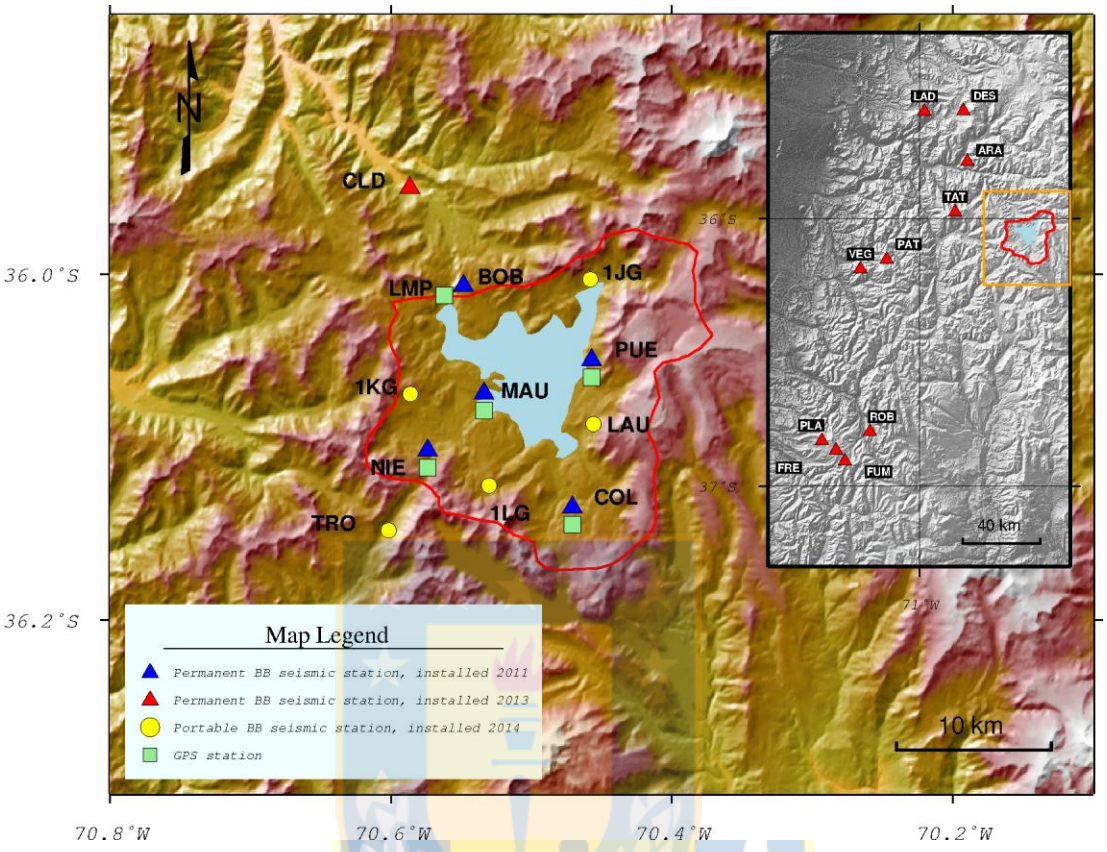

Figure 2.2 Distribution of seismic stations composing the LMVC seismic network used in this study. The main figure shows the 11 stations deployed inside the lake basin, whereas the inset shows locations of other 10 stations deployed by OVDAS on neighbors volcanoes. The red line shows the rim of the volcanic basin.

Here we consider continuous seismic records from April 2011 to October 2014 (~3.5 years). A first preliminary processing level over these data was applied as part of the routinely monitoring task at OVDAS. This

considers the manual recognition of individual events from the continuous seismic signal and extraction of basic information for each of them as amplitude, duration, energy, wave phases and preliminary seismic location. This preliminary processing recognized more than ~3200 volcanic seismic events of shallow depth (<8 km) related to the internal dynamic of LMVC. A second, post-processing level was implemented in this work with the aim to refine the location and characterization of the recognized seismicity. This includes following procedures:

2.4.1 Seismic events classification

The seismic signals related to each recognized event was classified following Lahr et al (1994) and Chouet (2003), which is based on the waveform appearance on the seismic records, as well as additional elements that help to discern about its seismic source. Thus, we established three main kinds of volcanic signals: volcano-tectonic events (VT) related to brittle fracturing of rocks induced by magmatic activity, long period events (LP) that suggest a genesis related to fluids movement or pressures changes of volcanic conduits, and tremor signals (TR) which origin are similar to LP

events, but with a sustained excitation through the time that can last by hours or days.

2.4.2 Seismic location methods and crust model determination

Using as a starting point a database of 1060 preliminary located events, we performed a relocation process using the Join Hypocenter Determination (JHD) algorithm (Crosson, 1976; Ellsworth, 1977; Thurber, 1983). For this, the local crustal velocity model was refined using VELEST (Kissling et al., 1994) considering only the 163 events having the best quality (gap <180°, ERH and ERZ > 2.0 Km). As initial model we used the 1D model proposed by Bohm et.al (2002) for the central part of Chile. Our model is divided in 20 horizontal layers of 1 km thickness. We divided the procedure into three phases: 1) we relocated the preliminary earthquakes, fixing the velocities distribution suggested by Bohm et. al (2002), and a new epicenter distribution was obtained, as well as the delays for each seismic station and the error of the solution. This procedure was done iteratively to reach the best solution with low error that better represented the P and S phases observed. 2) The epicenters were fixed and the velocity for each layer was varied iteratively in order to find the 1D crust model

velocity distribution with the lower error. 3) With the new 1D velocity model the hypoDD method (Waldhauser and Ellsworth, 2000) was applied to minimize the errors and improve the accuracy of the epicenter distribution.

2.4.3 Seismic swarms determination and cross-correlation analysis

Cross-correlation analysis is a method commonly used in seismological studies with the aim to determine the degree of similitude between waveforms of a seismic dataset (Poupinet et al., 1984). This allows recognizing seismic families or multiplets in a specific region, which makes possible an analysis of its recurrence, time progressions and spatial distributions. Correlation studies have been applied successfully to autodetect and classify seismic events, improving for instance locations of small magnitudes events (Shelly et. al 2013). Autodetection of events as based in waveform correlation has been specifically effective in cases where there is a high rate of events productivity in short lapse time, as seismic swarms (Shelly et. al 2007). As we show below, a series of seismic swarms can be recognized from seismic records of the LMVC zone. With the aim to evaluate the waveform similitude between each seismic swarm, a

cross-correlation analysis was done, searching to establish temporal variations of the waveforms included into each swarm episode. For this we isolate each seismic event and choose five seconds since the P wave time arrive, after a Butterworth bandpass filter (0.5-15Hz) was applied. The Cross Correlation Function (CCF) compares the seismic signal between pair of events, with CCF values between 0 and 1, being 1 the maximum similitude value. In our case, events with correlation coefficients higher than 0.7 were included into a same seismic family.

2.4.4 Seismic energy

We computed the seismic energy for each seismic swarm with the aim to provide a meaningful physical magnitude for comparison between discrete seismic episodes. To compute seismic energy Et we used the approach proposed by Boatwright (1980), assuming the media as an isotropic elastic homogeneous half space:

$$E_t = 2\pi\rho_s V_p d^2 \int A^2 \, \Delta_t$$

Where,

A = sum of seismic amplitude of the entire seismic swarm record.

ρS = solid density.

Vp = P wave velocity.

d = distance between seismic source to reference station

Δt = delta time of calculation.

For this analysis, we choose NIE as the reference station because it is the closest one to the swarm source (2 km from seismic swarm source).

2.4.5 Focal mechanism determination

To obtain the focal mechanism solutions we used the FOCMEC software packaged (Snoke et al., 1984) included into SEISAN program (10.1 version). This tool uses the first P wave polarities of a given set of stations, search all possible plane fault solutions that better represent the distribution of polarities into the focal sphere, search iteratively the strike, dip and rake for the two nodal planes that well separated the compressive and distensive polarities, assuming a pure double couple moment tensor. We selected those events with a well-constrained seismic location, at least 10 observations, and good azimuthal distribution of the stations. We only

allow two (over ten) polarity errors in order to guarantee a good constraint of the focal mechanism solution.

2.5 Results

2.5.1 Classification of Seismic Activity

We applied the classification criteria for volcanic events suggested by Lahr et al. (1994) and Chouet (2003) to continuous seismic records obtained during April 2011 and December 2014 at station NIE. From a total of 3218 preliminarily recognized events related with the dynamic of the volcanic system, 2568 of them were classified as volcano-tectonic (VT) events (80% of the total sample), 362 as long-period (LP) events (11% of the sample) and 279 as tremor pulses (9% of the sample). This shows a clear tendency of the volcanic system to generate seismicity related with the brittle fracturing of crustal material (Fig. 2.3).

A prominent aspect of the seismic activity detected at LMVC, which is notable in the daily number of recorded seismic events (Fig. 2.3), is the periodic occurrence (every 2 to 3 months in average) of swarms of VT events. We define a swarm as a group of more than 50 events occurring

during less than one hour. Using this criteria, swarm episodes are formed by a number between 63 to 300 seismic events of local magnitude between 0.1 and 2.2 occurring in restricted time spans of 25 to 180 minutes. Each of the 14 swarms recognized here are marked by vertical arrows in Fig. 2.3, whereas Table 2.1 presents some characteristic parameters for each episode.

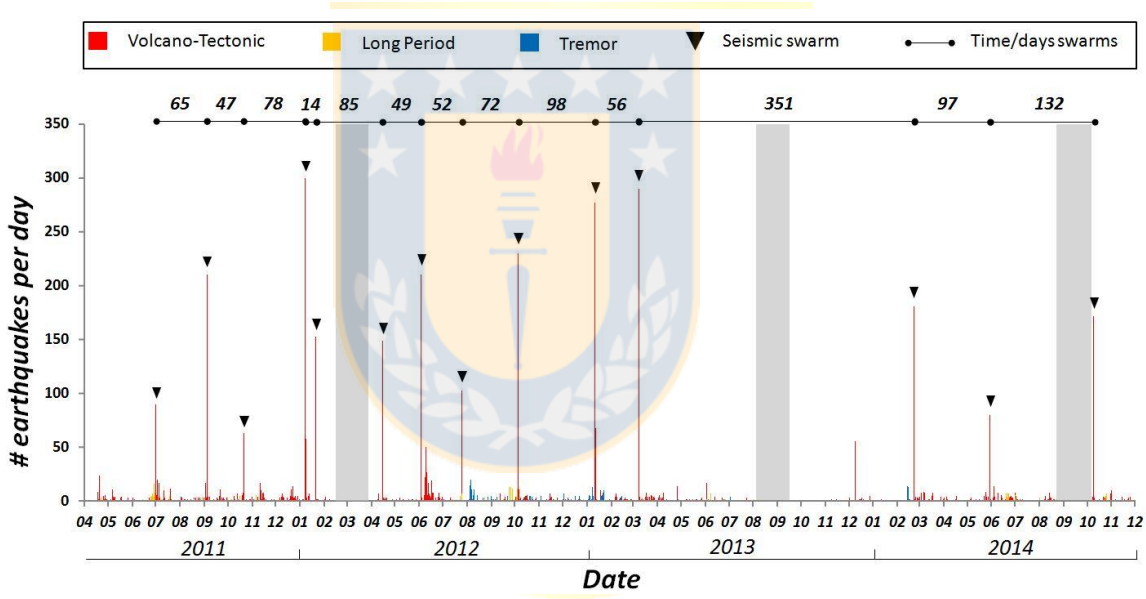

Figure 2.3 Temporal evolution of volcano seismicity as recorded at station NIE. Graph shows number of earthquakes per day for the entire study period, recognizing different types of events (volcano-tectonic in red, long period in yellow, and tremor in blue). Inverted black triangles denote occurrence of swarms of volcano-tectonic events. Numbers at the top of the figure shows amount of days between swarms. Grey bars indicate gaps in data record.

Table 2.1 Quantitative parameters of VT seismic swarms occurred in the LMVC.

Episode	Date dd-mm-yy	Number of Events	Duration (minutes)	ML Max	Energy (108 Joules)	Time between swarms (days)
1	01-Jul-11	90	25	1.2	0,9	-
2	04-Sep-11	210	90	1.9	2,7	65
3	21-Oct-11	63	160	1.5	0,6	47
4	07-Ene-12	300	167	1.8	13,4	78
5	21-Ene-12	153	180	1.4	1,1	14
6	15-Abr-12	149	70	1.7	5,9	85
7	03-Jun-12	210	160	2.2	68	49
8	25-Jul-12	103	55	1.2	0,6	52
9	05-Oct-12	230	180	1.7	13,9	72
10	11-Ene-13	277	180	1.9	155,7	98
11	08-Mar-13	290	150	1.7	2,3	56
12	22-Feb-14	181	170	0.9	0,5	351
13	30-May-14	80	30	1.0	0,8	97
14	09-Oct-14	172	100	2.1	4,2	132

The seismic activity related with the dynamics of fluids (LP and TR), shows a low level of occurrence compared with VT events, with average values of less than 1 event/day, low velocity amplitudes (0.5-2 um/s) and

reduced displacement lower than 2 cm2. It was possible to obtain the location of one relatively large (ML=1.3) LP event. This occurred in February 20th 2014 (2 days before swarm number 12) and recorded clear P-wave arrivals at 10 stations. The determined epicenter is located near of the SW vertex of the area suggested as the source of surface deformation by the InSAR studies (Fig. 2.5). Due to the low energy of the rest of the LP seismicity, locations could not been determined. However the distribution of amplitudes associate with these events in the stations where they are mostly observed (MAU and NIE) suggests that most of the LP seismicity is generated in the same area. The spectrums of this type of seismicity have frequencies between 1 to 5 Hz with a dominant peak around 3 Hz (Fig. 2.4). This frequency distribution was observed in all stations, suggesting that it correspond to sources frequencies. However, it was not possible to characterize this type of seismicity with a greater detail.

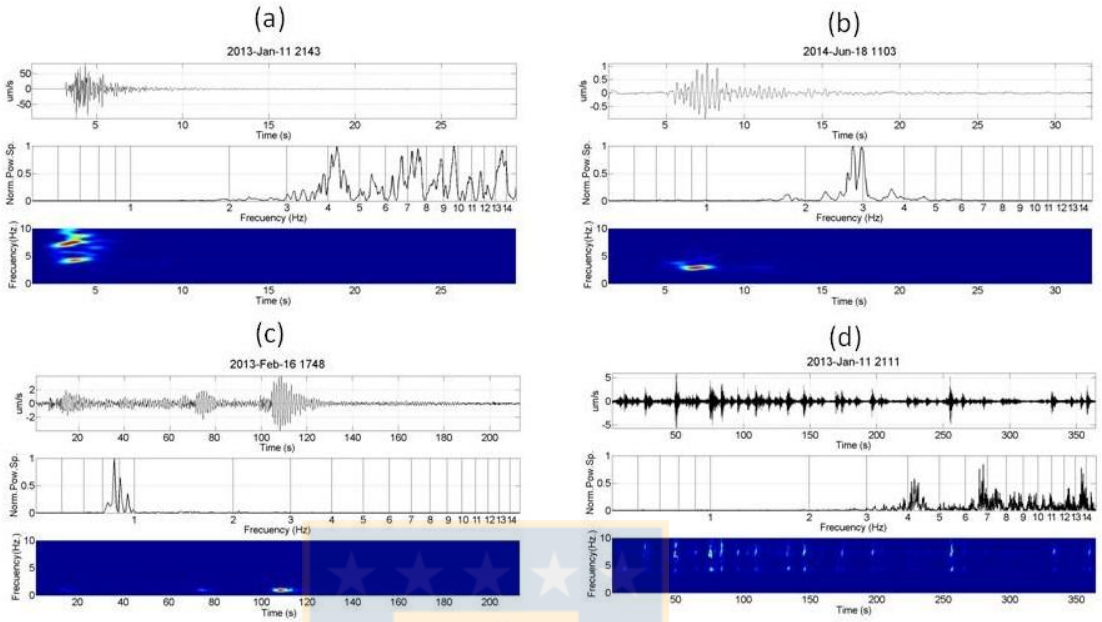

Figure 2.4 Examples of seismic records. For each subfigure we show the complete waveform (upper panel), frequency spectrum and spectrogram. a) typical volcano-tectonic (VT) event belonging to seismic swarms, b) long period (LP) event, c) tremor (TR), and d) portion of a VT seismic swarm. VT events like in a) present signals with frequencies between 1 to 20 Hz, while the LP and TR events present a narrow band with frequencies lower than 4 Hz.

2.5.2 1D Velocity model and seismicity relocation.

We use P- and S-phases readings of the preliminary located seismicity to derive a local 1D seismic velocity model with Velest (Kissling et al., 1994). Table 2.2 shows the obtained P-wave and S-wave velocity model and compared it against the regional velocity model of Bohm et al.

(2002), which was the starting model for the iterative inversion. We note that our model has smaller P-wave velocities than the regional model, mostly between 0 and 5 km depth where the difference is larger than 1 km/s (5.5 km/s for Bohm et al., 2002 compared to 4.4 km/s in our model). This difference is expected since the regional model was constructed for an area located 500 km southward of LMVC characterized by a crystalline plutonic basement of the volcanic arc that contrast with mostly volcano-sedimentary rocks forming the basement of LMVC.

Table 2.2 P and S velocity model and Vp/Vs ratio of 1D velocity model obtained in this work compared with the regional model of Bohm et al. (2002).

	This Work			**Bohm et al. (2002)**		
Depth (km)	***V_p (km/s)***	***V_s (km/s)***	***V_p/V_s***	***V_p (km/s)***	***V_s (km/s)***	***V_p/V_s***
-3	4,31	2,28	1,89	4,39	2,40	1,83
1	4,39	2,69	1,63	4,39	2,40	1,83
2	4,46	3,06	1,46	5,51	3,19	1,73
5	5,65	3,20	1,77	6,28	3,60	1,74
15	6,00	3,47	1,73	6,28	3,60	1,74
20 (fixed)	6,89	3,93	1,75	6,89	3,93	1,75
35 (fixed)	7,40	4,15	1,78	7,40	4,12	1,80
45 (fixed)	7,76	4,35	1,78	7,76	4,55	1,71
55 (fixed)	7,94	4,46	1,78	7,94	4,55	1,75
90 (fixed)	8,34	4,69	1,78	8,34	4,77	1,75

Based on this new velocity model, we applied JHD (Crosson, 1976; Ellsworth, 1977; Thurber, 1983) and HypoDD (Waldhauser and Ellsworth, 2000) to relocate the seismicity. Figure 2.5 shows the distribution of the epicenters, with seismicity concentrated in several clusters that can be associated with different possible sources. The first cluster is located in the western region of the studied area and is related to a relatively large (Mw=6.2) crustal earthquake occurred in June 6th 2012 and its aftershock sequence, composed by nearly 600 events. NEIC and GCMT catalogues reported a dextral strike-slip focal mechanism along a NNE fault plane, consistent with our own solution based on first P-wave motion at 17 stations. A NNE-oriented nodal plane is suggested by the alignment of aftershocks in this direction, coinciding with the orientation of regional structure that we call here Melado Fault (Fig. 2.5). Lupi and Miller (2014) suggest that this earthquake and its aftershocks could be related to static stress transfer from the Mw= 8.8 Maule 2010 earthquake toward a crustal fault.

The source area of the repetitive seismic swarms described in section 2.5.1 is located in the SW sector of the complex, with hypocenters fluctuating between 2 and 5 km depth. This area coincides with the SW vertex of the sill modeled as the source of InSAR-observed surface deformation (Fournier et al., 2010; Feigl et al., 2014; LeMevel et al., 2015), and match well with the zone along of the Troncoso fault where Miller et al. (2016) reported mass changes by microgravity measurements, during 2013 and 2004, calculating residual gravity changes of 124±12 µGal and an excess mass close to 9.2 $X10^{10}$kg. Furthermore, the area of the swarms corresponds to a notable structural intersection (as described below) and is characterized by the presence of centers of postglacial rhyolitic emissions (Hildreth et al., 2010). Similarly, a cluster of seismicity located in the SE extreme of the lake basin is closely related to one of the most active rhyolitic volcanic centers (called Barrancas by Hildreth et al., 2010), where Andersen et al. (2016) recognized at least 13 eruptive phases during the last 2.5 My.

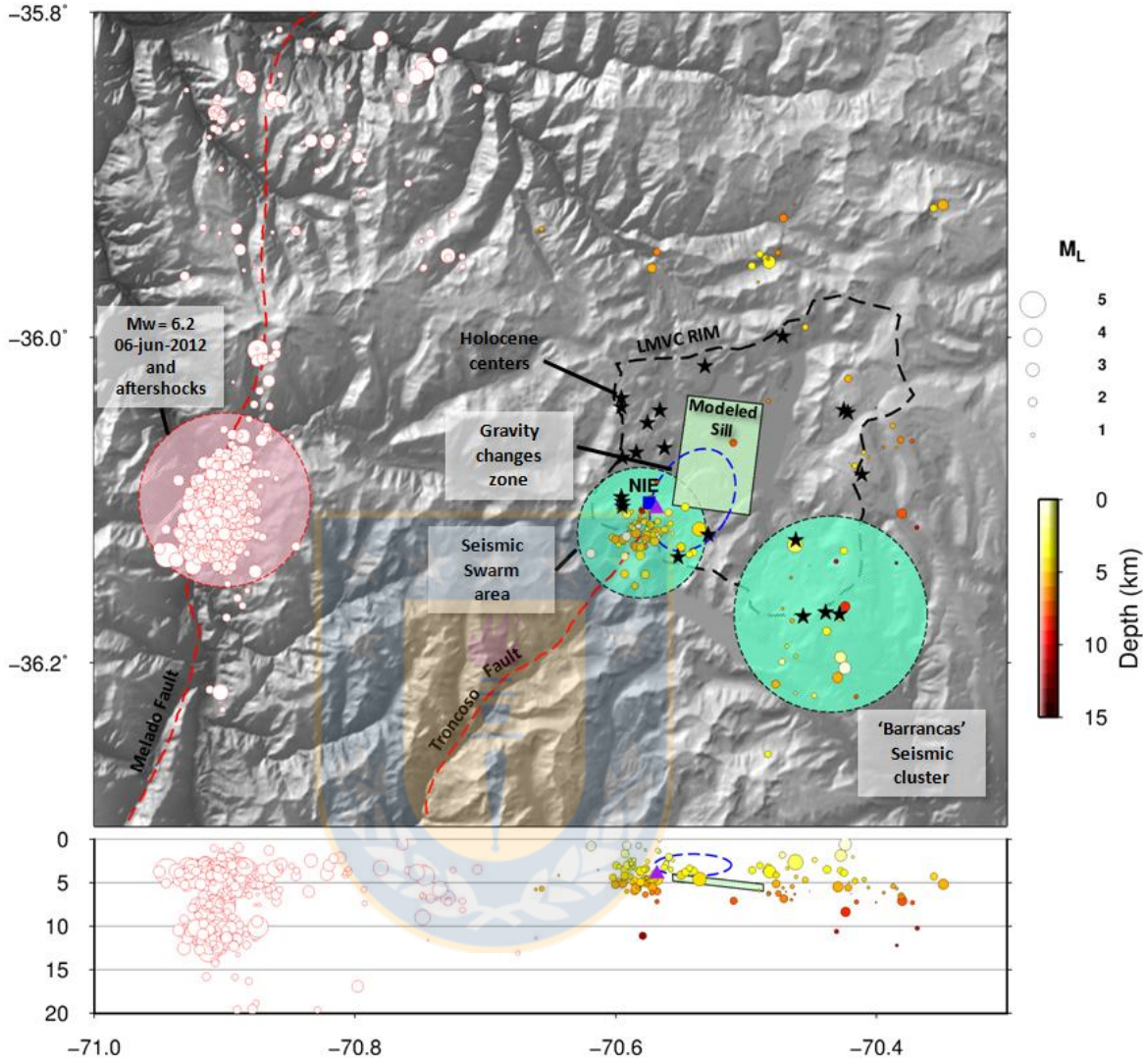

Figure 2.5 LMVC seismic location map between April 2011 and December 2014. LMVC volcano-tectonic events are color-code by depth and scaled by magnitude. Three clusters of seismic activity stand out. The pink circle marks the occurrence of a tectonic earthquake Mw=6.2 occurred in June 6th of 2012 and the sequence of ~600 aftershocks, tectonic earthquakes are represented by red circles without color bars. The green circles are two clusters of activity located at the border of the LMVC, which are situated near to some volcanic centers with recognized Holocene activity (black starts). The left-hand area is related to the occurrence of seismic swarms. The right-hand cluster is located close to one of the most active volcanic center called 'Barrancas'. The purple triangle on the seismic swarm area

shows the location of an energetic LP event. The blue square shows the reference seismic station 'NIE'. The green rectangle represent the sill modeled by InSAR and GPS data (Fournier et al. 2010 and Feigl et al. 2014) and the discontinuous blue ellipsoid shows the zone where Miller et. al (2016) reported an excess mass by microgravity measurements.

2.5.3 Cross correlation of VT swarms episodes

We performed a correlation waveforms analysis using cross correlation functions (CCF) that focused on seismicity related to the VT swarms at the SW region of the complex. We took those events with S-P arrival times less than 1.5 seconds at NIE reference station. Figure 2.6 shows the distribution matrix of cross correlation values obtained applying the CCF algorithm to the 450 events grouped in 14 swarms. This analysis allows us to recognize the level of similarity between events belonging to each swarm and between different swarms, being useful for the identification of families of swarms as characterized by a high level of correlation between them. The inspection of Fig. 2.6 suggests that 13 swarms can be grouped in 3 different families. Family F1 is composed by swarms E1, E8 and E13; family F2 is the most numerous and includes swarms E2, E4, E7, E9, E10 and E14; and family F3 with swarms E3, E5, E11 and E12. Swarm E6 has one of the strongest auto-similarity between

events belonging to the same swarm but shows very little similarity with the other 13 swarms grouped into the recognized families. A detailed inspection of Fig. 2.6 allows suggesting that E6 could be potentially related to family F2.

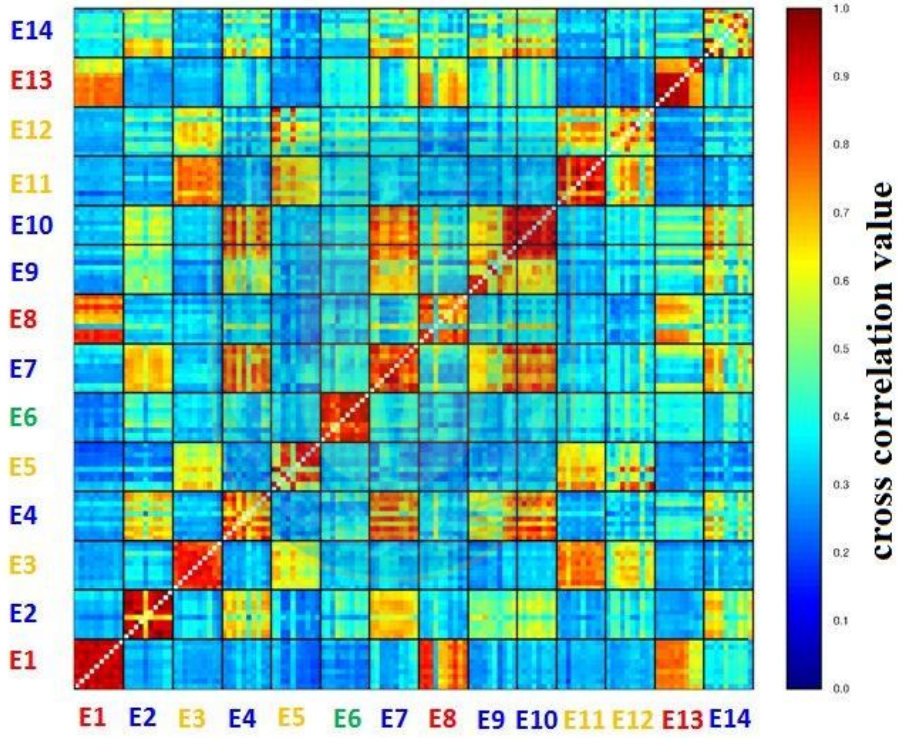

Figure 2.6 Matrix showing the correlation values computed for all events belonging to seismic swarms. Warm/cold colors represent high/low correlations values. The alphanumeric code below and at the left hand of the figure represent each one of the fourteen recognized seismic swarm episodes. The colors of the alphanumeric code represents families; red is for family 1 (F1) including swarms E1, E8 and E13; blue is for family 2 (F2) including E2, E4, E7, E9, E10 and E14); orange is for family 3 (F3)

including swarms E3, E5, E11 and E12; and green is for the isolated swarm episode E6.

We used the matched-filter technique to obtain the stacking of all the events included in each family by normalizing the amplitude and filtering the signals to a common reference (as used for instance at Villarica Volcano by Richardson and Waite, 2013). Figure 2.7 shows the stacked waveform for the three recognized families allowing a comparison of amplitude and phase for direct and coda waves of the seismic signals. This analysis shows that each family is characterized by a given temporary correspondence in scale of the amplitude and arrival time of the direct phases, mostly for the first 4 seconds after arrival of the P wave.

In addition, the comparison between the stacked waveform for each family shows differences on S-P values (less than 0.3 sec). Family 2 has the larger S-P of ~0.7 s, followed by Family 1 with S-P of ~0.5 s and Family 3 with S-P of ~0.4 s. These differences are explained by variation in the distance between the specific location of the source of each seismicity family and the references station NIE. In addition, we note that the stacked

waveform of families F1 and F3 are suggestively similar one to each other (mostly within 2 seconds after the arrival of the S wave) with much more high frequency energy than the one observed for family F2. These observations could indicate that F1 and F3 are rupturing relatively closer patches of the same fault with similar frictional properties, and that these notably differ from the properties of another fault being ruptured by family F2.

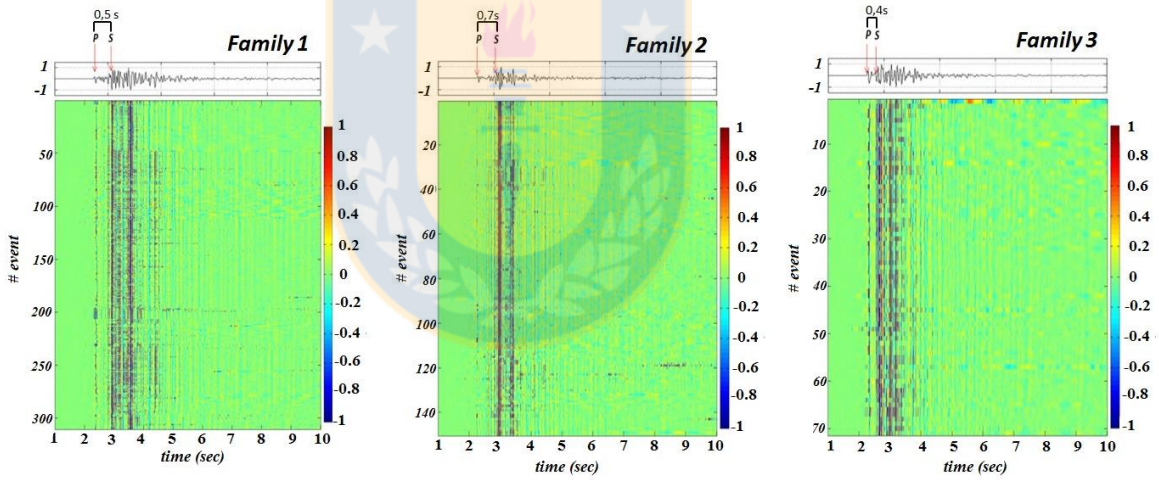

Figure 2.7 Stacking of volcano-tectonic events as grouped by the corresponding family. The stacked signals are for the vertical component at seismic station NIE. To apply the matched filter technique, the amplitudes of events were normalized between 1 (red) and -1 (blue) and a standard butterwort band pass filter was applied (0.5 – 12 Hz). Note the stability of the direct phase and the differences of the S-P values between families (shown at the top of each panel), suggesting differences in the location of the each family.

2.5.4 Temporal evolution of swarms

We analyze now how the recognized seismic swarms evolved in time. Figure 2.8 shows the number of events composing each swarm, duration of the swarm, maximum local magnitude (from Table 2.1) and total seismic energy (computed as explained in section 2.4.4). We first note that all these parameters are roughly correlated one to each other (with the exception of the duration for the first 5 swarms), and then we concentrate in describing temporal variations of calculated energy, which should be more clearly related with the physical phenomena behind these swarms. We recognized that our study period began 4 years after uplifting process started; consequently we present here only a snapshot of 4 year of the seismic behavior of the volcano system.

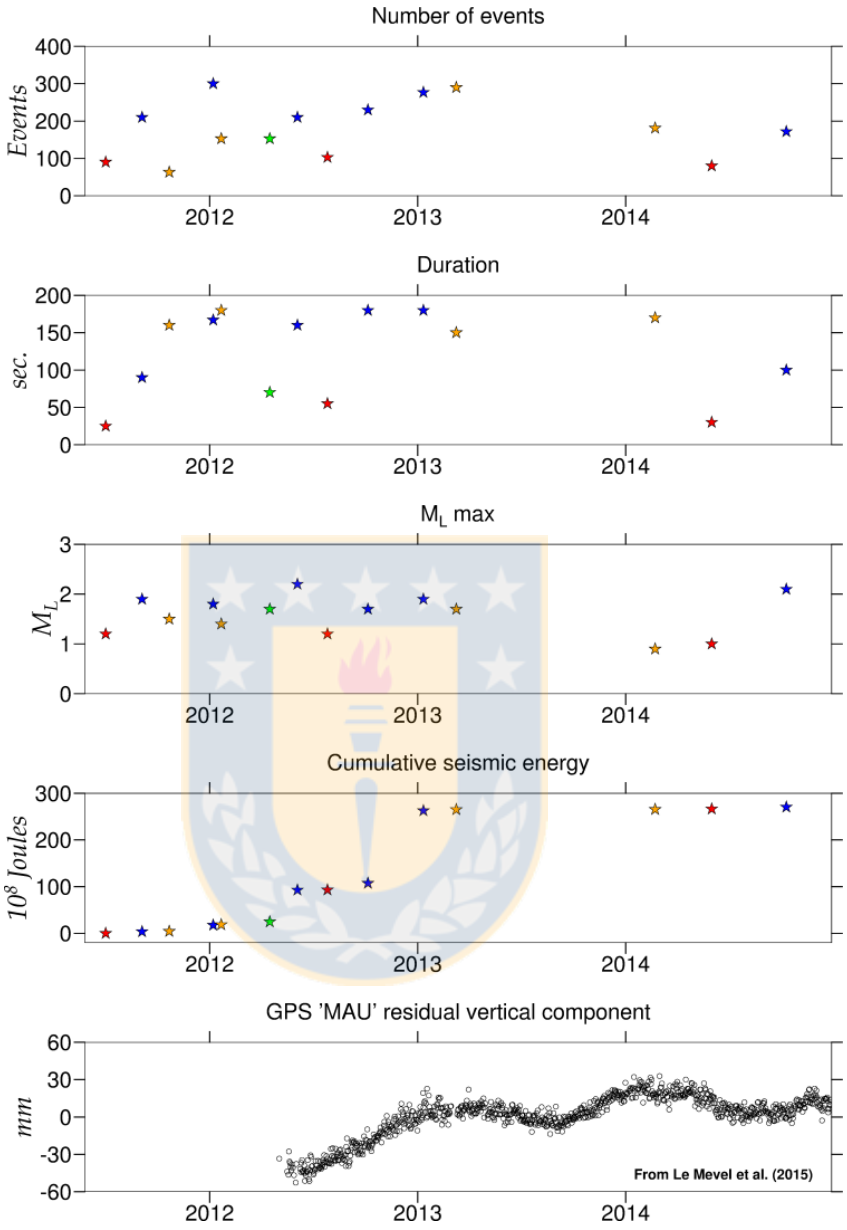

Figure 2.8 Temporal evolution of VT swarm´s parameters during the study period. Colors for each swarm represent families as in figure 6. The X axis format is 'month-year'. Family F2 (blue points) contains the most energetic seismic swarms. The grahs below shows the variation of deformation rates from 2012 to 2014 extracted from the Le Mevel et.al (2015), note that during April 2012 and January 2013 when the deformation rates were increasing the cumulative energy rise due to the most energetic swarm episodes were recorded.

We note that the energy of the swarms sequence as a whole (i.e. independent of its family) was gradually increasing from relatively low values in July 2011 to a maximum in January 2013 (swarm E10). After this, the next swarm was notably less energetic and afterwards no swarms were recorded for nearly a year (although a gap in data recorded by the seismic network between August and September 2013 could perhaps masks another swarm?). In February 2014, a low-energy swarm (E12) marked a re-start of swarm activity, which continued with other two swarms during this year with smoothly increasing energies.

The evolution of the cumulative energy with time is interestingly related with a more or less clear shift in the activity of the three recognized seismic families. The episodes related to swarm included into family 2, usually demark large increases of the cumulative energy. As each family is likely related to the repetitive rupture of an individual and isolated seismogenic fault patch, this observation suggests certain degree of mechanical interaction between these isolated patches, as discussed below. Also interesting is to note (Table 2.1 and Figure 2.8) that swarms belonging

to families F1 and F3 had always energies lower than $1.1x10^8$ joules (with the exception of swarm E11 of family F3 that occurred just after the maximum release of energy associated to swarm E10 in January 2013, see table 2.2). Swarms of family F2 were always more energetic than this threshold marking all the cumulative energy leaps in figure 2.8. The similar behavior of families F1 and F3 in terms of released energy and their notable difference with family F2 is complementary to observations revealed by the cross-correlation analysis of section 2.5.3. A phase to remark occurred between April 2012 and January 2013, at this time the cumulative energy has the larger leap observed that temporally match with a period reported by Le Mevel et al. (2015) where the deformation rates were increasing (see Fig 2.8.). Additionally, after this period Miller et al. (2016) reported mass changes by microgravity measurements, during 2013 and 2004, calculating residual gravity changes of 124±12.

2.5.5 Focal mechanism and field evidence for the source of the seismic swarms

The improvement of the seismic network in January 2014 occurred mostly around the region where the swarms were previously detected (Fig. 2.2), with the aim of refining their location and to solve their focal mechanisms. During 2014, three swarms (one for each family) were recorded, allowing a better location of events than those registered before this year, and the computation of focal mechanisms by P-wave first motion method for several relatively large events. A total of seventeen focal mechanisms were solved and are shown in figure 2.9 along with their epicenter location. Three well-located events of swarm E14 (family F2) are grouped near the intersection of a clear SW-NE topographic lineament coinciding with Cajón de Troncoso valley and a more diffuse WNW-ESE lineament parallel to the orientation of Laguna Fea (Fig. 2.9). Focal mechanisms of this swarm are dominated by a strike-slip motion that is compatible with either dextral sense along a SW-NE structure or sinistral sense along the WNW-ESE lineament. By the other hand, events belonging to swarms E12 (family F3) and E13 (family F1) are clustered 2-3 km westward of the location of swarm E14 along the continuation of the

WNW-ESE lineament and at constant depth of 4-5 km. The three focal mechanisms obtained for events of swarm E13 are almost purely strike-slip with nodal planes rather similar to those computed for E14. Focal mechanisms for events of E12 (6 in total) show a more heterogeneous character both in its kinematics (mix of strike-slip, normal and reverse motion) and orientation of nodal planes, although with a dominance of directions similar to the other two swarms. Fig. 2.9 also shows other 3 events also located along the WNW-ESE lineament but toward the east of its intersection with the NE-SW Troncoso lineament. The epicenter of these events coincides with the emission vent of Las Nieblas rhyolitic flow, one of the most recent (<2 ka) postglacial eruptive products (Singer et al., 2014). Focal mechanisms of these quakes are similar to those of E14 and E12 but with a significant normal component along a NE-SW plane.

With the aim of exploring the structural character of topographic lineaments concentrating the activity of seismic swarms, we performed a field reconnaissance of the area surrounding the intersection of the Troncoso lineament with the WNW-ESE lineament (Fig. 2.10). Along the

southern prolongation of the former, the basement of the LMVC (volcano-clastic and intrusive rocks of Oligo-Miocene age) is affected by brittle faulting expressed as sub-horizontal striation parallel to the valley (Fig. 2.10D and 2.10E), which corroborates that Troncoso is not only a morphologic lineament but a real fault. Integrating structural measurements at observed fault planes along the Troncoso fault, we obtain a fault solution remarkable similar to the dominant focal mechanisms of swarms, i.e. almost pure strike-slip along a NE-SW plane of dextral motion or WNW-ESE plane of sinistral motion. We prefer the first alternative because of the regional orientation of the fault, and suggest that at least those events belonging to E14 are likely rupturing the northern prolongation of the Troncoso fault. However, these events do occur at the intersection of this fault with the WNW-ESE lineament, along which we found morphological evidence of normal faulting along a roughly EW plane (Fig. 2.10G) and subvertical striation at several fault planes (Fig. 2.10F). The integrated fault plane solution resulting from these structural data (Fig. 2.10C) shows a more heterogeneous deformation that is dominated by a normal motion along a WNW-ESE plane with a week component of strike-slip. Although the kinematics of this fault solution is only roughly compatible with

computed focal mechanisms, we think that events located near the vent of Las Nieblas flow and those of swarms E12 and E14 are likely related to this WNW-ESE structure, being less clear its relation with swarm E14.

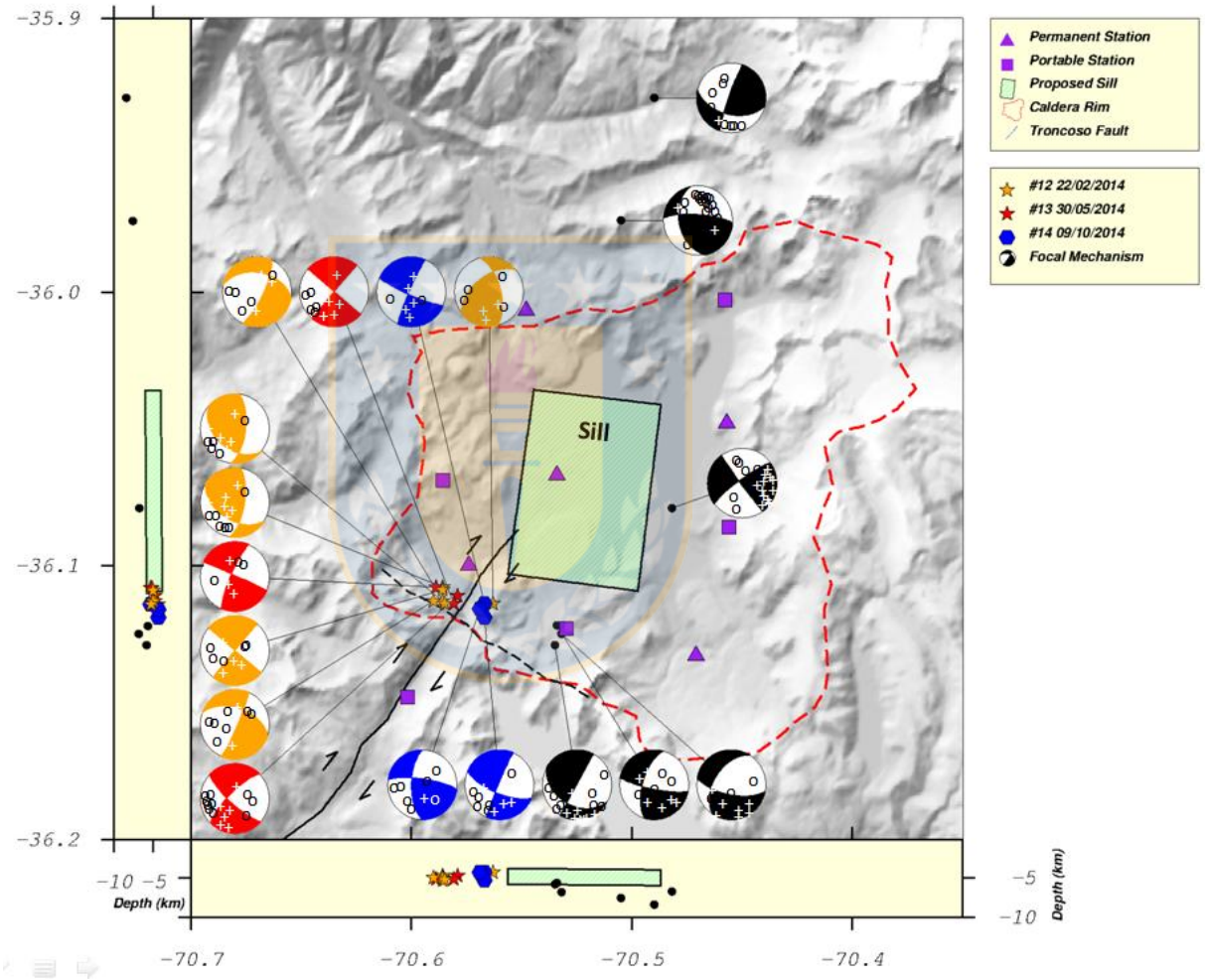

Figure 2.9 Focal mechanism and locations for 18 well-located VT events recorded by the full seismic network operative during 2014. Colors of events denote seismic families as in figure 6. Focal mechanisms show polarities with 'o' for distensive motion and '+' for compressive motion. The green rectangle represents the location of the sill modeled by InSAR studies.

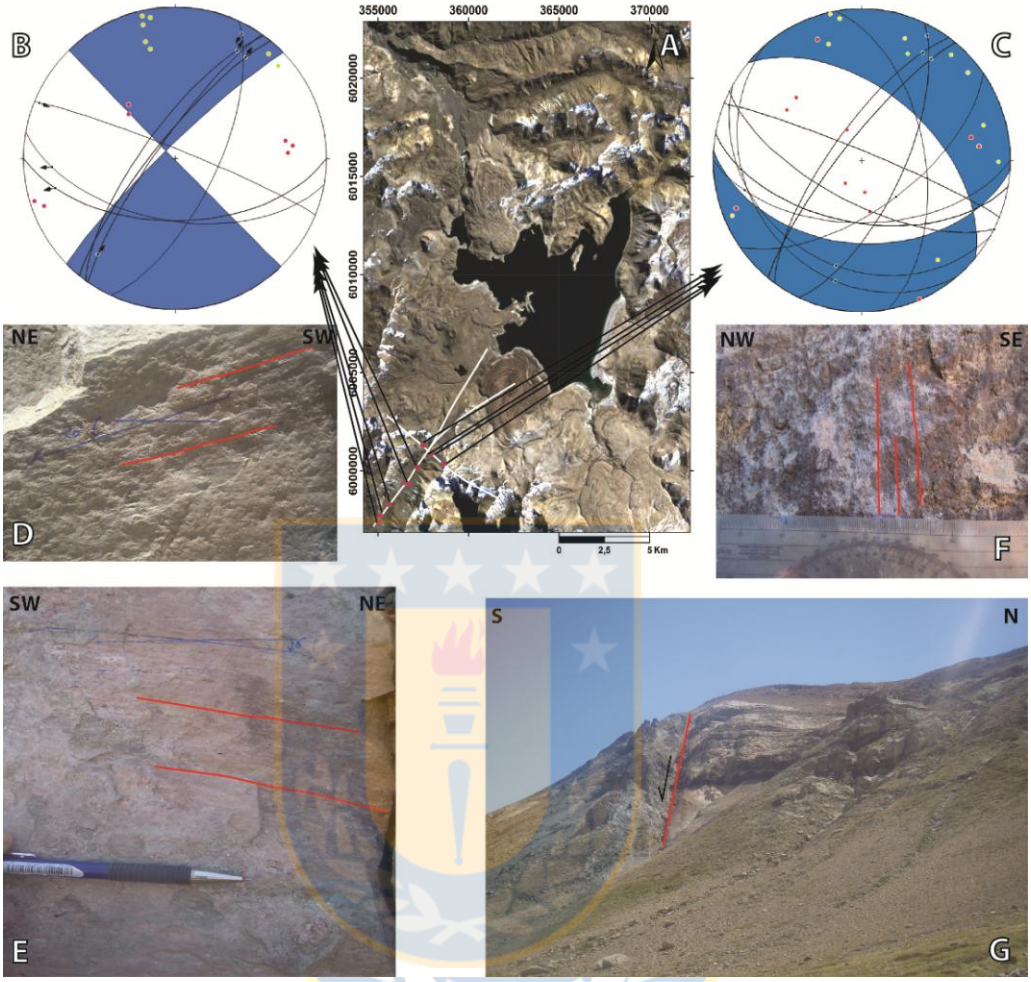

Figure 2.10 Field recognition of structures near the region of the VT seismic swarms. A) Satellite image of LMVC showing the location of structural observations (red points) and associated topographic lineaments (white lines). B) Strain diagram showing the best double-couple fault plane solution fitting data acquired at different sites along the NE-SW Troncoso Fault. C) Strain diagram showing the best double-couple fault plane solution fitting data acquired at different sites along the WNW-ESE lineament. D) and E) photographs of outcrops exhibiting evidences of sub-horizontal estriae at Troncoso fault evidencing dominant strike-slip motion. F) photograph of outcrop exhibiting evidence of sub-vertical estriae near WNW-ESE fault suggesting dominant vertical motion. G) photograph of the WNW-ESE lineament suggesting normal motion of the structure.

2.6 DISCUSSION AND CONCLUSION

The most prominent feature of crustal seismicity recognized by our study as accompanying the large inflation episode evidenced at LMVC by InSAR studies (Fournier et al., 2010; Feigl et al., 2014; LeMevel et al., 2016), is the existence of short (0.5 to 3 hours long) seismic swarms composed by tens to hundreds of small-magnitud (ML<2.2) quakes recurring every 2-3 months (in average) near the SW corner of the lake basin. The waveform correlation analysis that we applied to the recorded swarm seismicity allows recognizing three different seismic families which activity alternate over the 3.5 years period of this study (Fig. 2.6). Two of these families (F1 and F3, labeled with red and orange color, respectively in Fig. 2.7, Fig. 2.9 and Fig. 2.11) share some significant features, like certain similarity of their stacked waveform, their relatively low energy and their hypocentral location (for well-recorded events) along a WNW-ESE lineament showing field evidence of normal faulting, although computed focal mechanisms are more consistent with strike-slip motion of this fault (mostly for F3, see Fig. 2.9). Family F2 (labeled with blue color in Fig. 2.7, Fig. 2.9 and Fig. 2.11) by the other hand has a distinctive stacked waveform with larger S-P arrival times, larger integrated energy of the swarms and a

location at the intersection of the WNW-ESE lineament with the NE-SW Troncoso fault. Strike-slip focal mechanisms for F2 events are consistent either with sinistral motion along the WNW-ESE fault or dextral motion along the Troncoso fault (Fig. 2.9), which fits with the structural evidence recognized in the field (Fig. 2.10).

Into this context our main finding is to discover that the SW corner of the sill proposed as source of surface uplift by geodetic studies (Feigl et al., 2014, LeMevel et al., 2015 and 2016) roughly coincides with a seismically active structural intersection where a complex spatio-temporal interaction between both faults seems to be likely activated by the inflation of the proposed sill. We discuss here how these phenomena could be causatively connected.

Swarms of volcano-tectonic (VT) seismic events have been long described at siliceous volcanic complexes like Laguna del Maule. The pioneer work of Hill (1977) proposes that this type of repetitive seismic activity does occur in fault-controlled systems with a critical combination of

fluid injection into the faults and changes in the level of regional stress loading the fault system. Rapid deformation of the upper crust by the inflation of the magma reservoir below LMVC can transfer stresses to the structural framework of the volcanic system, as also proposed for other volcanic complexes (Karymsky Volcanic Group, Walter, 2007; Mt Etna, Feuillet et al., 2006; Cerro Negro, Díez et al., 2005). Into this model, the mechanical interaction between active shallow faults loaded by tectonic stresses and the inflationary source atop the magma reservoir promote the generation of crustal seismicity, eventually triggering the cyclic rupture of frictional asperities along different faults. The periodic alternation between swarms belonging to families F1 and F3 by one side and those of family F2 by the other (Fig. 2.8) suggests that certain degree of interaction does exist between the fault segment generating F1 and F3 along the WNW-ESE structure and the asperity associated with swarms of family F2 at the intersection of this fault with the Troncoso fault. It seems possible that the activity of a swarm in one fault can transfer stresses to the other fault, adding to those continuously loaded by the inflation of the magmatic source.

Assuming a constant rate of stress loading as driven by a constant rate of upper crustal inflation, the cyclicity of the swarms could be partially controlled by the rate of fault healing (Marone, 1998), i.e. the rate at which friction is reconstituted along the ruptured fault patch after each seismic swarm. Once the fault is healed, locking of the fault plane is re-established and the interseismic phase of strain buildup restarts around that patch. Into this model, the time step between swarms of the same family could give an indication of the efficiency of healing at each patch. However the rate of upper crustal inflation as observed by geodetic methods was not constant during the studied period, as shown by LeMevel et al. (2015, 2016). These authors noted a coincidence between the moment when the uplift rate recorded at GPS stations near the center of the inflation region starts decreasing in January 2013 and the occurrence of the largest seismic swarm. Our results confirm that this swarm, E10 belonging to family F2 (Fig. 2.8), was the most energetic of the entire sequence recorded between 2011 and 2014. Moreover, it seems apparent that before E10, the energy of F2 swarms was gradually increasing, whereas F1 and F3 swarms keep always at lower energies (see table 2.1 and Fig. 2.8). This suggests to us that the seismogenic asperity associated with F2 would be more strongly

coupled to the inflation source than those related to F1 and F3, which activity could be seen as a secondary response of the fault system to the primary mechanical interaction between the inflating sill and the fault intersection located close to its SW corner.

A complementary mechanism to explain the repetitive nature of seismic swarms (as also envisaged by Hill, 1977) is the possible interaction of the fault frame with a confined, highly-pressurized hydrothermal system. VT seismic swarms in other rhyolitic systems like Yellowstone and Long Valley (Shelly 2013; Massin, 2013) have been related with the episodic rupture of faults as it shear strength decreases once pore pressure reach a certain threshold due to the constant fluid injection at high pressure from a deeper hydrothermal reservoir. In this case, the occurrence of a seismic swarm breaks the hydraulic seal represented by the fault, allowing the release of fluids to shallower levels. This temporally lowers the fluid pressure inside the reservoir and at pores of the fault, increasing in this way the shear strength of the fault plane that can lock again sealing the hydraulic system once more and re-building elastic stresses. Since the hydrothermal

reservoir is still active, this starts building-up internal pressure again until the fault ruptures in a new swarm episode when this highly-pressurized fluid invades pores of the fault. This mechanism could be also applicable to swarms recorded in LMVC, moreover after considering that the region of the swarms (mostly for F2) coincides with the epicenter of the recognized LP activity (commonly associated with the movement of fluids). Supporting this idea, temporal gravity changes documented by Miller et al. (2017) have been interpreted as a consequence of hydrothermal fluids circulating in an arrange of NE-SW oriented faults modeled as elongated tabular prisms (Fig. 11) whose SW tip roughly coincides with location of seismic swarms.

Our field evidence of dextral strike-slip brittle faulting along the Troncoso fault coinciding with focal mechanisms of the energetic seismic family (F2) located at it trace, helps to constrain a regional structural model of the LMVC useful to understand the interaction of the deep source of surface deformation with the fault system. We schematize this model in Figure 2.11 summarizing all the relevant results that have been recently published for LMVC. We favor a structural model with Troncoso fault as

the western master fault of a SW-NE oriented dextral pull apart basin, as also suggested by Miller et al. (2016) based on the relation between the fault and location of a low density anomaly recognized from modeling gravity data. Similar models considering transtensional tectonic regimes associated with pull apart basins along strike-slip structural systems have been proposed for Central Andean Mio-Pliocene calderas (Riller et al., 2001), the Taupo volcanic zone (Spinks et al., 2005), large caldera systems in California including Long Valley (Riley et al., 2012) and Ilopango Caldera in Salvador (Saxby et al., 2016). We think that the base of such tectonically-controlled pull-apart basin can serve as the roof of the magmatic reservoir, as schematized in fig. 2.11. This scheme considers the structure proposed by Andersen et al. (2017) for the magmatic plumbing system under LMVC that integrated its temporal and geochemical evolution. This includes a large, long-lived crystal rich reservoir that is sporadically intruded by mafic recharge from the lower crust and develops internal mush zones of magma mingling, mixing and hybridization from which crystal-poor, rhyolitic eruptable magma can be extracted and cumulated in an upper holding zone. This latter zone in our scheme coincides with the base of the pull-apart basin and with the source region of

surface uplift. This model as applied to LMVC could allow to clarify the observed synchronicity between rapid surface uplift as produced by magmatic intrusion and/or hydrothermal pressurization at the base of the pull-apart basin with seismic activity of the master fault bounding the basin. Exploring this model requires a detailed correlation analysis of surface deformation and seismic activity aided by modeling stress transfer between different sources, something that we are facing for a future contribution.

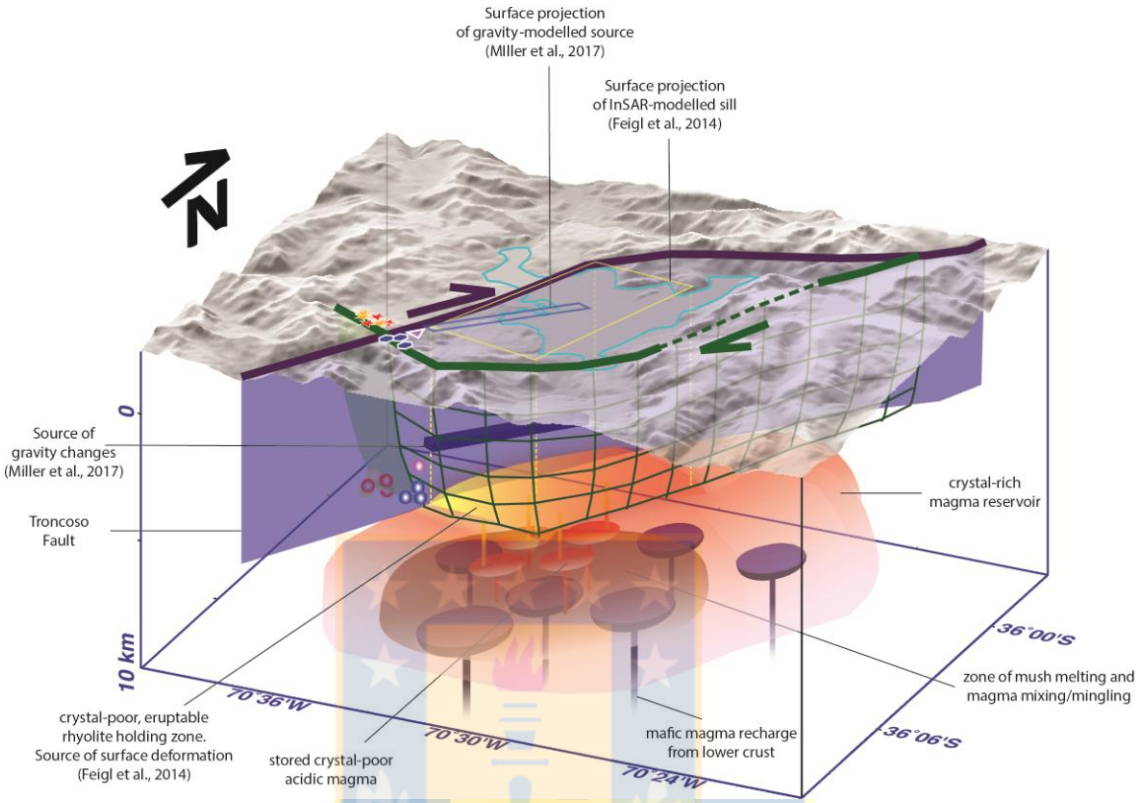

Figure 2.11 3D conceptual model explaining the relationship between crustal structure and magmatic plumbing system underneath Laguna del Maule Volcanic Complex. Hypocenter of seismic swarms recognized in our study are shown as spheres and their epicenters at the surface are marked with symbols and colors of seismic families as defined in figures 7 and 9. These seismic swarms are located at the intersection of Troncoso fault with an ENE-oriented lineament (family F2, blue) and along this latter lineament (families F1 and F3). Troncoso fault forms the western structural limit of a NE-SW oriented dextral pull-apart basin, at which base is located the sill modeled as the source of surface uplift imaged by InSAR (Feigl et al., 2014). This in turn coincides with the roof of an extensive magmatic reservoir (as imagined by Andersen et al., 2017) where crystal-poor eruptable rhyolitic magma is likely being cummulated. The scheme also includes the prismatic source of gravity changes proposed by Miller et al. (2017), which SW tip coincides with the SW corner of the inflating sill and roughly with the epicenter of an energetic LP event (purple triangle at the surface) above the hypocenters of F2 swarm.

2.7 Acknowledgements

This research has been partly partially funded by Observatorio Volcanologico de los Andes del Sur (OVDAS) belonging to Sernageomin (National Geological Survey), US NSF grant EAR-1322595 with Brad Singer (University of Wisconsin-Madison) as PI, and Chilean Fondecyt project 1151175 (Andres Tassara as PI). The Concepción University supports the first author providing a doctoral student grant. We would like to say thank to the OVDAS electronic team and specially the electronic engineer Christian Delgado to participate in the fieldwork seismological deployment and the regular service of the seismic stations, and the seismological team of OVDAS to support the authors performing the primary processing of the seismic data. Most figures were generated using GMT software by Wessel and Smith (1991).

CAPITULO 3: Repetitive volcano seismic swarms triggered by static stress transfer from sustained volcano deformation: the example of Laguna del Maule Volcanic Complex – Chile.

Submitted to Journal of Volcanology and Geothermal Research

Cardona, Carlos[1,2]; Tassara, Andrés[2]; Cordova, Loreto[1]; Delgado, Christian[1]; Franco, Luis[1,2]; Gil-Cruz, Fernando[1]; Morales, Sergio[1]; Basualto, Daniel[1,2];

[1] Observatorio Volcanológico Chileno, Servicio Nacional de Geología y Minería. Rudecindo Ortega 03850, Temuco, Chile.

[2] Universidad de Concepción, Departamento de Ciencias de la Tierra, Chile.

3.1 Resumen

Recientemente dos relevantes procesos geológicos activos han sido detectados en el Complejo Volcánico Laguna del Maule (CVLM): Un gran proceso de alzamiento vertical relacionado con la actividad de un cuerpo riolítico de magma localizado a 5 Km de profundidad, que produce una deformación cortical a tasas consideradas como una de las más altas medidas mundialmente en un volcán que no esté activamente en erupción, y enjambres sísmicos volcano-tectónicos cíclicos cuya localización coincide con un número de rasgos claves: Dos de los centros volcánicos más activos durante el holoceno; la intercepción del borde de la cuenca volcánica y una falla strike-slip activa; el vértice SW del sill modelado por estudios InSAR como fuente de la deformación; una zona donde estudios gravimétricos sugieren un cambio de masa debido a la reciente inyección de magma. Nosotros presentamos un estudio que involucra observaciones sísmicas y GPS para mostrar como las fuentes de ambos procesos podrían estar conectadas. Parece existir una conexión temporal entre ambos procesos, ya que periodos de incrementos/decrementos de las tasas de alzamiento podrían correlacionar con periodos cuando un mayor/menor número de enjambres sísmicos fueron registrados. A través del modelamiento de

esfuerzos tipo coulomb, nosotros sugerimos que el proceso de inflación causante de las sorprendentes tasas de alzamiento superficial podría afectar el campo de esfuerzos local del área, promoviendo el deslizamiento en fallas vecinas. Algunos aspectos como la geometría, estado de esfuerzos, magnitud, localización y disposición de la fuente que produce la deformación y la fuente productora de la sismicidad, podría jugar un rol relevante para explicar cómo éste proceso trabaja y la aparente conexión.

3.2 Abstract

Two relevant and active geological processes have been recently detected at Laguna del Maule Volcanic Complex (LMVC): A large surface uplift process related to the activity of a rhyolitic magma body located at 5 km depth that produce a crustal deformation with rates considered as one of the highest worldwide ever measured at a volcano that is not actively erupting, and cyclic volcano-tectonic seismic swarms which location coincide with a number of key features: Two of the most active Holocene volcanic emission centers; interception between the rim of the volcanic basin and an active NE-SW strike-slip fault; the SW vertex of the sill

modeled by InSAR studies as the source of surface uplift; a zone where gravimetric studies suggest a mass changes due to recent magma injection. Here we present a study that involves seismic and GPS observations to show how the sources of both processes could be connected. There seems to be a temporal connection between both processes, since periods of increasing/decreasing uplift rates could correlate with periods where a greater/smaller number of seismic swarms were recorded. Through Coulomb stress modeling we suggest that the inflation process causing the astonishing surface uplift rates could affect the local stress field of the area, promoting the failure on neighbor faults. Some aspects as the geometry, stress state, magnitude, location and disposition of the source that produce the crustal uplift and the source that produce the seismicity, could play a relevant role to explain how this process work and the apparent connection.

Key words: Rhyolitic volcanic complex, coulomb stress changes, cyclic volcano seismic swarms, sustained volcano deformation.

3.3Introduction

3.3.1 Tectonic frame and Geology

The south-central part of Chile (33°S – 46°S) is tectonically dominated by the active oblique convergence between Nazca and South American plates (Cembrano and Lara 2009; Lavenue and Cembrano 1999; Bonali et al, 2013). This obliquity impose the partitioning of convergence between large subduction earthquakes and a complex intra-arc dextral-transpressional fault systems, which is related to the Liquiñe-Ofqui Fault Zone (LOFZ) south of 37°S and a less well-know system to the north. These intra-arc fault systems are strongly connected to the Southern Volcanic Zone (SVZ) of the Andes, a very active Holocene-to-recent magmatic arc with more than 60 volcanic centers considered as active volcanoes (Siebert et al, 2002), of which 25 been considered as historically actives. A relevant aspect of the SVZ is the presence of large rhyolitic calderas located in the rear-arc that have been producing large explosive eruptions during the Holocene and extensive ignimbritic quaternary deposits, as Calabozo and Diamante Calderas, and Puelche and Laguna del Maule volcanic fields.

The Laguna del Maule Volcanic Complex (LMVC) is located 230 km eastward of the epicenter of the Mw8.8 2010 Maule earthquake (Fig. 3.1) and is formed by 130 holocene volcanic vents surrounding a 9x11 km lake. The LMVC comprises more than 350 km3 of volcanic products in the last 1.5 Ma, and has been particularly active during the post-glacial period, producing a concentric ring of 36 separate silicic eruptions between 25 ka (Hildreth et al, 2010) and ~2 ka ago (the most recent eruption; Andersen et al, 2017 and 2018). These recent eruptions were from 24 vents that produced mainly rhyodacite and rhyolite lava flows and domes covering ~100 km2. This is the greatest concentration of post-glacial rhyolite in the Andes (Singer et al, 2014).

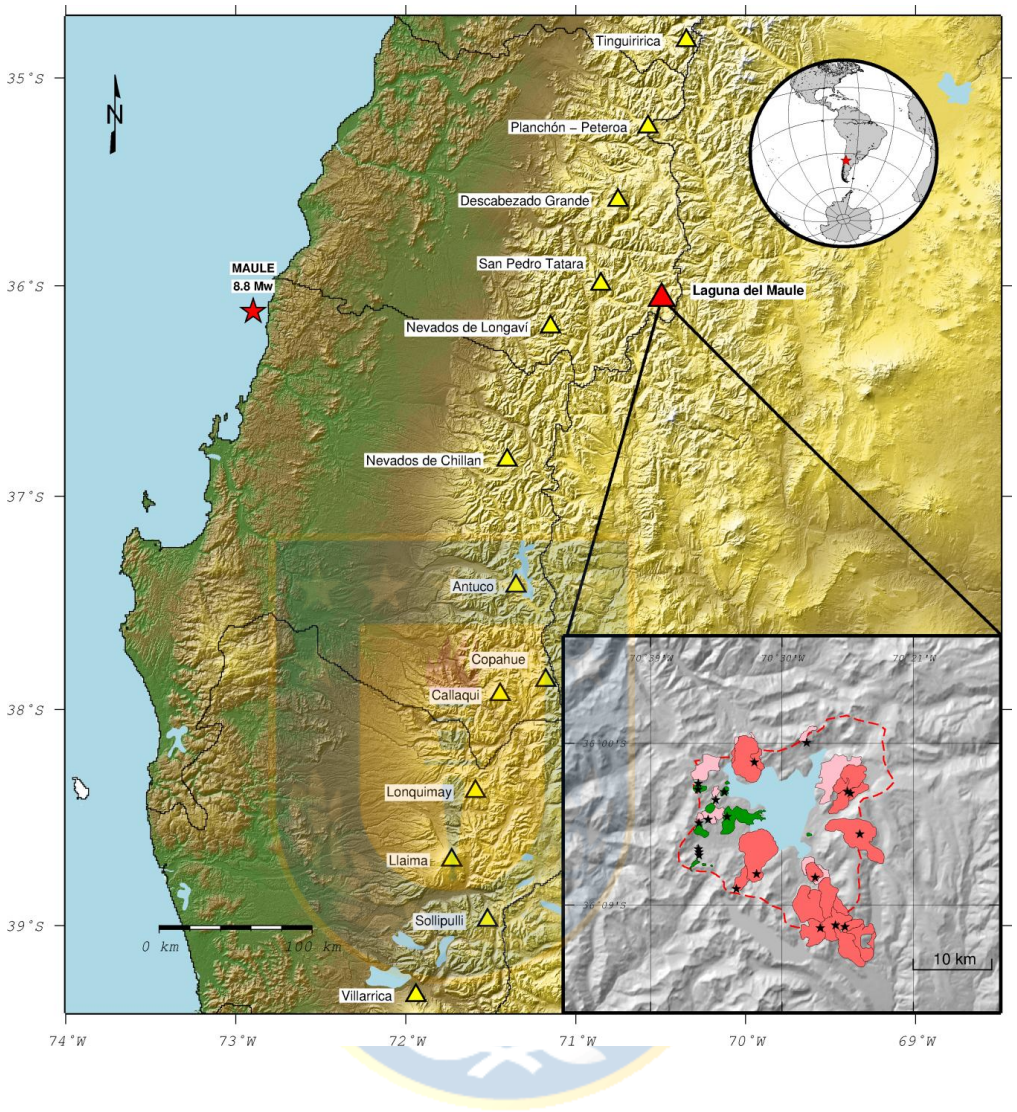

Figure 3.1 Laguna del Maule Volcanic Complex (LMVC) location. Image showing the Southern Andes active volcanoes (yellow triangles) and LMVC (red triangle), the red star shows the epicenter of the Mw=8.8 27-feb-2010 Maule earthquake. The below inset shows the simplified geological map (from Hildreth et al., 2010), showing the postglacial geological products (pink=rhyolites; lightpink=rhyodacites; green=andesites. The black stars are the volcanic vents and the red discontinuos line is the rim of the volcanic basin.

3.3.2 Recent volcanic processes

Multidisciplinary studies have reported an ongoing extraordinary crustal inflation process at LMVC. Volcanic deformation was initially studied by Fournier et al (2010) through interferometric analysis of synthetic aperture radar images (InSAR), using ALOS images, for a period from January 2007 and January 2008. The study founded a huge volcanic uplifting centered in the SW part of the lake, with an uplifting rate close to 18.5 cm/yr, which was model as sourced in a sill located at 5 km depth. The deformation rate was considered as one of the highest ever measured at a volcano that is not actively erupting (Singer et al. 2014). Later on, Feigl et al (2014) recalculated the LMVC deformation using SAR images acquired between 2007 and 2012, complementing the modeling with permanent GPS data calculating an uplift velocity up to 28 cm/yr and suggesting as model of the deformation a sill geometrically similar to that suggested previously. Lately, Le Mevel et al (2015) using interferograms from different agencies and supporting the modeling with five permanent GPS and six campaign GPS stations, suggested that the volcano deformation rates has a sustained and exponentially increasing behavior between 2007 and 2013, reaching maximum values of 24 cm/yr. After January 2013 the velocity field has a

inflexion point showing a deceleration, where deformation rates showed values close to 19 cm/yr, the inflexion point of the velocity fields coincided with the most energetic seismic swarm recorded ever in the LMVC (Le Mevel, et al. 2015, Cardona et.al 2018). The previous InSAR and GPS works suggested that the rate of deformation was negligible from 2003 and 2004, and it should have started some time before 2007.

In April 2011 OVDAS deployed a seismic portable network composed by five broadband stations and five GPS stations, in order to determine the activity level of LMVC. Later, the network was enhanced installing the telemetric component of the previous stations and adding one more permanent broadband station in January 2012. During 2014 OVDAS deployed a temporary network composed by 5 broadband seismic stations. Finally, as part of a NSF project leaded by the Wisconsin University, in which agencies and universities from USA, Chile, Canada and Argentina were participating, 38 temporary seismic stations were deployed between 2015 and 2016 (Fig. 3.2), reaching 49 seismic stations in total between 2011-2016.

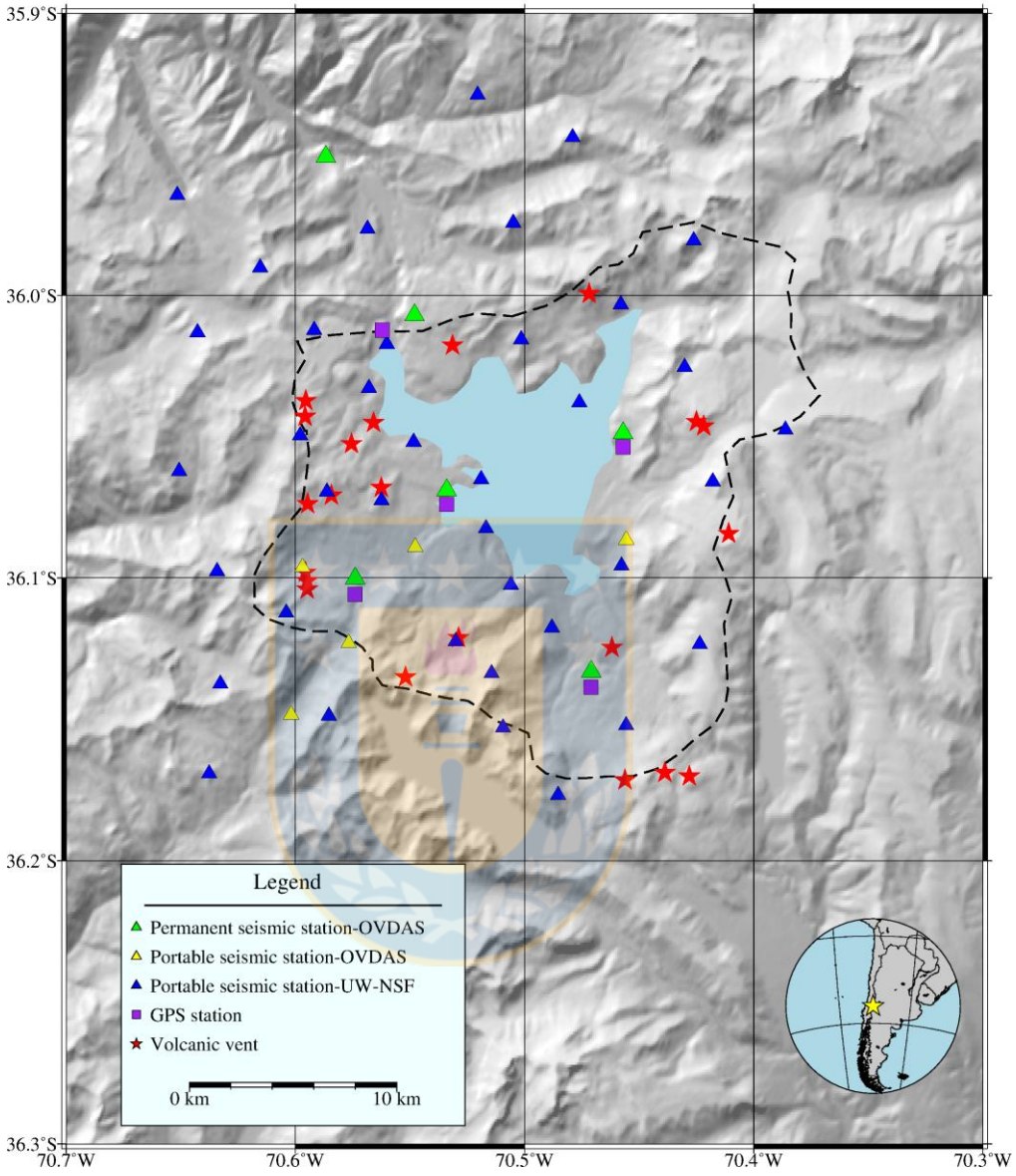

Figure 3.2 Network of LMVC between 2011 and 2016, composed by 49 seismic (permanent and portable stations) and 5 GPS stations, the black dash line demark the rim of the volcanic basin.

The seismic record acquired showed that LMVF is a volcanic zone seismically active, since there were recorded shallow cyclic seismic swarms located in the SW portion of the basin (Cardona et al., 2018). The swarm epicenter zone have a spatial correlation with others relevant geological structures as: (1) the rim of LMVF, (2) two of the most active emissions center during the Holocene period, (3) the interception between the rim of the volcanic basin and an active NE-SW strike-slip fault (Troncoso fault), and (4) the SW vertex of the sill suggested by the InSAR studies (Fig. 3.3), and (5) the location of ongoing mass addition recognized by microgravity studies (Miller et. al 2016, 2017), probably associated with influx of hydrothermal and magmatic fluids.

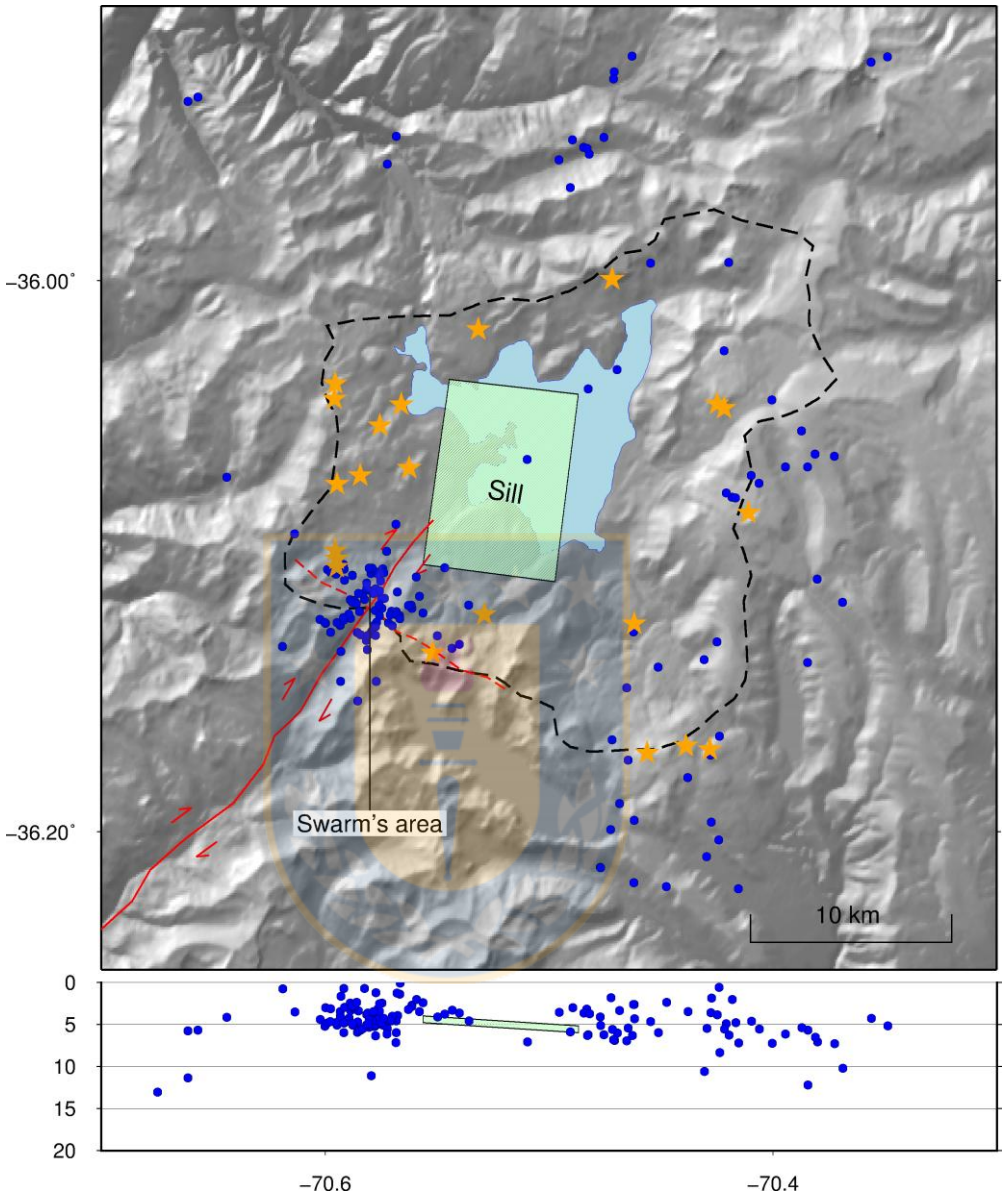

Figure 3.3 Recent actives volcanic processes at LMVC, the blue dots represent the locations for VT earthquakes from 2011 to 2016, note the seismic swarm area located close to the rim of the volcanic basin, two of the most active emissions center (orange stars) during the Holocene period, the interception between the rim of the volcanic basin (discontinuous black line) and an active strike-slip fault (red line), and the SW vertex of the sill suggested by the InSAR studies (green rectangle).

3.4 Methodology

The main aim of this work is to understand the physical link between the ongoing inflation process and the generation of seismic swarms. As initial hypothesis we suggest that the uplift process and the astonishing rates measured could affect the local stress field of the area, promoting the failure on neighbor faults, where some aspect as the geometry, stress state, magnitude, location and disposition of both sources could play a relevant role to explain how this process work and the apparent connection.

To validate the hypothesis is essential resolve the source mechanism for both processes. In relation to the inflation process, recently published works resolve the source, reaching analogous results, and suggesting as source of the deformation a magmatic chamber located to 5 km depth, centered in the SW of the volcanic basin (see Fig. 3.3). Additionally, we construct GPS time series complementing the data published in the works of Feigl et. al. (2014) and Le Mevel et. al (2016). We used the GIPSY software (release 6.1) from the Jet Propulsion Laboratory to obtain daily GPS station coordinates and velocities for five GPS stations located around of LMVC.

We performed a linear regression of the data to determine the average of the uplifting rate for each station, and subsequently we did a graph that show the variation of each point to the general tendency (Δrate) to determine periods when the magnitude of the rate increasing and decreasing with time.

To resolve the source associated to the seismic swarm episodes, we analyze the seismic activity recorded by the composed seismic network. Firstly, we make a seismic classification follow a combination of Lahr et al. (1994) and Chouet (2003) criteria, and then we construct time series of daily occurrence for the volcanic seismicity observed. Afterward, we separated from the database those episodes recognized as 'swarm episodes' (more than 50 volcano-tectonic events per hour), calculating the seismic energy by the equation proposed by Boatwright (1980). Subsequently, for signals categorized as volcano-tectonic (VT), we did a relocation process using HypoDD software (Kissling et al., 1994) with the crustal velocity model developed by Cardona et al. (2018). Finally, for those events with a clear P wave phase and more than 10 stations recorded, the focal mechanisms were obtained using the FOCMEC program (Snoke et al.,

1984) searching the fault plane that better represented the first P wave's motion.

To examine the hypothesis initially proposed as mechanism of connection between both processes, a Coulomb stress calculation was done. To calculate static stress changes we used Coulomb 3.3 software (Toda et. al. 2005), which is based on Okada's (1985) equations, being essential to have a good approximation of the sources involved in the estimation, considering that small variations in the sources could gave us contrasting results. The calculations are based in the assumption described by Toda et al. (2005), where the static stress changes are related by the displacement of a structure 'source' (fault , dike or point) in a elastic half space. The program resolve the shear and normal components of the stress change on specified "receiver" fault planes, using the Coulomb failure criterion, $\Delta\sigma f = \Delta\tau s + \mu' \Delta\sigma n$, where $\Delta\sigma f$ = change in failure stress on the receiver fault caused by slip on the source fault(s), $\Delta\tau s$ = change in shear stress, positive when sheared in the direction of fault slip, $\Delta\sigma n$ = change in normal stress,

positive if the fault is unclamped, μ' = effective coefficient of friction on the fault.

We take values of coefficient of friction de 0.4, Poisson's ratio of 0.25 and Young's module of 8x103 bars, previously predetermined. Once the plausible structures and geometries that produce the volcano uplift and the seismic swarms were established, we chose as source of stress a magma body with the disposition suggested by Fournier et. al (2010), Feigl et. al. (2014) and Le Mevel et. al (2016), which consist a sill located at 5 km depth, an azimuth close to 11° and 20° of dipping, with approximately 9 km length and 5 km width, and a opening rate of 1 m by year. As receiver structure, we take those seismic events located into the seismic swarm area, determining all the focal mechanism for events with at least 10 stations and stable solutions.

3.5 Results

3.5.1 Seismic activity

Initially a seismic database from 2011-2016 for the LMVC was created, extracting the seismic events related to volcanic processes. More than 5600 seismic events were categorized, then a daily occurrence graph including each type of event was obtained (Fig. 3.4). A total of 82% of the volcano seismic events correspond to volcano-tectonic (VT) earthquakes, but yet more importantly is the recurring record of seismic swarm along time, being recognized 21 seismic swarms in total.

We separate the seismic swarm activity into three noteworthy stages. The first stages comprise a period of time between July 2011 and March 2013. During this stages a greater number of seismic swarm were recorded, 11 in total. The total seismic energy related to each seismic swarm episode during this stage show a tendency to increase with the time. In fact, to the end of this stage did occurred the most energetic seismic swarm ever recorded in LMVC. This phase was followed by a declination of the seismic swarm productivity, extended by one year of stillness, without seismic

swarm activity. During the second stage between February 2012 and January 2016, 9 seismic swarms were recorded, with seismic energies are comparatively lower than the previous stage. This stage mark the reawaken of the seismic swarm activity, with seismic energy showing a slightly tendency to increase with the time, but more randomly than stage 1. However, in this stage it could be distinguish two periods where the energy increase gradually, the first one between February 2014 and March 2015, and the second one between August 2015 and December 2015. Finally, the third stage comprises a period between January 2016 and December 2016, during which only one seismic swarm was recorded, marking an apparent quiescence of the seismic swarm activity (Fig. 3.4).

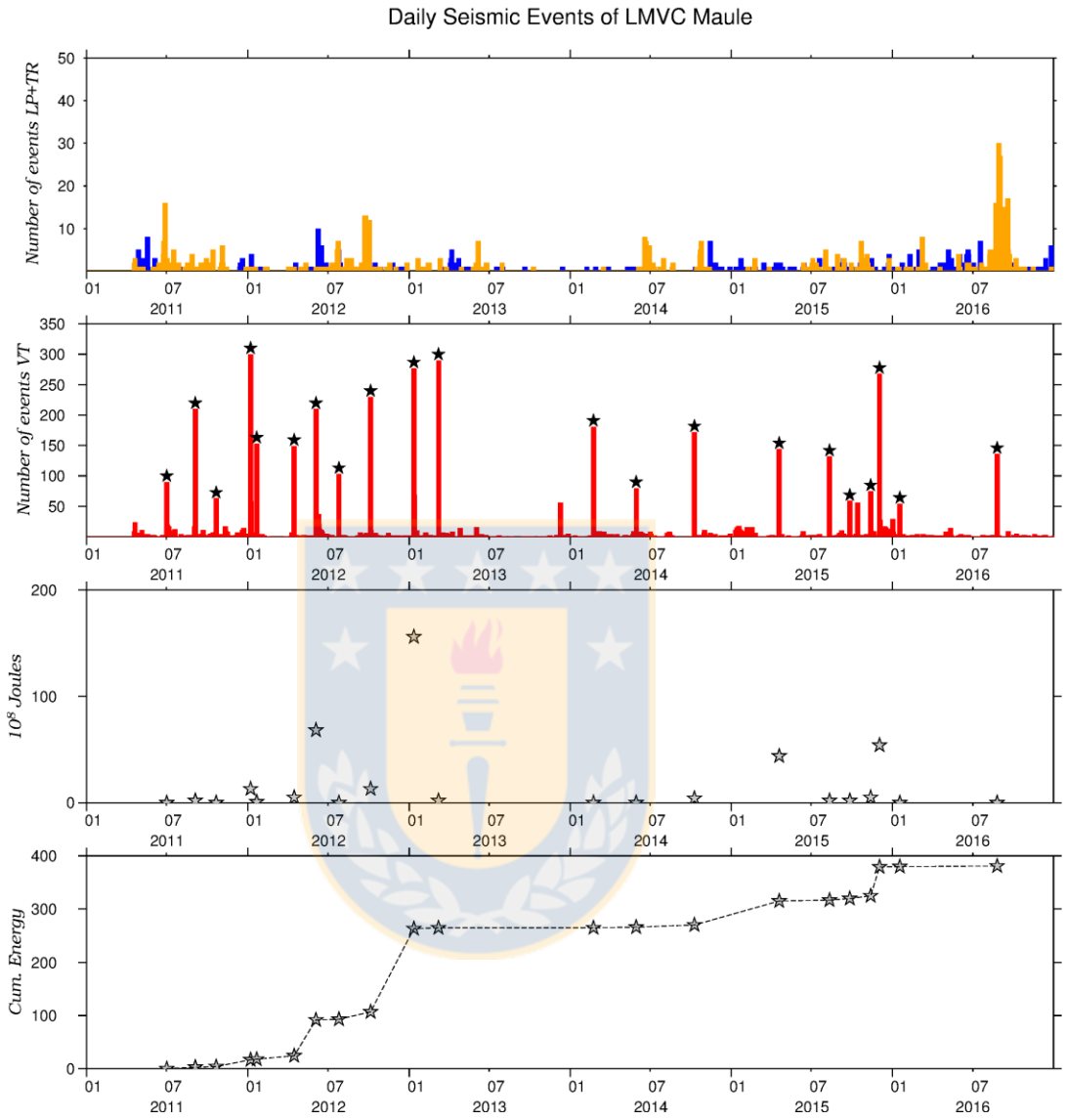

Figure 3.4 Volcano seismic activity of LMVC recorded by day between 2011 and 2016. The upper graph shows the long period (orange arrows) and tremor events (blue arrows), the graph in the middle shows the volcano-tectonic events recorded; the black stars demark the occurrence of seismic swarm's (21 in total). The below graph shows the seismic energy calculated for each seismic swarm episode. Between July 2011 and January 2013, a great number of swarm's were recorded and the energy calculated for each episode having a slightly tendency to increase with the time, then from 2014 to 2016 a random behavior was observed.

3.5.2 Volcano crustal uplift

In relation to uplift process, the tendency of the time series of the GPS stations between 2011 and 2016 shows coherent result relate to a source placed in the SW region of the complex, as was previously suggested by Fournier et .al (2010), Feigl et al. (2014) and Lemevel et al. (2015, 2016). The station located close to SW portion of the lake ('Maule' GPS station) reveal the higher annual media uplifting rates with values close to ~20 cm/y in the vertical component, followed in descending order of magnitude by Nieblas (9.3 cm/y), LDMP (6.2 cm/y) and Puelche (5.7 cm/y) stations (see the GPS velocity time series in fig. 3.5 and GPS velocity vectors in Fig. 3.6). We derive vertical residual graphs subtracting the linear trend for each station, in order to observe temporal changes of the uplift rates (gray lines into Fig. 3.5). In a general context, we could separate the time series into three phases. The first one between April 2012 and January 2013 include a period where the uplifting rates gradually increased to reach a maximum value close to 23 cm/y. After that the second stage comprises a phase extended by two years, between January 2013 and February 2015, showing a stability of the deformation rates with average values close to 20

cm/y. Into this phase a particular annual oscillated behavior was observed, that could be due to seasonal changes because the peaks are positioned on summer season and the valleys are placed on winter season. Finally, the third stage comprises a period of time between April 2015 and December 2016, where the uplifting rates were gradually decreasing to a minimum value close to 17 cm/y (see MAU station in Fig. 3.5).

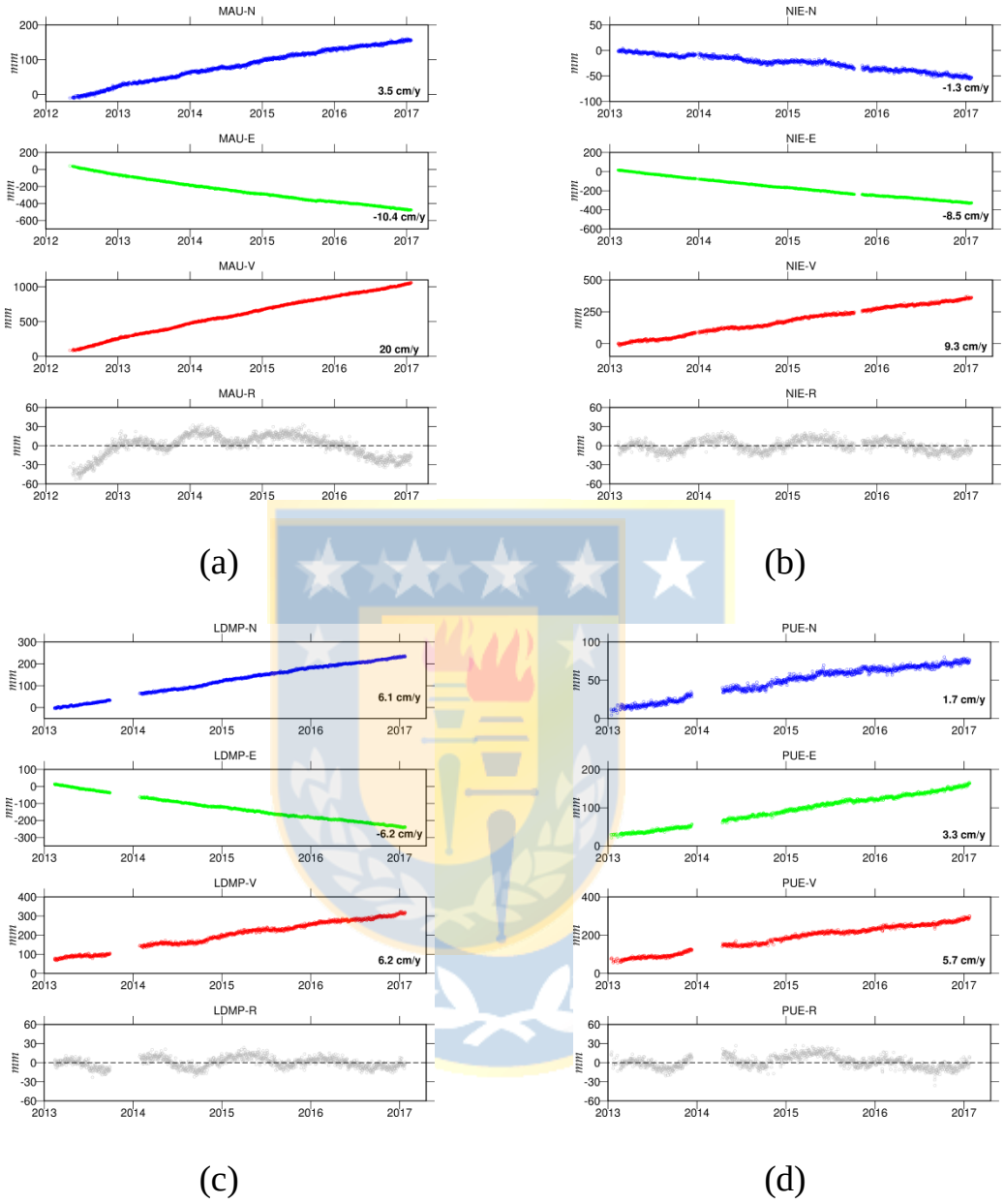

Figure 3.5 GPS velocities for stations (a) MAU, (b) NIE, (c) LDMP and (d) PUE. The blue lines correspond to north component, the green lines correspond to east component and the red lines correspond to vertical component. The gray line corresponds to the residuals for each daily measurement subtracted from the linear trend of the vertical component. In total, the closest station (MAU) has a cumulative GPS velocity value of ~1000 mm in five years, one of the most remarkable worldwide crustal volcano deformations, ongoing process.

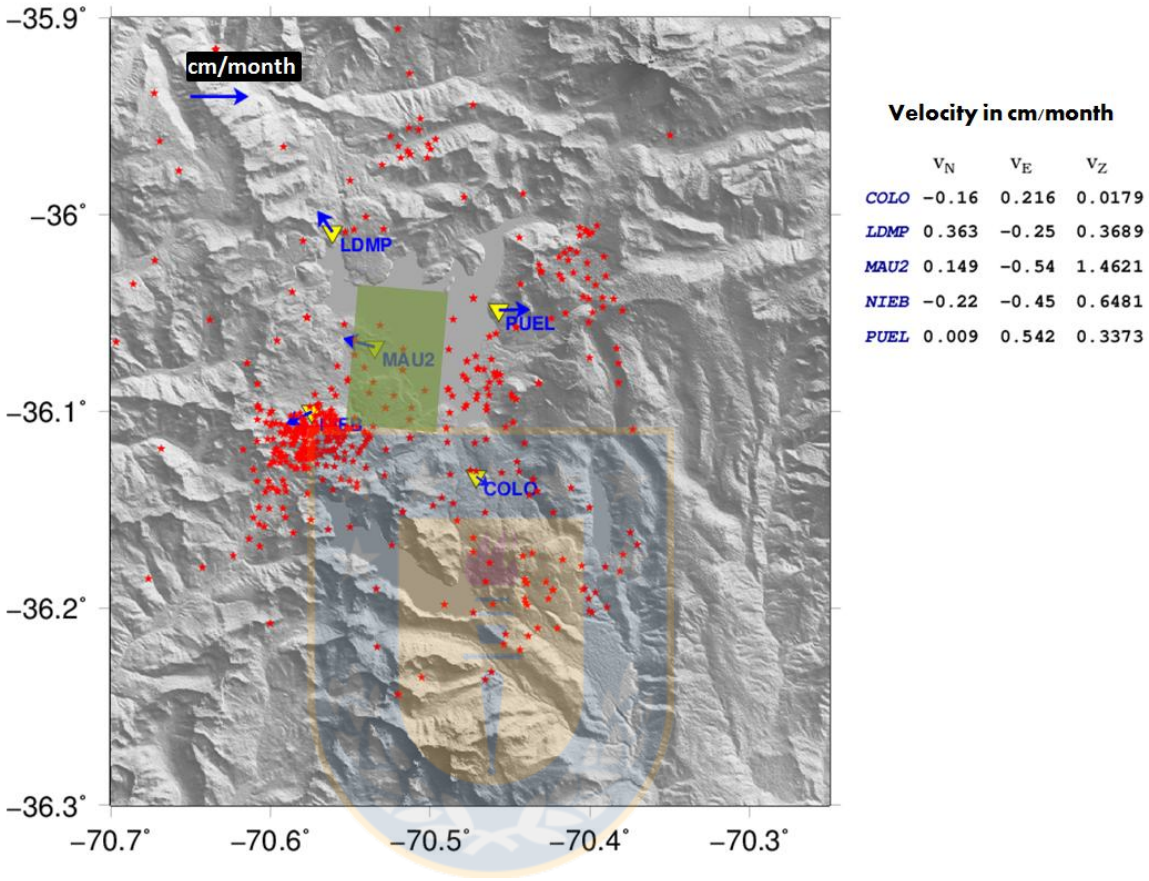

Figure 3.6 GPS horizontal velocities vectors (blue arrows) for stations MAU, NIE, PUE, LDMP and COLO. The red stars are the locations for VT earthquakes. The green rectangle shows the location of the sill modeled by INSAR Studies.

3.5.3 Coulomb stresses analysis

To define the receiver structures we computed eighteen focal mechanisms in order to resolve the source that produces the repetitive seismic swarms

episodes, selecting only the better seismic events recorded. This means those well located events, with an impulsive arrive of P phase, a ratio signal/noise up to 5 and at least 10 station with an optimum coverage of the focal sphere. The results of the focal mechanisms suggest the activity of a strike-slip fault, SW-NE trending and high dipping as source producing the seismic swarms episodes. Afterward, we defined the source of stresses as an opening sill coinciding with the source defined by previous InSAR studies, whereas the receiver structure is defined by the strike-slip fault. We model the Coulomb stress changes, assuming an isotropic and homogenous half-space. The normal stress distribution map showed a positive zone (unclamped) at the western zone of the sill, showing highest values close to 15 MPa. The region of maximum Coulomb stresses fits well with the seismic zone related with the strike slip fault that produces the cyclic volcano tectonic seismic swarms (Fig. 3.7a). In addition, Miller et .al (2017) by microgravimetry measurement suggested a mass injection over this zone and along of the Troncoso Fault, between 2013 and 2014, as well as the unclamped zone spatially fits with the zone where was detected LP seismic activity close to the north section of the Troncoso fault (Cardona et al., 2018), which could suggest fluid circulation over this zone.

On the other hand, the shear stress map for strike-slip faults SW-NE trend (29° strike, 90° dip and 130° rake) exhibit an positive anomalous zone, with values of stresses close to 18 MPa, located in the SW vertex of the sill (see Fig. 3.7b, red colors represent charge of stresses to promote dextral faulting), where strike slip faults with dextral component could be triggered by the uplift source. This anomalous zone spatially connect with the zone where approximately more than 70% of the volcano-tectonic earthquakes does occur over the past five year at the LMVC and mostly of the repetitive seismic swarm were located.

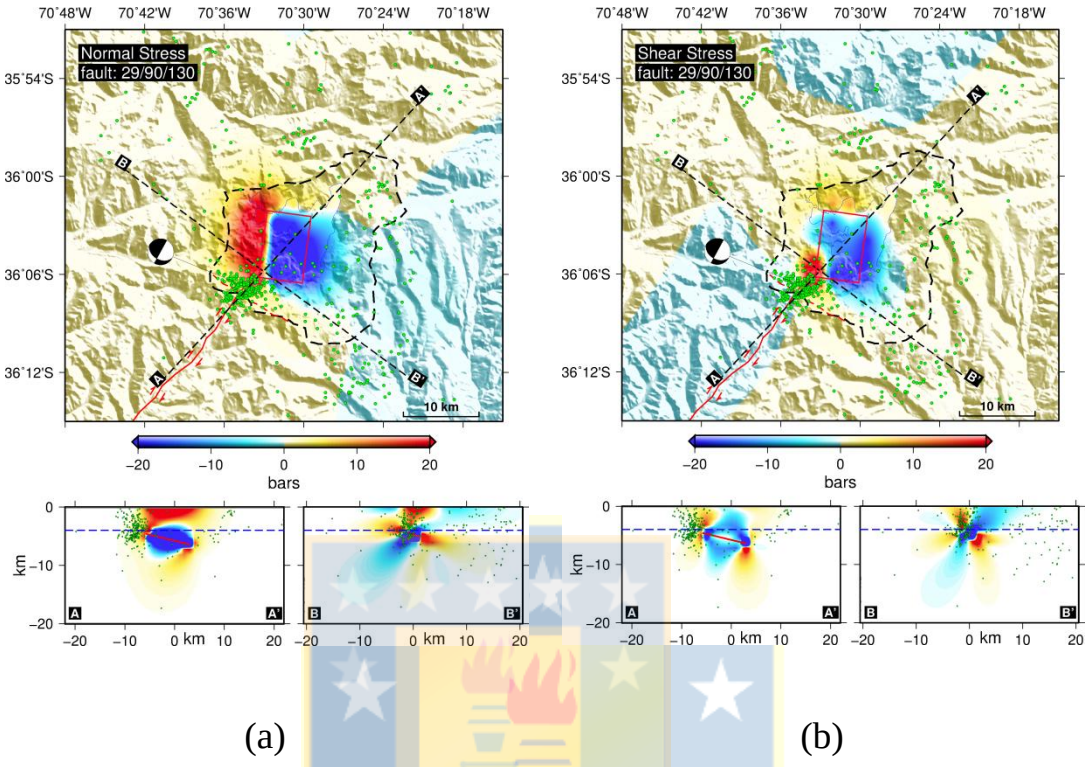

(a) (b)

Figure 3.7 Coulomb stress distribution at LMVC assuming as source structure a sill located 5 Km depth and as receiver structures strike-slip faults SW-NE trend. (a) Normal stress distribution, note that the positive zone (red colors-unclamped) is located at west portion of the volcanic basin, the high values are located from 0 to 4 km depth, the unclamped zone have spatial connection with the cluster where are located the VT seismic swarm episodes. (b) Shear stress distribution, as noteworthy aspect the positive zone is located close to the SW vertex of the sill modeled by previous InSar studies, this zone contain more than 70% of the VT earthquake located between 2011-2016 at the Laguna del Maule volcanic basin.

3.6 Discussion and conclusions

The interaction between volcanic system and active faults has been a topic broadly discussed recently. Transfer of stresses from big earthquakes has been suggested as mechanism to promote volcano eruption or at least promoting temporal changes on volcanic systems. In this sense, some authors suggested that static stress from big earthquakes could induce changes in the local stresses of the volcanic systems promoting the cracks opening, facilitating the magma rising and/or increasing the pressure of the magmatic chambers that could induce thermodynamic changes into the magmatic fluids inducing the gas nucleation. Alternatively, some cases have showed that volcano activity could promote activity over neighbors faults system promoting tectonic seismicity in a specific zone, being suggested as mechanism the static stresses from volcanic systems that could change the local stress of the fault promoting its failure. Other mechanisms associated with increasing of the pore pressure or hydrothermal and magmatic fluids diffusivity that promote the fault sliding has been also suggested.

Our main finding was the recognition of an anomalous zone at LMVC located in the SW part of the basin, where recent studies using diverse methodologies have detected volcano activity that could be summarized as follow:

1- An active volcano deformation process generating uplifting rates with annual media values close to 25 cm/y, the source of this process has been modeled as a sill located 5 km depth (Fournier et al. 2010, Feigl et al. 2014). This process has been active at least over the past nine year (Le Mevel et al. 2016).
2- The inflating region includes most of the 16-Km-by-14-km ring of rhyolitic vents (Feigl et .al, 2014). Close to the SW vertex of the sill are located one of the youngest emission center 'Nieblas' (Hildreth et al., 2010; Singer et al., 2014: Andersen et al., 2017).
3- In the SW portion of the modeled sill has been recognized a mass changes between 2013 and 2014 by means of microgravity measurements (Miller et al., 2016) suggesting a mechanism of hydrothermal fluids intrusion into existing voids along Troncoso fault.

4- Repetitive seismic swarms located over The Troncoso Fault and an WNW-ESE lineament that roughly coincides with the SW vertex of the Sill and the microgravity zone anomaly, where a complex spatio-temporal interaction between both faults seems to be likely triggered by the inflation process (Cardona et al. 2018).

From those evidences it is clear for us that in the SW portion of the LMVC currently has occurred a series of crustal processes surrounding a magma body located 5 km depth triggered by a new pulse of magma injection, but the available evidence at the moment is insufficient to demonstrate the coupling level between those processes. For instance, Miller et al. (2017) suggest that there will be a discrepancy and time correspondence between deformation and gravity changes, however suggesting some kind of magma-tectonic interaction mechanism that allows shallow mass addition triggered by deeper magma injection. In order to add more evidences to discern about of the coupling level between those processes, a new contribution of our work was the temporal comparison between the behavior of the seismic activity occurring in the SW part of the

basin and the time series of the uplift process using GPS data. In a general overview, there seems to be a temporal association between both processes, considering that there are periods where increasing in the uplift rates correlate well with periods where a greater number of more energetic seismic swarms were registered. On the other hand, periods where the uplift rates were gradually decreasing, temporary correlate well with the period where a smaller number of seismic swarms were recorded and the seismic energy calculated were comparatively lower. From 2012 and 2016, we could separate this general behavior into three stages. The first stage comprises a period of time between January 2012 and January 2013, where uplift rates were gradually increasing and finishing in a peak of deformation rate value close to 35 cm/yr (higher value ever measured). This peak value match in time with the most energetic seismic swarm ever recorded at LMVC (see fig. 8). During this period a high productivity of seismic swarm was observed, being recorded 11 seismic swarm in total. The next phase, during the years 2013, 2014 and 2015 (see fig. 3.8) demark a period of time where the deformation rates have low variations from the media value, and we could observe during this stage a cyclic annual behavior of consecutives increases and decreases of the uplifting rates (perhaps due to seasonal

factors). During this phase the energy and occurrence of seismic swarm are comparatively lower than the before phase, being recorded nine seismic swarms during three years. Finally, the stage third (after January 2016) marked a period where the uplift rates show a slightly tendency to decrease, with only one seismic swarm was recorded, showing a quiescence of the seismic swarm activity.

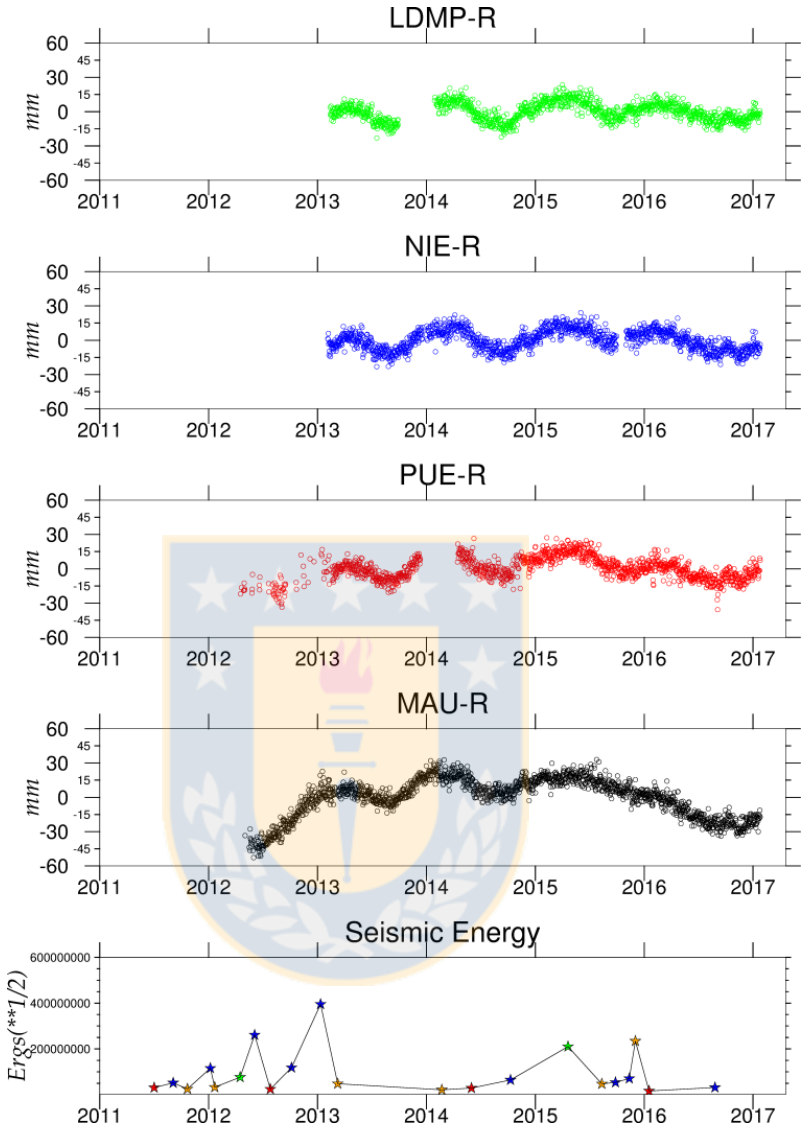

Figure 3.8 Temporal comparison between GPS velocity residuals subtracting linear trend for LDMP (green), NIE (blue), PUE (red) and MAU (black) stations, and seismic energy (below) for each swarm episode. A stage to highlight occurred between July 2011 and January 2013, during this period the GPS velocities shows a tendency to increase and the seismic swarm productivity was comparatively higher than others periods and the seismic energy has a tendency to increase through the time. Between 2013 and 2015 the deformation rates doesn't have significant changes where stationeries changes were observed. After 2016 when the deformation rates were decreasing and low seismic swarm productivity was observed.

Other remarkable aspect has relation to the spatial correspondence between the anomalous zones observed by static stress transfer calculation and the cluster of activity related to seismic swarm activity. Normal stresses predicted by static stress transfer from the sill show a positive zone (unclamped zone) located to west portion of the sill that matches well the area where a mass changes between 2013 and 2014 by microgravity measurements (Miller et al. 2017) was observed and the location of the seismicity related to fluids movements described by Cardona et al. (2018). This suggests that there will be located a brittle zone and pathways that promote the circulation of hydrothermal and magma fluids to shallow levels (see Fig 3.7a and Fig 3.8). In addition, the shear stress changes map predict a zone located in the SW vertex of the sill, where strike slip faults dextral component (charge of stress are red colors into Fig. 3.7b) could be triggered by stresses from the deformation source. If we compare this anomalous zone with a seismic density map for LMVC (Fig. 3.9) we could see that most of the volcano-tectonic activity occurred between 2011 and 2016 has been located in a particular patch along Troncoso Fault, matching clearly with the zone that the Coulomb stress calculation predict, suggesting to us that both process could be causatively connect.

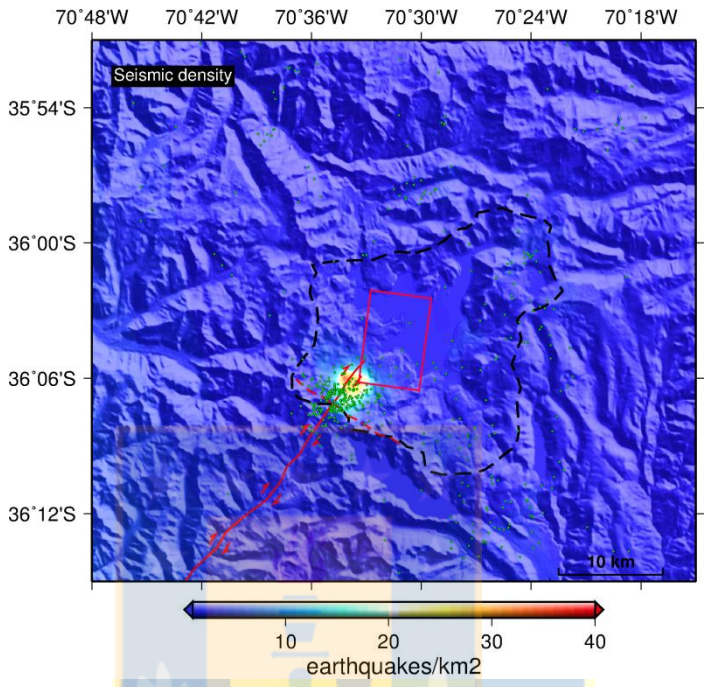

Figure 3.9 Seismic density map for locatable VT earthquakes between 2011 and 2016. To obtain the density map, the area was divided in 1km x 1km squares, counting the number of events into each square. The distribution shows a relevant zone with high earthquake productivity, located in the SW portion of the basin, in the SW vertex of the modeled sill and close to Troncoso fault.

3.7 Acknowledgements

This research has been supported by Observatorio Volcanologico de los Andes del Sur (OVDAS) belonging to Sernageomin (National Geological Survey), US NSF grant EAR-1322595 with Brad Singer

(University of Wisconsin-Madison) as PI, and Chilean Fondecyt project 1151175 (Andres Tassara as PI). We thank to seismological team of OVDAS to perform the primary processing of the seismic data. Most figures were generated using GMT software by Wessel and Smith (1991).

CAPITULO 4. CONCLUSIONES

- Unas de las principales observaciones de este trabajo de investigación fue corroborar la existencia de actividad sísmica superficial asociada con la dinámica actual del complejo volcánico Laguna del Maule, que acompaña temporalmente un proceso inflacionario cortical, el cual ha sido relacionado con la actividad de un cuerpo magmático presumiblemente de composición riolítica, que ha gatillado una serie de anomalías detectadas por estudios multiparamétricos, que incluyen observaciones sísmicas, geodésicas, microgravimétricas, magnetotelúricas y petrológicas.

- Un aspecto destacable en el proceso de caracterización de la sismicidad asociada al Complejo Volcánico Laguna del Maule, para un periodo de tiempo comprendido entre los años 2011-2016, fue el reconocimiento de enjambres de eventos sísmicos volcano-tectónicos, siendo detectados 21 episodios en total, que fueron localizados en el extremo SW de la cuenca volcánica. Los enjambres

ocurren cada 2-3 meses en promedio, presentan duraciones entre 0.5 a 3 horas y magnitudes locales inferiores a 2.2. Un análisis de correlación de las formas de onda de los enjambres permitió el reconocimiento de cuatro familias sísmicas, cuya actividad se alterna durante los 5 años que analizó este estudio.

- Dos de las familias sísmicas identificadas (E1 y E3, etiquetadas con color rojo y naranja en las figuras 2.7, 2.9 y 2.11, en el capítulo 2) comparten algunas características importantes, como la similitud de su forma de onda apilada, y su localización epicentral a lo largo de un lineamiento WNW-ESE, sobre el cual se identificaron evidencias de campo de un fallamiento normal, sin embargo, los mecanismos focales determinados para eventos sísmicos de estas familias son más consistentes con fallamientos strike-slip con componente dextral.

- Por su parte, la familia sísmica E2 (etiquetada con color azul en las figuras 2.7, 2.9 y 2.11, en el capítulo 2) tiene una forma de onda distinta, presenta valores de S-P mayores y la energía sísmica es comparativamente mayor. Los eventos sísmicos de esta familia

fueron localizados en la intersección de la falla Troncoso (dirección NE-SW) y un lineamiento WSW-ENE. Un alto porcentaje de los mecanismos focales obtenidos para sismos de esta familia fueron asociados con fallamientos de dirección WSW-ENE de componente sinestral, o fallamientos con dirección NE-SW de componente dextral, esto último es concordante con el rumbo de la falla Troncoso y las evidencias estructurales reconocidas en campo.

- Dentro de este contexto, el principal hallazgo del proceso de caracterización de la señales sísmicas observadas en el CVLM, fue descubrir que la esquina SW del sill propuesto como fuente de alzamiento por los estudios geodésicos (Feigl y otros, 2014; LeMevel y otros, 2015, 2016) aproximadamente coincide con una intersección estructural, activa sísmicamente, donde una compleja interacción espacio-temporal entre la falla Troncoso de dirección NE-SW y un lineamiento WNW-ESE, podría ser activado por el proceso inflacionario.

- Observaciones de campo realizadas a lo largo de la falla Troncoso revelan micro estructuras asociadas con fallamientos strike-slip dextrales, que coinciden con los mecanismos focales determinados para la familia sísmica E2, localizada sobre la traza. Nosotros proponemos un modelo conceptual para el CVLM, con la falla Troncoso como una falla maestra de una cuenca 'pull apart dextral', orientada SW-NE, que limita la cuenca en su costado W. El rol de la falla Troncoso en la actividad del sistema volcánico también es sugerido por Miller y otros (2016) basado en la relación espacial de una anomalía de baja densidad reconocida por datos gravimétricos y su ubicación a lo largo de la falla Troncoso.

- La alternancia periódica entre enjambres sísmicos de las diferentes familias y su localización en diferentes estructuras y segmentos de falla, que acompañan temporalmente el proceso inflacionario, hace pensar que podría existir cierto grado de interacción entre los procesos generadores de sismicidad y deformación cortical. Nosotros sugerimos que la fuente inflacionaria podría promover sismicidad cortical, por transferencia de esfuerzos hacia el marco estructural del

sistema volcánico, como una respuesta mecánica de la corteza a los esfuerzos inducidos por la fuente de deformación, la cual puede gatillar rupturas de asperezas a lo largo de las fallas cercanas al sistema volcánico. Una observación que podría apoyar este modelo, es la correspondencia temporal cuando la tasa de alzamiento comenzó a decrecer en enero de 2013 y la ocurrencia del enjambre más energético registrado en el CVLM.

- De acuerdo los resultados de la investigación, un hallazgo importante es el reconocimiento de una zona anómala ubicada al SW de la cuenca volcánica, donde confluyen una serie de procesos, tales como: 1- El vértice SW del sill modelado como fuente del proceso de alzamiento, modelado por los estudios InSAR, 2- Un cambio de masa que sucedió entre los años 2013 y 2014, observado a través de medidas gravimétricas, 3- La ubicación de uno de los centros de emisión volcánica riolíticos más jóvenes 'Nieblas', y 4- Enjambres sísmicos localizados en la intersección de dos estructuras sísmicamente activas.

- El mapa de distribución de esfuerzos tipo coulomb, asumiendo como fuente productora de esfuerzos la fuente de alzamiento (sill ubicado a ~5km de profundidad) y estructuras receptoras fallas strike-slip de componente dextral (falla Troncoso), predice una zona de transferencia de esfuerzos de cizalla ubicada al extremo SW de la cuenca, que corresponde espacialmente con el cluster de actividad sísmica tipo enjambre, y donde el 80% de la actividad VT fue localizada entre los años 2011 y 2016. A su vez, una segunda zona donde se encontraron cambios positivos de esfuerzos normales (unclamping), correlaciona espacialmente con la zona donde Miller y otros (2016) reportan cambios de masa ocurridos entre los años 2013-2014, y donde fueron localizados algunos eventos sísmicos tipo LP. De acuerdo a lo anterior, se sugiere que la falla Troncoso podría ser una zona de debilidad cortical, a través de la cual fluidos hidrotermales y/o volcánicos podrían estar siendo movilizados.

Referencias

Andersen, N.L., Singer, B.S., Jicha, B.R., Beard, B.L., Johnson, C.M., Licciardi, J.M., (2017). Pleistocene to Holocene growth of a large upper crustal rhyolitic magma reservoir beneath the active laguna del Maule volcanic field, central Chile. J. Petrol. 2017, Vol. 58, No1,85-114, doi: 10.1093/petrology/egx006.

Andersen, N; Singer, B.; Costa, F.; Fournelle, J.; Herrin, j.; Fabbro, G., (2018). Petrochronologic perspective on rhyolite volcano unrest at Laguna del Maule, Chile. Earth and Planetary Science Letters 493 (2018) 57-70. doi:10.1016/j.epsl.2018.03.043.

Boatwright, J., (1980). A spectral theory for circular seismic sources: simple estimates of source dimension, dynamic stress drop, and radiated seismic energy. Bull. Seismol. Soc. Am. 70 (1), 1 – 27.

Bohm M., Luthb S., Echtler H., Asch G., Bataille K., Bruhn C., Rietbrock A., Wigger P., (2002). The Southern Andes between 36° and 40°S latitude: seismicity and average seismic velocities. Tectonophysics 356, 275– 289.

Bonali FL; Tibaldi A; Corazzato C; Tormey DR; Lara LE., (2013). Quantifying the effect of large earthquakes in promoting eruptions due to stress changes on magma pathway: the Chile case. Tectonophysics 583:54–67.

Cardona, C; Tassara, A.; Gil Cruz, F.; Lara, L. E.; Morales, S.; Kohler, P.; Franco, L., (2018). Crustal seismicity associated to rapid surface uplift at Laguna del Maule Volcanic Complex, Southern Volcanic Zone of the Andes. Journal of Volcanology and Geothermal Research. Volume 353, p. 83-94. doi:10.1016/j.jvolgeores.2018.01.009.

Cembrano, J.; Lara, L., (2009). The link between volcanism and tectonics in the southern volcanic zone of the chilean andes: a review. Tectonophysics 471, 96 – 113.

Chouet, B., (2003). Volcano seismology. Pure and applied geophysics, 160 739-788.

Cordell, Darcy., Unsworth, Martyn J., Díaz, Daniel., (2018). Imaging the Laguna del Maule volcanic field, central Chile using magnetotellurics: evidence for crustal melt regions laterally offset from surface vents and lava flows. Earth and Planetary Science Letters, 488 (2018): 168–180. doi:10.1016/j.epsl.2018.01.007

Crosson, R.S, (1976). Crustal structure modeling of earthquake data,1, Simultaneous least squares estimation of hypocenter and velocity parameters. J. Geophys. Res., 81, 3036-3046,1976.

Díez, M.; La Femina, P. C.; Connor, C. B. ; Strauch, W.; Tenorio, V., (2005). Evidence for static stress changes triggering the 1999 eruption of Cerro Negro Volcano, Nicaragua and regional aftershock sequences.

GEOPHYSICAL RESEARCH LETTERS, VOL. 32, L04309, doi:10.1029/2004GL021788, 2005.

Drake, R.E., (1976). Chronology of Cenozoic igneous and tectonic events in the central Chilean Andes-latitudes 36°30' to 36°S. Journal of Volcanology and Geothermal Research 1*:* 265-284.

Ellsworth, W.L, (1977). Three-dimensional structure of the crust and mantle beneath the island of Hawaii. Ph D thesis, MIT, Massachussetts, USA,1977.

Feeley, T.C., Dungan, M.A., Frey, F.A., (1998). Geochemical constraints on the origin of mafic and silicic magmas at Cordón El Guadal, Tatara-San Pedro Complex, central Chile. Contributions to Mineralogy and Petrology 131*:* 393-4.

Feigl, K. L., H. Le Mével, S. T. Ali, L. Córdova, N. L. Andersen, C. DeMets, and B. S. Singer, (2014). Rapid uplift in Laguna del Maule

volcanic field of the Andean Southern Volcanic zone (Chile) 2007–2012, *Geophys. J. Int.*, **196**(2), 885–901, doi:10.1093/gji/ggt438.

Feuillet, N., Cocco, M., Musumeci, C., Nostro, C., (2006). Stress interaction between seismic and volcanic activity at Mt Etna. *Geophys. J. Int.* (2006) 164, 697–718 doi: 10.1111/j.1365-246X.2005.02824.x.

Fournier T.J., Pritchard M.E., Riddick S.N., (2010). Duration, magnitude, and frecuency of subaerial volcano deformation events: New results from Latin America using InSAR a global synthesis. Geochemistry Geopshysics Geosystems G3, an electronic journal of the earth sciences. Volume 11, Number 1, 19 January 2010. Pag 1-29.

Frey, F.A.; Gerlach, D.C.; Hickey, R.L.; López, L., (1984). Petrogenesis of the Laguna del Maule volcanic complex, Chile (36°S). Contributions to Mineralogy and Petrology 88*:* 133-149.

González-F., O.; Vergara, M., (1962). Reconocimiento geológico de la Cordillera de los Andes entre los paralelos 35º y 38º latitud sur. Universidad de Chile, Instituto de Geología, Publicaciones 24: 121 p.

Hildreth W., Godoy E., Fierstein J., Singer B., (2010). Laguna del Maule Field. Eruptive history of a quaternary basalt-to-rhyolite distributed volcanic field on the Andean range crest in central Chile. Boletin No 63, 2010. Subdirección Nacional de Geología. Sernageomin. 145 pág.

Hildreth, W., and Moorbath, S. (1988). Crustal contributions to arc magmatism in the Andes of Central Chile. Contributions to Mineralogy and Petrology, 98, 455-89.

Hill, D. P., (1977). A model for earthquake swarms, J. Geophys. Res., 82,1347–1352.

Kissling, E., Ellsworth, W. L., Eberhart-Phillips, D., and U. Kradolfer, (1994). Initial reference models in local earthquake tomography, J. Geophys. Res., 99, 19'635-19'646.

Lahr, J.C., Chouet, B.A., Stephens, C.D., Power, J.A. and Page, R.A., (1994). Earthquake classification, location and error analysis in a volcanic environment: implications for the magmatic system of the 1989-1990 eruptions at Redoubt Volcano, Alaska. Journal of Volcanology and Geothermal Research, 62(1-4): 137-151.

Lavenu, A.; Cembrano, J., (1999). Compressional and transpressional-stress pattern for Pliocene and Quaternary brittle deformation in fore arc and intra-arc zones (Andes of Central and Southern Chile). Journal of Structural Geology, Vol. 21, p. 1669-1691.

Lupi, M. and Miller, S. A., (2014). Short-lived tectonic switch mechanism for long-term pulses. Solid Earth, 5, 13–24, 2014. doi:10.5194/se-5-13-2014

Le Mevel H., Feigl K., Ali T., Cordova L., Demets C., Singer B., (2012). Rapid Uplift during 2007-2002 at Laguna del Maule Volcanic Field, Andean Southern Volcanic Zone. American Geophysical Union Meeting. San Francisco, December de 2012. Poster.

Le Mével, H., Feigl, K. L., Cordova, L., DeMets, C. & Lundgren, P. (2015). Evolution of unrest at Laguna del Maule volcanic field (Chile) from InSAR and GPS measurements, 2003 to 2014. Geophysical Research Letters 42, 6590–6598.

Le Mével, H., Gregg, P. M. & Feigl, K. L. (2016). Magma injection into long-lived reservoir to explain geodetically measured uplift: Application to the 2004–2014 episode at Laguna del Maule volcanic field, Chile. Journal of Geophysical Research 121, 6092–6108.

Marone, C., (1998). The effect of loading rate on static friction and the rate of fault healing during the earthquake cycle. Nature, 391(6662), 69-72.

Massin, F., J. Farrell, and R. B. Smith, (2013). Repeating earthquakes in the Yellowstone volcanic field: Implications for rupture dynamics, ground deformation, and migration in earthquake swarms, J. Volcanol. Geotherm. Res., 257, 159–173.

Miller, C. A., Williams-Jones, G., Fournier, D. & Witter, J. (2016). 3D gravity inversion and thermodynamic modeling reveal properties of shallow silicic magma reservoir beneath Laguna del Maule, Chile. Earth and Planetary Science Letters 459, 14–27.

Miller, C. A., H. Le Mével, G. Currenti, G. Williams-Jones, and B. Tikoff, (2017). Microgravity changes at the Laguna del Maule volcanic field: Magma-induced stress changes facilitate mass addition, J. Geophys. Res. Solid Earth, 122, doi:10.1002/2017JB014048.

Munizaga, F., (1978). Geología del complejo volcánico Laguna del Maule. Memoria de Titulo (Inédito), Universidad de Chile, Departamento de Geología: 157.

Okada, Y., (1985). Surface deformation to shear and tensile faults in a half space, Bull. Seism. Soc. Am., 75, 1135-1154.

Poupinet, G.; Ellsworth, W. L.; and Frechet, J., (1984). "Monitoring Velocity Variations in the Crust Using Earthquake Doublets: An Application to the Calaveras Fault, California". *USGS Staff -- Published Research.* Paper 386.

Pritchard, M., J. Jay, F. Aron, S. Henderson, and L. Lara., (2013). Subsidence at southern Andes volcanoes induced by the 2010 Maule, Chile earthquake, *Nat. Geosci.*, *6*(8), 632–636, doi:10.1038/ngeo1855.

Richardson, J., and Waite, G., (2013). Waveform inversion of shallow repetitive long period events at Villarrica Volcano, Chile. J. Geophys. Res: Solid earth, VoL. 118, 4922– 4936, doi:10.1002/jgrb.50354, 2013

Riley, P.; B. Tikoff; and W. Hildreth., (2012). Transtensional deformation and structural control of contiguous but independent magmatic

systems: Mono-Inyo Craters, Mammoth Mountain, and Long Valley Caldera, California, Geosphere, 8, 740–751, doi:10.1130/GES00662.1.

Riller, U.; Petrinovic, I.; Ramelow, J.; Strecker, M.; Oncken, O., (2001). Late Cenozoic tectonism, collapse caldera and plateau formation in the central Andes. Earth and Planetary Science Letters 188 (3-4): 299-311.

Rodríguez C., Selles D., Dungan M., Langmuir C., Leeman W., (2007). Adakitic Dacites Formed by intracrustal cristal fractionation of water-rich parent magmas at Nevado del Longaví volcano (36.2°S; Andean Southern Volcanic Zone, Central Chile). Journal of Petrology, Volume 48, Number 11, Pages 2033-2061. doi:10.1093/petrology/egm049.

Saxby, J., Gottsmann, J., Cashman, K., Gutiérrez, E., (2016). Magma storage in a strike-slip caldera. Nat. Commun. 7, 12295. http://dx.doi.org/10.1038/ncomms12295.

http://www.nature.com/doifinder/10.1038/ncomms12295.

Shelly, D. R., G. C. Beroza, S. Ide., (2007). Non-volcanic tremor and low frequency earthquake swarms, Nature, 446, 305–307, doi:10.1038/ nature05666.

Shelly, D.R; Hill D.P; Massin, F; Farrell, J; Smith, R.B, Taira, T., (2013). A fluid-driven earthquake swarm on the margin of the Yellowstone caldera. Journal ofF Geophysical Research: Solid Earth, Vol. 118, 1–15, doi:10.1002/jgrb.50362, 2013.

Siebert, L., Simkin, T., (2002). Volcanoes of the world: an illustrated catalog of Holocene volcanoes and their eruptions. www.volcano.si.edu.

Singer, B., Andersen, N., Le Mevel, H., Feigl, K., DeMets, C., Tikoff, B., Thurber, C., Jicha, B., Cardona, C., Cordova, L., Gil, F., Unsworth, M., Williams-Jones, G., Miller, C., Fierstein, J., Hildreth, W., Vazquez, J., 2014. Dynamics of a large, restless, rhyolitic magma system at Laguna del Maule, southern Andes, Chile. GSA Today24, 4–10. http://dx.doi.org/10.1130/GSATG216A.1.

Snoke, J. A., J. W. Munsey, A. C. Teague, and G. A. Bollinger, (1984). A program for focal mechanism determination by combined use of polarity and SV-P amplitude ratio data, Earthq. Notes 55, no. 3, 15.

Spinks, K.; Acocella, V.; Cole, J., Bassett; K., (2005). Structural control of volcanism and caldera development in the transtensional Taupo Volcanic Zone, New Zealand. Journal of Volcanology and Geothermal Research 144, 7–22.

Stern, Charles R., (2004). Active Andean volcanism: its geologic and tectonic setting. Rev. geol. Chile v.31 n.2. doi: 10.4067/S0716-02082004000200001.

Thurber, C. H., (1983). Earthquake locations and three-dimensional crustal structure in the Coyote Lake area, central California, J. Geophys. Res. 88, 8226-8236.

Toda S, R. S. Stein, K. Richards-Dinger, and B. Serkan., (2005). Forecasting the evolution of seismicity in southern California: Animations built on earthquake stress transfer. Journal of Geophysical Research 110(B5): B05S16.

Waldhauser, F., and W. L. Ellsworth, (2000). A double-difference earth-quake location algorithm: Method and application to the northern Hay-ward fault, Bull. Seismol. Soc. Am., 90, 1353–1368.

Walter, T.R., (2007). How a tectonic earthquake may wake up volcanoes: Stress transfer during the 1996 earthquake–eruption sequence at the Karymsky Volcanic Group, Kamchatka. Earth and Planetary Science Letters 264 (2007) 347–359.